AVCO EVERETT RESEARCH LABORATORY

a division of
AVCO CORPORATION

EXPERIMENTAL INVESTIGATION OF ADVANCED SUPERCONDUCTING MAGNETS

SUPERCONDUCTING STRIP AND ITS USE IN MAGNETS

Ethan Hoag

FINAL REPORT
Contract No. NAS 8-5279
September 1964

prepared for

GEORGE C. MARSHALL SPACE FLIGHT CENTER
NATIONAL AERONAUTICS AND SPACE ADMINISTRATION
Huntsville, Alabama

EXPERIMENTAL INVESTIGATION OF ADVANCED SUPERCONDUCTING MAGNETS

SUPERCONDUCTING STRIP AND ITS USE IN MAGNETS

by

Ethan Hoag

FINAL REPORT

AVCO-EVERETT RESEARCH LABORATORY
a division of
AVCO CORPORATION
Everett, Massachusetts

Contract No. NAS 8-5279

September 1964

prepared for

GEORGE C. MARSHALL SPACE FLIGHT CENTER
NATIONAL AERONAUTICS AND SPACE ADMINISTRATION
Huntsville, Alabama

TABLE OF CONTENTS

INTRODUCTION

An experimental investigation has been carried out to study the characteristics of superconducting strip in the context of its use for practical superconducting magnet construction. Particular attention has been directed toward such practical aspects as superconducting to normal joints, superconducting to superconducting joints, critical current characteristics of wide samples suitable for large coil construction, current density distribution, and heat treatment.

A strip coil using approximately 6.8 kg of Nb 25% Zr Strip was constructed in order to test the actual applications of the principles learned. The coil incorporated many of these and performed satisfactorily, but did not perform as well as an equivalent wire coil.

The study has been broad and exploratory in nature and a considerable portion of the effort has been expended in developing the necessary tooling and measurement techniques.

While drawing conclusions in some areas, questions have been raised in others. These are vital to successful coil construction and deserve further study.

I. SUPERCONDUCTING TO NORMAL CONNECTIONS

1. Introduction

Joints between power leads and superconductors and between superconductors can be a source of error in experiments on superconductivity and of trouble and expense in superconducting magnets.

The following is a presentation of a theoretical and experimental program that was carried on to (1) develop a reliable contact that could be used in high field superconducting magnets, (2) analyze the mechanism whereby current is transferred to a superconductor, (3) establish design parameters that would permit comparative measurements to be made on various types of joints and (4) to establish a testing procedure for making such comparative measurements.

2. Theoretical Analysis

2.1 Current Transfer

The transfer of current into a superconductor from a normal conductor in a contact can be idealized by the circuit shown in Fig. 1. In an actual contact, the surface resistance may vary along the length of the contact, especially in one which is made by crimping the normal material around the superconductor at several points. For the purpose of this analysis, it is assumed that an average uniformly distributed surface resistivity exists between the superconductor and the normal conductor.

Initially, all the current is in the normal conductor. The transfer starts at the beginning of the contact between normal conductor and the superconductor. Let us assume initially that the temperatures are low enough so that the superconductor remains in its superconducting state with zero resistance throughout the length of the contact.

If we write the circuit equations for a length Δx of the ladder network shown in Fig. 1 and then allow Δx to approach zero, the equation for the current in the normal conductor is:

$$\frac{d^2 In}{dx^2} = \frac{In}{x_s^2} \tag{1}$$

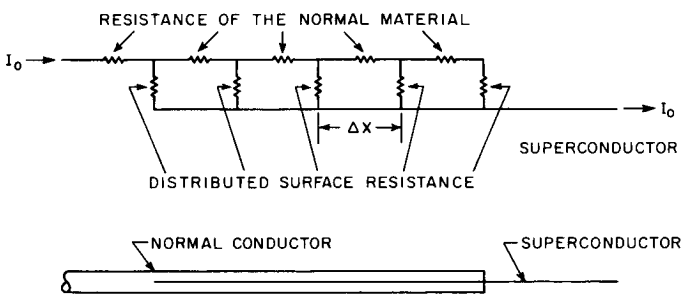

Fig. 1 Idealized circuit diagram for the transfer of current from a normal conductor.

where

$$x_s = \sqrt{\frac{S}{r}}$$

and the quantities r and S are defined as follows:

r = resistance per unit length of normal conductor [Ω/cm]

S = surface resistance of unit length of contact [Ω cm]

The boundary conditions are:

In = I_o at x = 0 and

I = O at x = ℓ

This results in an equation for the current in the normal conductor

$$I_n = I_o \frac{\sinh \frac{\ell - x}{x_s}}{\sinh \frac{\ell}{x_s}} \tag{2}$$

and the current in the superconductor

$$I_S = I_o \left[1 - \frac{\sinh \frac{\ell - x}{x_s}}{\sinh \frac{\ell}{x_s}} \right] \tag{3}$$

The potential V of the normal material above the potential of the superconductor is given locally by the current flowing through the surface resistance:

$$V = -S \frac{d I_n}{dx} = \frac{S I_o}{x_s} \frac{\left(\cosh \frac{\ell - x}{x_s} \right)}{\sinh \frac{\ell}{x_s}} \tag{4}$$

The voltage at x = 0 divided by I_o represents the resistance of the contact:

$$R_c = \left. \frac{V}{I_o} \right]_{x=0} = \frac{S}{x_s} \coth \frac{\ell}{x_s} = r\, x_s \coth \frac{\ell}{x_s} \tag{5}$$

The above expression for contact resistance is plotted in Fig. 2, and shows that for long contacts (ℓ/x_s large) the contact resistance is equal to the resistance of a length x_s of the normal conductor. For short contacts ($\ell/x_s < 1.0$) the contact resistance increases rapidly as ℓ/x_s decreases.

In some experiments the contact resistance has been measured using a potential difference at the end of the contact, ($x = \ell$). The measured resistance for this case is:

$$R_\ell = \frac{V}{I_o}\Bigg]_{x=\ell} = \frac{S}{x_s \sinh \ell/x_s} = \frac{r x_s}{\sinh \frac{\ell}{x_s}} \qquad (6)$$

This relationship is shown plotted in Fig. 2.

Measurement of R_ℓ is a measure of surface contact resistance for $\ell/x_s < 1.0$; for $\ell/x_s > 1.0$, $R_\ell \to 0$ and a low value does not necessarily mean that a low surface resistance has been achieved.

2.2 Temperature Distribution

The current transfer characteristics of a contact are only one half of the overall picture, since failure of a contact results when the combination of current and temperature to which the superconductor is subjected is inconsistent with its being able to remain superconducting.

We shall consider two types of contacts of normal conductor to superconductor. The two contacts are shown idealized in Fig. 3. (I) The first contact consists of a normal conductor which is exposed to helium up to the point where the superconducting-normal contact is made. (II) The second one consists of a contact that is cooled for its entire length.

The temperature distribution for each case is calculated from the one dimensional heat conduction equation:

$$k A \frac{\partial^2 T}{\partial x^2} - h P T + \frac{\text{Joule heat generation}}{\text{unit length of contact}} = 0 \qquad (7)$$

In the above equation k is the thermal conductivity which, for simplicity, is assumed independent of temperature, A is the cross sectional area of the normal conductor, P is the cooled perimeter, h is the heat transfer coefficient to the helium.

For the Case I where the conductor is cooled only before contact is made with the superconductor:

for $x \leq 0$:

$$kA \frac{\partial^2 T}{\partial x^2} - h P T + r I_o^2 = 0 \qquad (8)$$

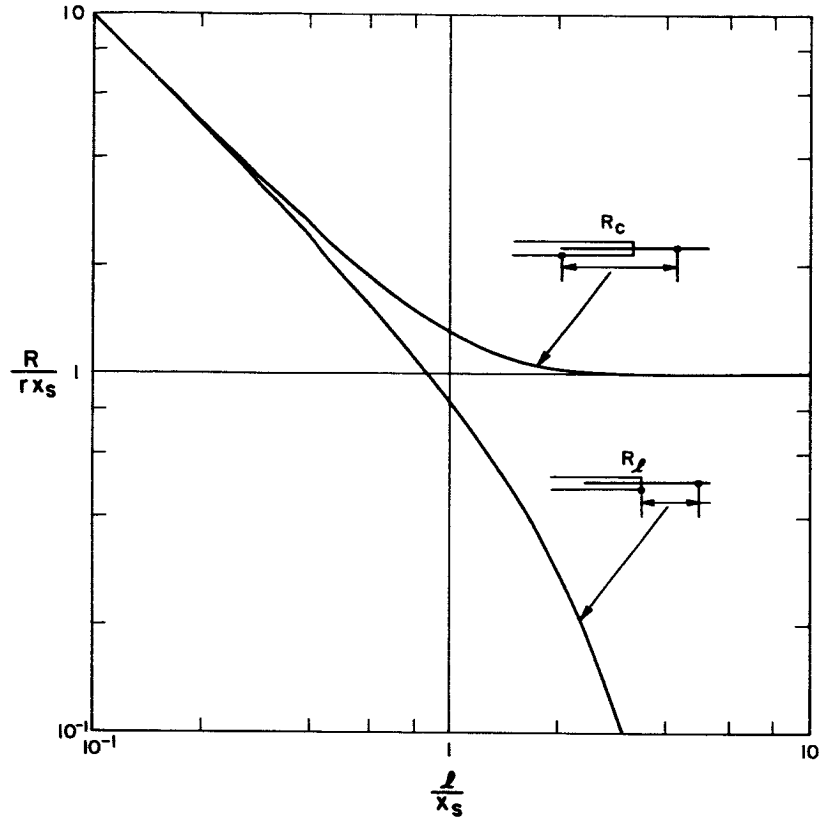

Fig. 2 The resistance of a contact as measured by (a) potential taps at the beginning of the contact and the superconductor (R_c) and (b) potential taps at the end of the normal conductor and the superconductor (R_ℓ). Both are shown plotted versus the length of the contact divided by the characteristic transfer distance x_s.

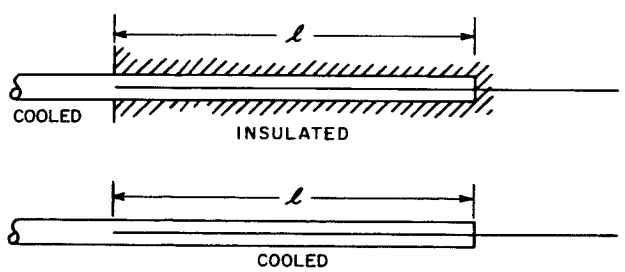

Fig. 3 Two idealized normal to superconductor contacts. The upper contact consists of a normal conductor which is exposed to helium up to the point where the contact starts, the lower contact is exposed to helium for its entire length.

A2294

A2291

For the region where the current is transferring into the superconductor the heat generated per unit length is given by:

$$\frac{\text{Joule Heating}}{\text{Unit Length}} = r I_n^2 + S \left(\frac{d I_n}{dx} \right)^2 \qquad (9)$$

the first term represents heat generated in the normal conductor and the second term heat generated in the surface resistance by the transfer of current from normal conductor to superconductor.

Substituting for I_n from Eq. (3) results in:

$$\frac{\text{Joule heating}}{\text{unit length}} = r I_o^2 \frac{\cosh 2 \frac{\ell - x}{x_s}}{\left[\sinh \frac{\ell}{x_s} \right]^2} = 0 \qquad (10)$$

For this contact we have assumed that the transfer of current takes place in the insulated part of the contact, so the temperature distribution is given by:

$$kA \frac{\partial^2 T}{\partial x^2} + r I_o^2 \frac{\cosh 2 \frac{\ell - x}{x_s}}{\left[\sinh \frac{\ell}{x_s} \right]^2} = 0 \qquad (11)$$

$$x \geq 0$$

Equations (8) and (11) together define the temperature distribution in the whole contact.

For simplicity we shall take the temperature T to represent the temperature rise above the cooling bath. The boundary conditions are then:

$T \neq \infty$ at $x \rightarrow -\infty$

$\frac{dT}{dx} = 0$ at $x = \ell$ (no heat conducted out of the end longitudinally)

$T, \frac{dT}{dx}$ continuous at $x = 0$

Using these boundary conditions together with Eqs. (8) and (11):

$$x \geq 0$$

$$\frac{hPT}{rI_o^2} = 1 + \frac{x_s^2}{4x_o^2}\left[\frac{\cosh\frac{2\ell}{x_s} - \cosh 2\left(\frac{\ell - x}{x_s}\right)}{\left[\sinh\frac{\ell}{x_s}\right]^2}\right] + \frac{x_s}{x_o}\coth\frac{\ell}{x_s}$$

$$x \leq 0$$

$$\frac{hPT}{r I_o^2} = 1 + \frac{x_s}{x_o}\, e^{\frac{x}{x_o}}\coth\left(\frac{\ell}{x_s}\right) \qquad (12)$$

where

$$x_o \equiv \sqrt{\frac{kA}{hP}}$$

Case II - For this case, the contact is cooled for its entire length and Eq. (11) is replaced by:

$$x \geq 0$$

$$kA\frac{d^2T}{dx^2} - hPT + rI_o^2\frac{\cosh 2\frac{\ell - x}{x_s}}{\left[\sinh\frac{\ell}{x_s}\right]^2} = 0 \qquad (13)$$

while the temperature in the region $x \leq 0$ is still obtained from Eq. (8). The boundary conditions remain unchanged (we still neglect any heat transfer out the end of the contact, so $dT/dx = 0$ at $x = \ell$).

The results for the temperature distribution are:

$$x \geq 0$$

$$\frac{hPT}{r I_o^2} = e^{-\frac{\ell}{x_o}} \cosh \frac{\ell - x}{x_o} \left[1 - \frac{\cosh 2\frac{\ell}{x_s} + \frac{2x_o}{x_s} \sinh \frac{2\ell}{x_s}}{\left(1 - \frac{4x_o^2}{x_s^2}\right)\left[\sinh \frac{\ell}{x_s}\right]^2} \right]$$

$$+ \frac{\cosh 2\left(\frac{\ell - x}{x_s}\right)}{\left(1 - \frac{4x_o^2}{x_s^2}\right)\left[\sinh \frac{\ell}{x_s}\right]^2} \qquad (14)$$

and

$$x \leq 0$$

$$\frac{hPT}{r I_o^2} = 1 + \left[e^{-\frac{\ell}{x_o}} \cosh \frac{\ell}{x_o} \left\{ 1 - \frac{\cosh 2\frac{\ell}{x_s} + 2\frac{x_o}{x_s} \sinh \frac{2\ell}{x_s}}{\left(1 - \frac{4x_o^2}{x_s^2}\right)\left[\sinh \frac{\ell}{x_s}\right]^2} \right\} \right.$$

$$\left. - 1 + \frac{\cosh 2\frac{\ell}{x_s}}{\left(1 - \frac{4x_o^2}{x_s^2}\right)\left[\sinh \frac{\ell}{x_s}\right]^2} \right] e^{\frac{x}{x_o}} \qquad (15)$$

2.3 Results of Theoretical Analysis

The results of the theoretical analysis are best shown in graphical form. Figure 4 summarizes the details of the current transfer and temperature analysis for a contact of length $\ell = x_s$, and $x_s = 2.5\, x_o$.

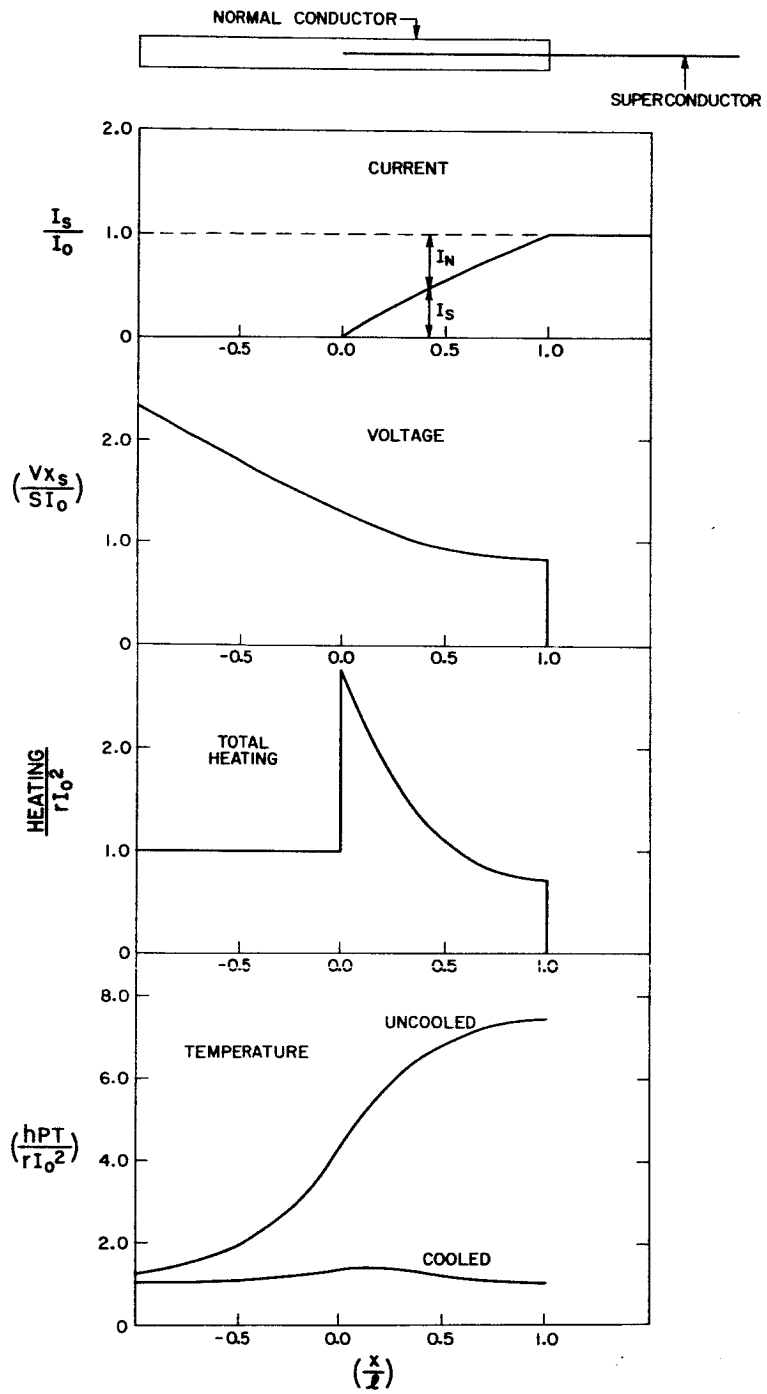

Fig. 4 This figure shows the theoretical variation of the current in the normal conductor, current in the superconductor, potential variation, total heating, and temperature distribution for cooled and uncooled contacts as a function of distance. The plots are made for $\ell = x_s$ and $x_s = 2.5\ x_o$.

The figure shows the current in the superconductor, current in the normal conductor, voltage in the normal conductor with reference to the superconductor, heating per unit length of contact, temperature distribution for the case of a contact with an insulated section in the region of the superconducting wire, and for the case where it is cooled for its entire length.

The heat generation per unit length requires a comment at this point. Until current transfer begins, the heat generation is merely the joule heating in the normal conductor. However, when the transfer of current begins, additional heating occurs at the interface between the normal conductor and the superconductor, since the current in the normal conductor is still close to its value before the transfer started, an increase in the heat generation occurs.

For a contact which is insulated in the region of current transfer, the maximum temperature occurs at the end of the contact ($x = \ell$) where the superconductor is required to carry the full current I_o flowing through the contact. From Eq. (12) the temperature at this point is:

$$\frac{hPT_e}{r I_o^2} = 1 + \frac{1}{2}\left(\frac{x_s}{x_o}\right)^2 + \frac{x_s}{x_o} \coth \frac{\ell}{x_s} \tag{16}$$

Note that the temperature rise T_e drops as ℓ increases.

If the superconductor cannot carry the current I_o, at the temperature T_e, then the superconductor becomes resistive.

In general, under a given set of conditions we can define a temperature rise above the cooling bath T_c which will make the superconductor resistive while it carries no current, also let us define a current I_c which can be passed through the superconductor while it is at the bath temperature. The current which can be passed through the superconductor I_o is a function of the temperature T_o, and falls from I_c at $T_o = 0$ to zero at $T_o = T_c$. As an approximation let us assume that this decrease in current carrying capacity is linear.

$$\frac{I_o}{I_c} = 1 - \frac{T_o}{T_c} \tag{17}$$

Using this relationship between current I_o and temperature T_o as well as Eq. (16) for the maximum temperature in the contact results in:

$$\frac{1 - \frac{I_o}{I_c}}{\left(\frac{I_o}{I_c}\right)^2} \geq \frac{r I_c^2}{hPT_c}\left[1 + \frac{1}{2}\frac{x_s^2}{x_o^2} + \frac{x_s}{x_o}\coth\frac{\ell}{x_s}\right] \qquad (18)$$

The inequality denotes the values of the expression on the right for the superconductor in the contact to remain superconducting up to a fraction I_o/I_c of the current it could carry if it were truly at the temperature of the surrounding bath.

For Case II, where the contact is cooled for its entire length, the maximum temperature occurs near the beginning of the contact, where the current has not yet fully transferred into the superconductor. From the temperature distribution in Eq. (14) and using Eq. (17), the allowable current in the superconductor can be obtained:

$$\left(\frac{hPT_c}{r I_c^2}\right)\frac{I_c^2}{I_o^2}\left(1 - \frac{I_a}{I_c}\right) = e^{-\frac{\ell}{x_o}}\cosh\frac{\ell - x}{x_o}$$

$$\left[1 - \frac{\cosh\frac{2\ell}{x_s} + \frac{2x_o}{x_s}\sinh\frac{2\ell}{x_s}}{\left[1 - 4\frac{x_o^2}{x_s^2}\right]\left[\sinh\frac{\ell}{x_s}\right]^2}\right] + \frac{\cosh 2\left(\frac{\ell - x}{x_s}\right)}{\left[1 - 4\frac{x_o^2}{x_s^2}\right]\left[\sinh\frac{\ell}{x_s}\right]^2} \qquad (19)$$

The actual current flowing in the superconductor at any point is given by Eq. (2) and varies along the length of the contact.

When the allowable current I_a, at any point becomes equal to the superconductor current I_s, the limiting condition is reached and any further increase in current through the contact makes the superconductor resistive.

In designing a contact Case I results in an expression (Eq. (18)) which is relatively easy to use. The Case II solution clearly shows that the temperatures are reduced from those of Case I and therefore contacts which satisfy Eq. (18) will have an additional safety factor if they are cooled over their whole length.

To see the effect of the individual variables on the contact performance we can write Eq. (18) in terms of primary quantities:

$$\frac{1 - \frac{I_o}{I_c}}{\left(\frac{I_o}{I_c}\right)^2} \geq \frac{r I_c^2}{hPT_c} + \frac{1}{2} \frac{SI_c^2}{kAT_c} + \sqrt{\frac{Sr}{hPkA}} \frac{I_c^2}{T_c} \coth \ell\sqrt{\frac{r}{S}} \qquad (20)$$

For values of I_o/I_c close to unity the left hand side of the equation becomes merely $1 - I_o/I_c$. From the above it is clear that a good contact has the following characteristics:

1. High thermal and electrical conductivity in the normal conductor
2. Low surface resistance
3. A length longer than $\sqrt{\frac{S}{r}}$
4. Good cooling as far as exposing the surface to the bath, as well as good thermal contact between the superconductor and the normal conductor.
5. High T_c obtained by placing contact in region of low field.

It is important to point out that the limitation on the contact is a thermal one, and that having a low resistivity alone does not insure good contact performance.

The onset of resistance in the superconductor in a contact may be catastrophic or gradual depending on the cooling available. Onset of resistance in the superconductor results in a new current distribution, with a new distribution of joule and surface heating, it is conceivable that the temperature distribution could readjust to a new stable situation resulting in a higher resistance in the contact, but not a catastrophic propagation of the resistive region. It is expected that this increase in contact resistance would be catastrophic in the case where the current transfer section is insulated, since the highest temperature occurs at the point where the superconductor is required to carry the most current, once this point becomes resistive, an unstable situation will probably result.

If the contact is cooled for its full length the appearance of resistance occurs at a point in the contact where the superconductor doesn't have to carry the full current, so that a new stable situation with a higher contact resistance is possible.

3. Experimental Investigation

3.1 Soldered Connections

Our initial policy in regard to superconducting to normal (SN) connections was to follow the methods already established with wire technology. Our first attempts were therefore in the area of ultrasonic soldering with indium tin solder and we did prepare a connection which performed reasonably well. Before tests were completed on this, however, we discovered that spot welding to copper strip afforded a much simpler and more desirable method.

At about the same time, we discovered that soldering with tin or indium in general, produces inherently high resistance connections because of a high resistivity alloy of tin or indium and copper which forms at the interface during the soldering operation.

Further testing of the soldered connection was therefore abandoned in favor of more pressing experiments. The results of the tests done on this strip are discussed in Appendix A.

3.2 Spot Welded Connections

Spot welding has been found to be by far the most successful method for making SN connections. No special cleaning or other preparation is required and a highly reliable connection can be made in a few minutes with a small spot welding apparatus.

Figure 5 shows a typical connection arranged for testing. It consisted of a copper strip 0.127 mm thick by 20 mm wide, with a Nb-25% Zr strip 0.051 mm thick by 3.00 mm wide, spot welded to it with 3 welds per cm. The spot welds were made with a Model 60A Raytheon spot welding apparatus using a 14 μ F capacitor setting and a heat setting of 3, and an electrode compression of 100 N. In Fig. 6, the reduced voltage (voltage divided by the current at which it occurred) as measured by means of the taps shown in Fig. 5, is plotted as a function of distance along the strip. This characteristic remained unchanged at all currents up to 375 A, the limit of our supply.

From the data shown in Fig. 6, the resistance of an individual spot weld was calculated to be approximately 1.07 $\mu\,\Omega$ (assuming that all spot welds have the same resistance). With this resistance, the characteristic length x_s can be calculated as 1.18 cm.

It is interesting also to note that 75% of the total current is transferred in by the first four spot welds, the current in the first spot weld is 112 A and the current density in the superconductor as it eminates radially out from the spot weld (assumed to be 0.0254 mm in diameter) is of the order of 10^4 A/m^2.

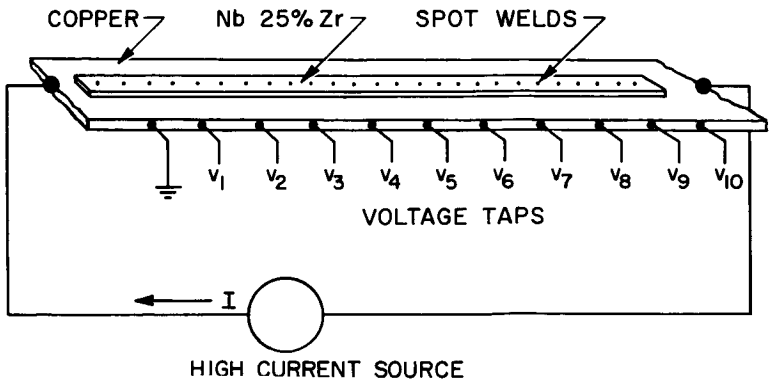

Fig. 5 Test arrangement for Spot Welded Superconducting to Normal Connection.

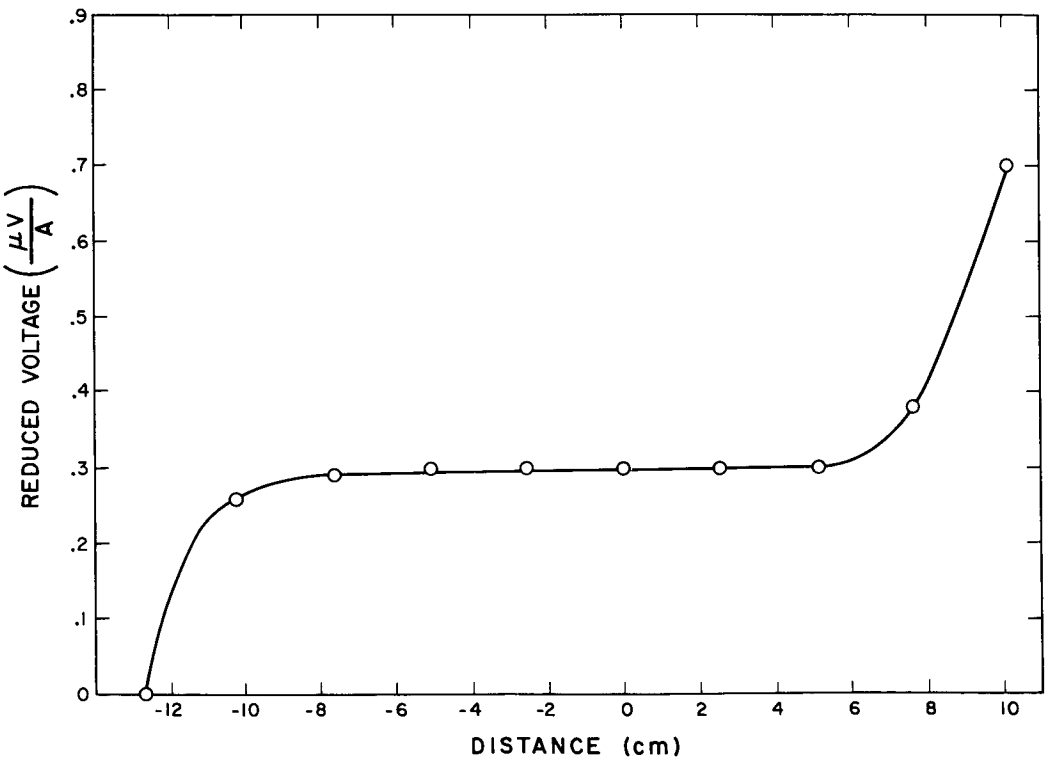

Fig. 6 Voltage Distribution along Superconducting to Normal Spot Welded Connections.

A2389
A2390

Unfortunately, this method was not discovered in time to make anisotropy or H-I measurements, but there is no reason to suspect poor performance in a field. Even if performance is poor, this is not necessarily a drawback since many SN connections can be made in low field regions.

Assuming a spot weld density of 10^6 welds/m^2 (which is quite easy to achieve), we can arrive at an equivalent surface resistivity of 10^{-12} Ω-m^2 which is equal to or better than the best values obtained by any method so far.

Connections of this type, in conjunction with nitrogen cooled leads, were in fact used very successfully in our last test of the strip coil.

3.3 Mechanical Pressure Type Connections

In early work, prior to this contract, we did work on pressure type connections with strip. Owing to the large area over which contact is made, and the high pressures necessary for good contacts, very bulky mechanical structures are required. Even at best, it was difficult to make consistently reliable connections. We decided, therefore not to pursue this method any further in this contract.

3.4 Conclusions

In general, our findings indicate that the success of SN connections is critically dependent on two key factors; the heat transfer away from the joint, and the resistivity of the interface between the superconducting and normal components.

The spot welding method satisfies both of these conditions. It is quick, inexpensive, and reliable, no expensive equipment is needed, and no special precautions need be taken in regard to surface cleanliness. Portable equipment can be used so that connections can be made at the construction site of a coil.

II. SUPERCONDUCTING TO SUPERCONDUCTING CONNECTIONS

In the early stages of the contract, our policy regarding superconducting to superconducting (SS) connections was one of conservatism since they were so essential to the construction of the strip coil. We therefore started testing several types of connections before the anisotropy testing apparatus was completed. This was done by means of a DC transformer apparatus with a small self-contained iron core magnet capable of producing 1 T only in the transverse direction.

We felt at that time that the heat of any welding process would seriously degrade the strip performance in a field and accordingly we concentrated our efforts on methods not requiring heat. Later when the anisotropy testing apparatus was completed and we were able to test resistance spot welds in a parallel field, we found that this was not so and that excellent connections could be made in this way. But in the meantime, considerable effort went into making and testing ultrasonic cold welded connections and several types of riveted connections. Since these are now of somewhat academic interest, we have relegated their discussion to Appendix B.

Immediately upon completion of the transverse field magnet, several resistance spot welds were tested and found to perform almost as well as the strip itself. A typical example of this is shown in Fig. 7 which compares a 3 mm wide by 0.051 mm thick Nb-25% Zr strip with a 3 mm wide, resistance spot welded, lap joint of the same material. The joint was made with an overlap of 6 mm and contained 15 welds, all of which were in the high field region. The welds were produced with a Raytheon Model 60A welder using a 1 μF capacitor setting, a heat setting of 3 and an electrode compression of 100 N.

These connections are ideal from all points of view, they are excellent electrically and mechanically, they can be produced with simple portable equipment in a few minutes with no particular attention paid to cleaning techniques, and their overall thickness is only twice that of the strip itself. They fit our needs so well that all other work on connections was concluded.

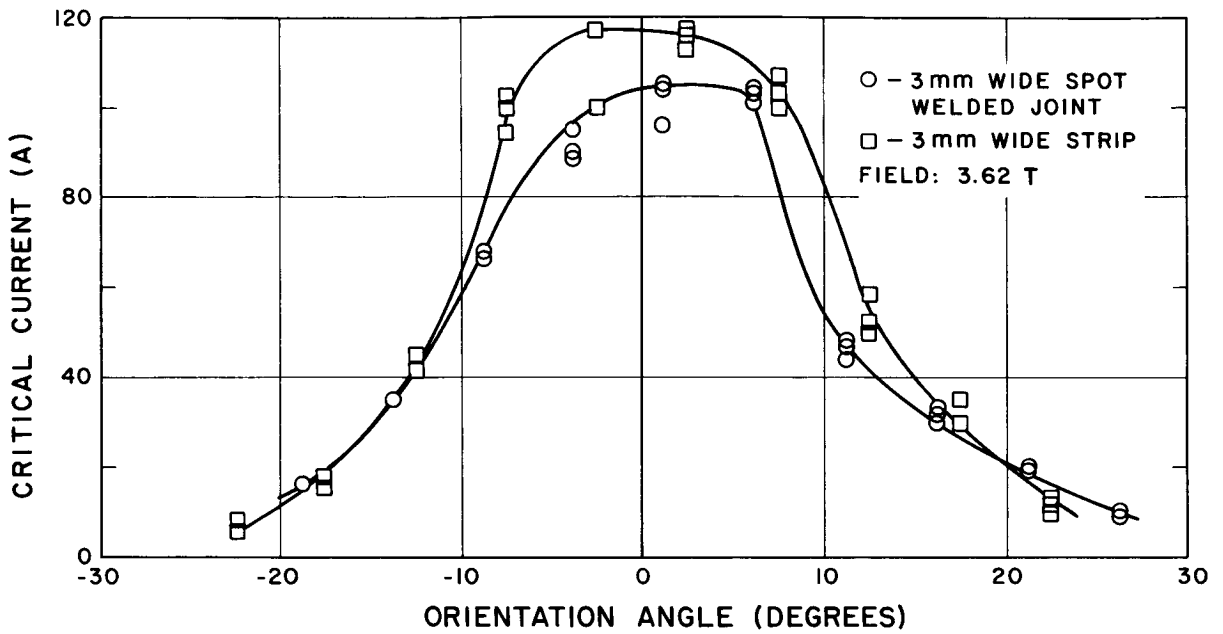

Fig. 7 Comparison of Spot Welded Superconducting to Superconducting Connection to Strip of Similar Width.

III. ANOMALIES IN THE ANISOTROPY OF WIDE SUPERCONDUCTING STRIPS

1. Introduction

Probably the most well known unique property of superconductors in strip form is their anisotropy with respect to magnetic field. Several workers have studied these effects; typical examples of such studies are embodied in the work of Walker and Fraser[1] and of Heise[2]. Their investigations seem to indicate with little doubt that the anisotropy is due to properties of the material (probably due to strains introduced during rolling) rather than of sample geometry.

These studies were done, however, on very narrow strips of small cross sections unsuitable for practical coil construction, and we therefore decided to perform tests of our own on wider samples.

Our data is in the form of H-I curves (critical current density as a function of magnetic field magnitude at constant orientation angle) and anisotropy curves (critical current density as a function of orientation angle at constant magnetic field magnitude).

In general, our experiments have confirmed that the anisotropy is an intrinsic property of the material, but with the wider samples, we have discovered certain anomalies which tend to limit the critical current to values much less than those observed with very small samples.

This anomalous behavior is of such importance to coil technology that we have devoted much of our effort to their study. We attribute them to external factors such as sample width, proximity of other conductors, electrical shunting and heat transfer. In the paragraphs which follow, we show the character of these anomalies and how they are affected by various external factors.

2. Experimental Procedure

In view of the large currents necessary to test the widths contemplated in our investigations, we have made use of a DC transformer for energizing the samples. As explained more fully in Appendix C, this device operates on the principle of conservation of magnetic flux and enables one to induce very large currents in the sample with very little primary current actually entering and leaving the helium. The induced sample current was measured by placing another transformer, similar to but smaller than the first, also in series with the sample and energizing it separately in such a way as to keep the core flux zero. The primary current in this second transformer is then proportional by the turn ratio to the sample current.

The magnetic field was produced by the iron core superconducting magnet described in Appendix D. This magnet has a maximum field of 4.1 T oriented at right angles to the helium dewar axis so that field orientation experiments can be conveniently executed by simply rotating the sample.

In our anisotropy measurements, the DC transformer with its sample was mounted on a rotating member, equipped with a 360^{o} protractor for measuring the orientation angle. The physical arrangement is shown in Figs. 8 and 9. A typical sample with a copper stabilizing strip spot welded to it is shown in Fig. 10.

All anisotropy curves were taken with respect to the orientation angle Θ as defined in Fig. 11.

3. Experimental Results

3.1 Width Effect

The effect of sample width on performance is shown in Fig. 12 where four anisotropy curves for different widths are compared. For strips wider than 1 mm the curves become truncated progressively more and more. In fact, as is seen in Table I, the total currents for all cases are roughly the same regardless of width.

Table I

Total Current vs. Strip Width for Field Parallel to Strip Plane ($\Theta = 0$)

Strip Width (mm)	Total Current (A)
1.32	121
3.07	128
4.8	80
10.0	132

In order to check and be sure that this was not simply faulty contacts, we performed the following two experiments.

In the first, we prepared two 3 mm wide samples, one a conventional spot welded loop and the other an endless loop with no joint at all. These were tested in zero field and quenched at 140 and 120 A respectively, thus proving the reliability of the spot welded contacts.

The second experiment was designed to prove that the quench did not occur in the transformer or measurement section (see Fig. 8).

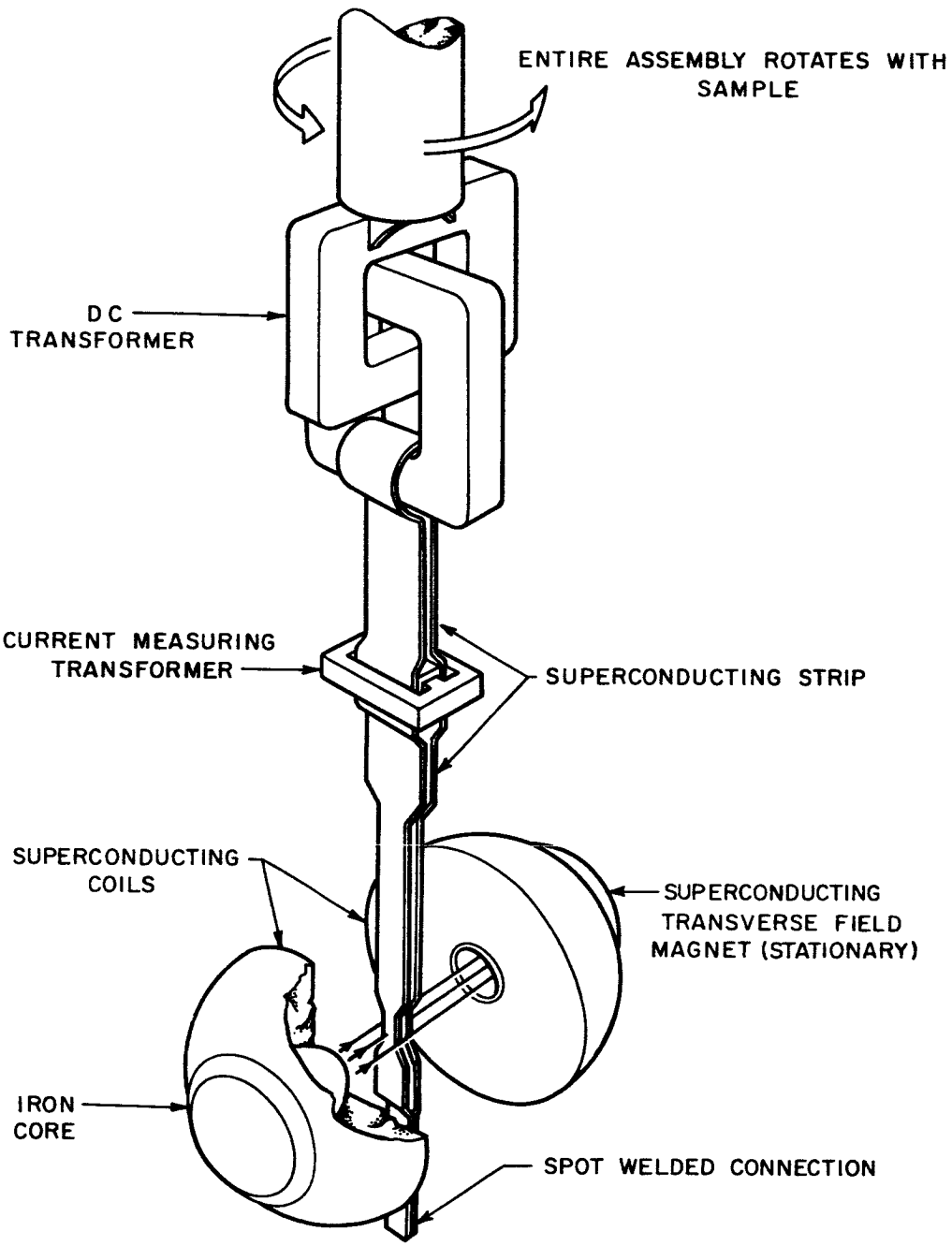

Fig. 8 Physical Arrangement of Sample in Anisotropy Testing Apparatus.

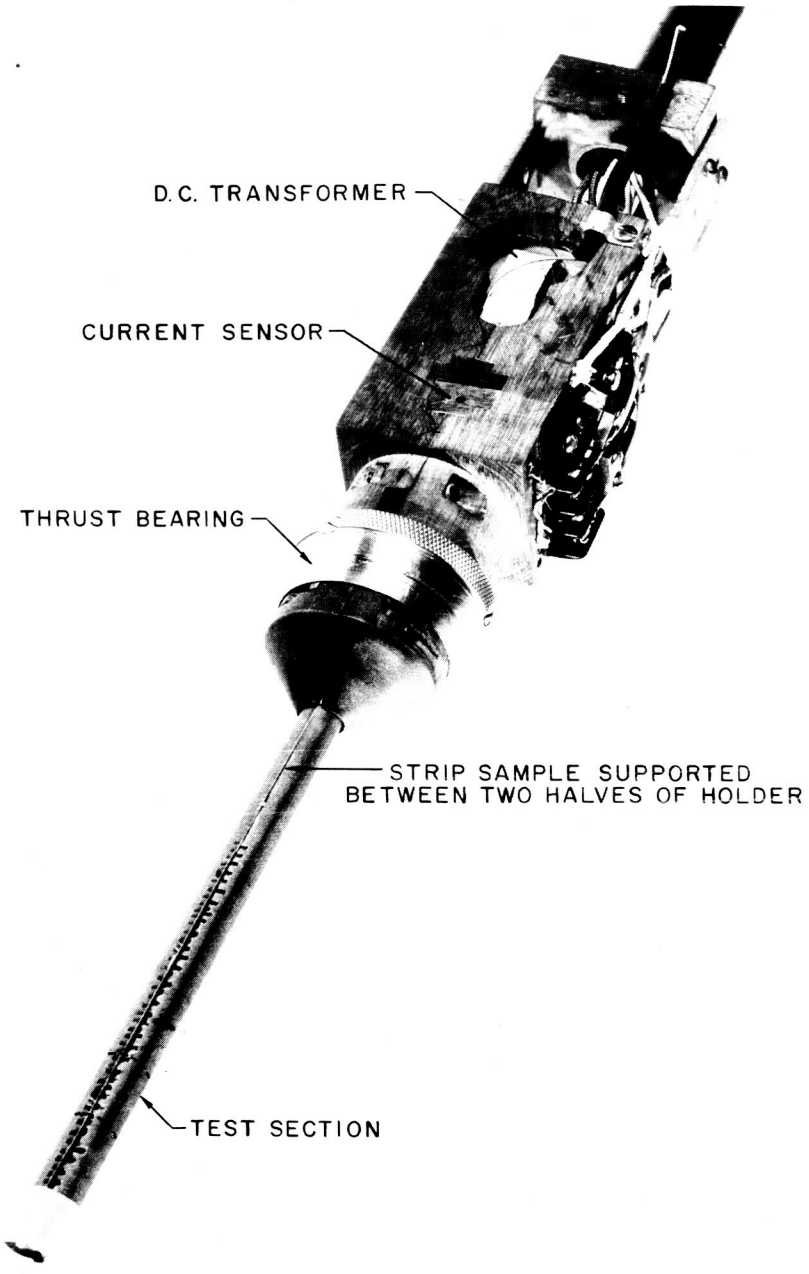

Fig. 9 Anisotropy Test Fixture.

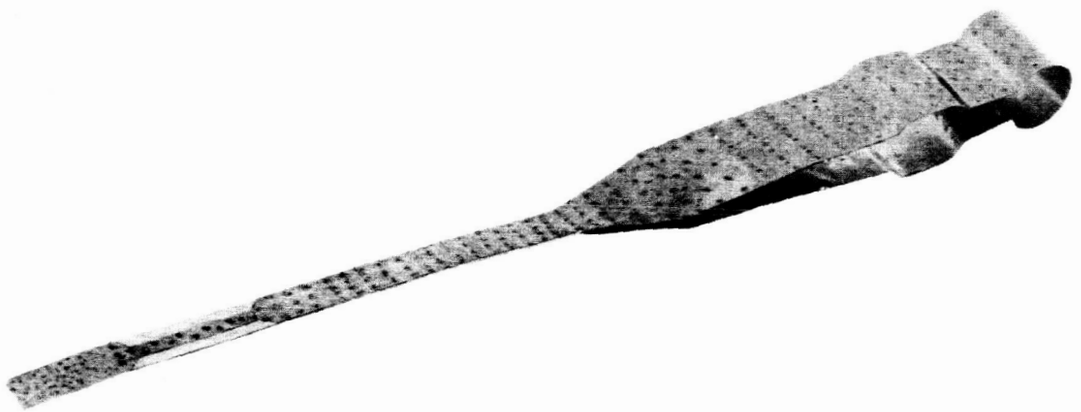

Fig. 10 Typical Sample

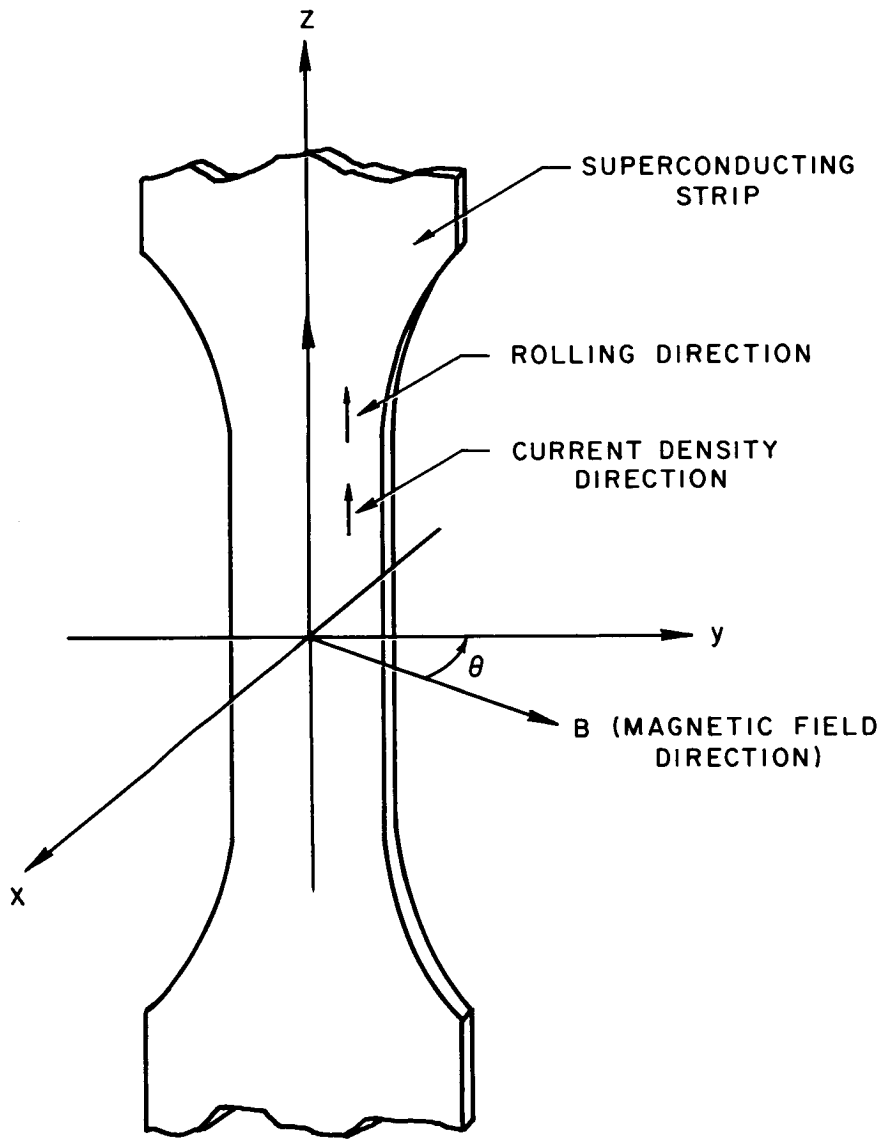

Fig. 11 Definition of Orientation Angle, Θ

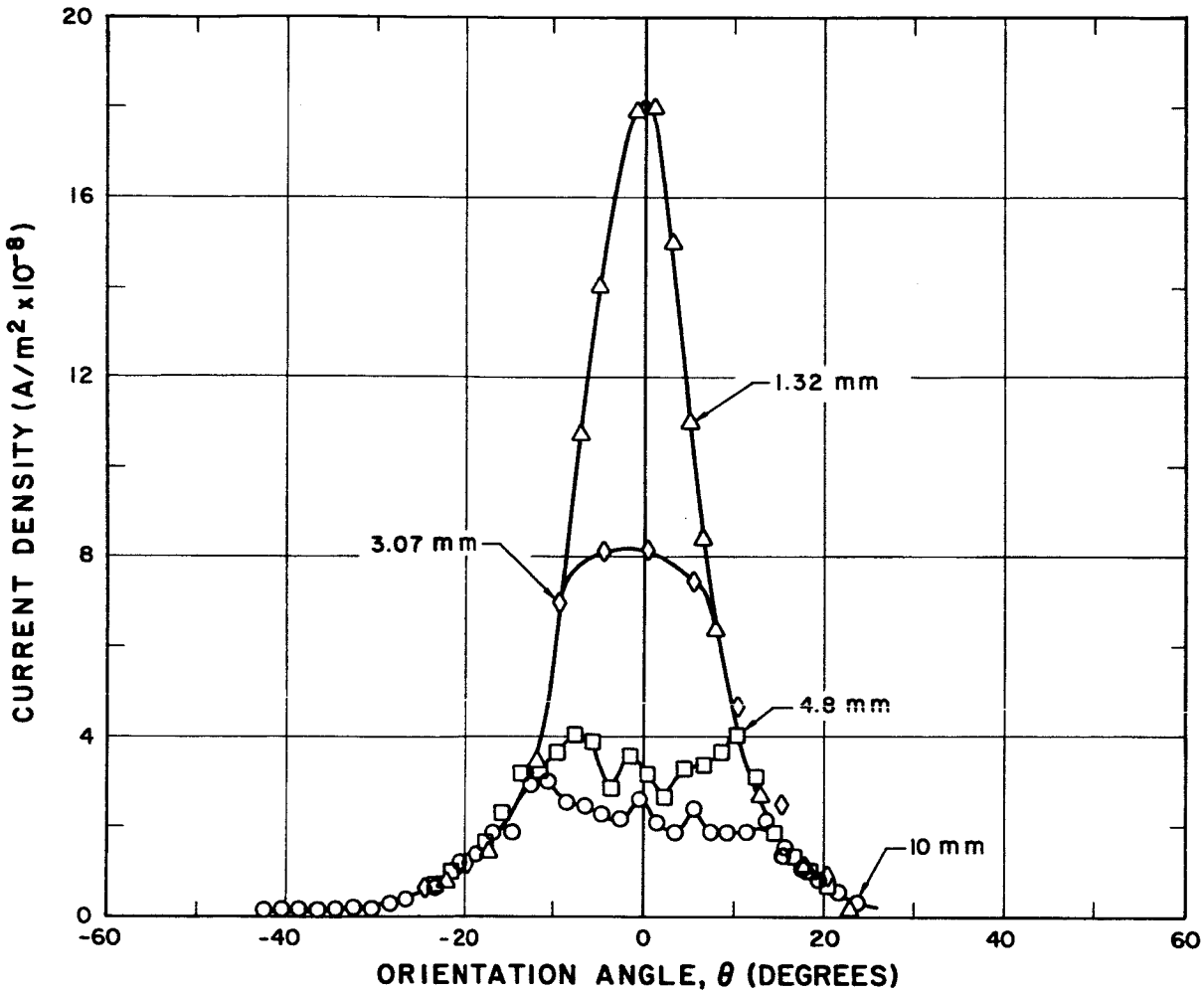

Fig. 12 The effect of Sample Width on Anisotropy

This was done by spot welding copper to the sample in the test section and across the spot weld only, so that if a quench occurred there, the escape of flux (and hence the current decay) would be very slow since it would have to diffuse out through a relatively long narrow channel filled with copper. If, on the other hand it quenched anywhere up in the transformer or measurement section (see Fig. 8) where it was not damped with copper, it would decay instantly. The anisotropy curve for this sample was quite truncated, yet every quench was slow, showing that all quenches (including those in the truncated region) occurred either in the test section or in the joint. Between these two experiments, we conclude that the quenches are occurring in the test section.

3.2 Proximity to Other Conductors

The class of effects relating to the proximity of other conductors on the critical current of a conductor encompasses a rather wide scope, particularly if one is liberal with his definition of "other conductors". To illustrate this point, we cite two examples, the coil and the wide strip. In a coil, we can easily consider adjacent turns to be equivalent to separate conductors at close proximity, even though they are really just other parts of the single conductor making up the coil. By the same token, we can consider a wide strip equivalent to two narrower strips in such close proximity that they are in contact.

In order to investigate this class of effects, we obtained anisotropy curves for the three types of geometries shown in Fig. 13 and compared them with results from single strips. Figure 13a is a 3 mm wide strip which has been slit down the center to form two parallel 1.5 mm samples in the test region; Fig. 13b shows two separate strips insulated from one another but both energized by the same transformer; Fig. 13c shows three strips energized in series to simulate conductors in a coil.

Figure 14 compares the results from the dual isolated strip and the results from the dual parallel strip with a single strip of the same total width. Except for a small difference in the character of the truncation, the dual parallel strip displays the same characteristics as the single strip. The isolated strip has a somewhat narrower curve but the truncation occurs at the same value. Figure 15 compares the triple series samples with single strips of various widths and also shows the effect of the separation, d, between the outgoing and returning strips.

The separation evidently has little effect on performance. The curve for 1 mm separation is almost identical to the 0.0025 mm separation.

Comparison with single strips show two effects. The first effect is displayed by the fact that the current density in the narrowest part of the triple strip is less than that of 3 mm single strips even though it is narrower. This implies some kind of proximity degradation.

The other effect is displayed by the fact that the total current passed by the three strips taken together is about twice that of a single strip of comparable overall width. This shows that with wide strips, (1 cm) performance

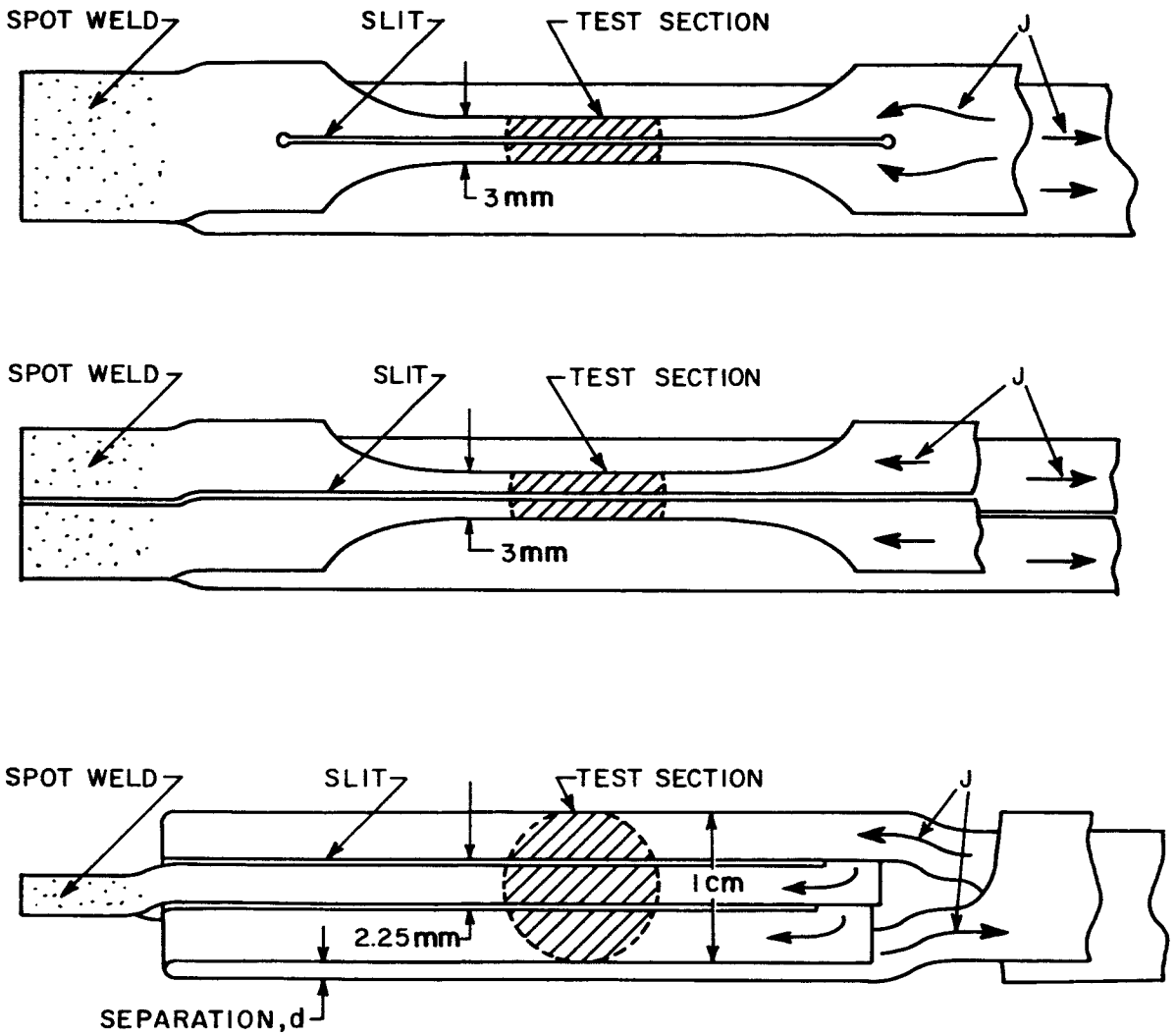

Fig. 13 Special Samples for Testing Proximity Effects

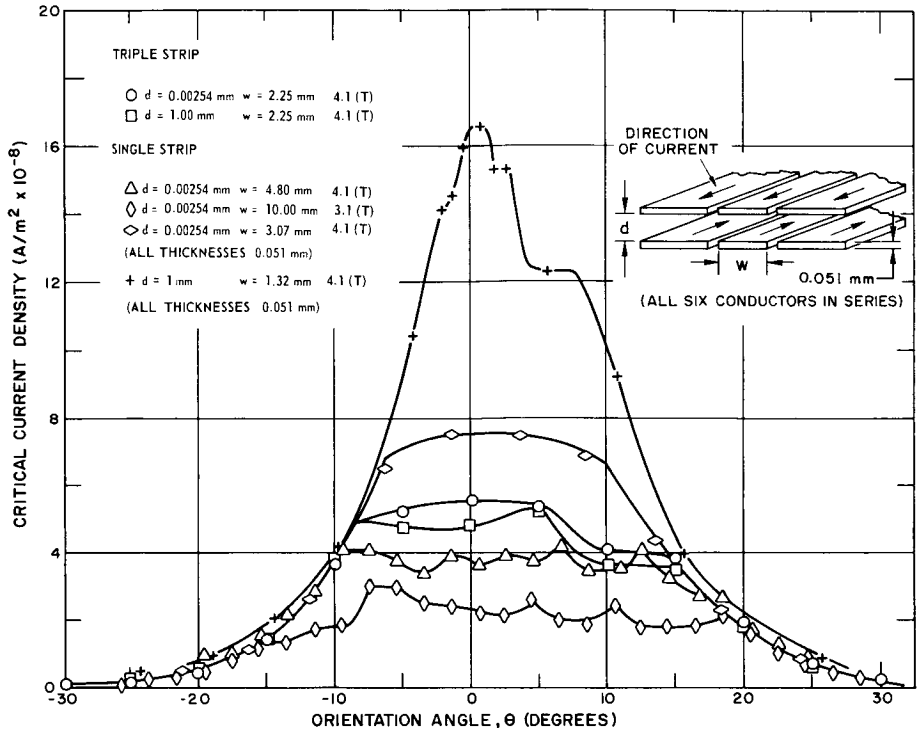

Fig. 15 Comparison of Triple Strip with Single Strips of Various Widths

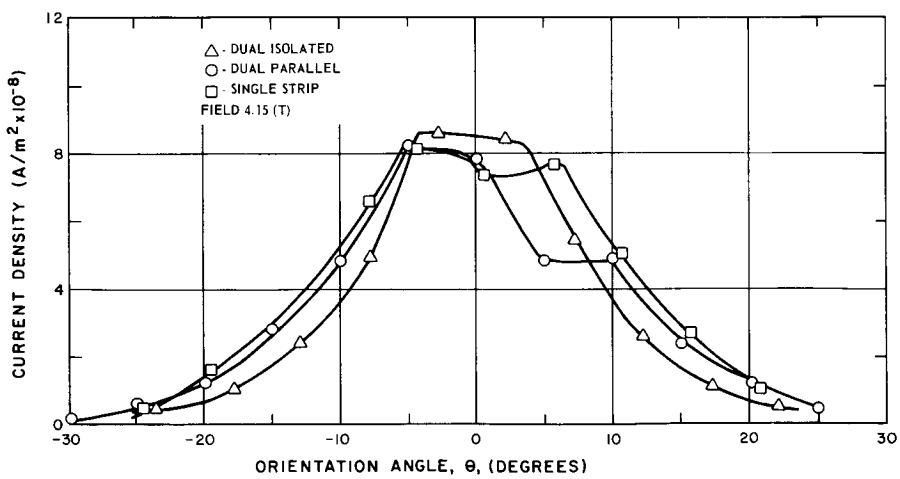

Fig. 14 Comparison of Dual Parallel Sample with Dual Isolated Sample and Single Sample of Similar Width

A2399

A2398

is improved by breaking them up into narrower units. This improvement is evidently less pronounced on narrower strips as in the case of the dual strips (3 mm overall) cited above. There the degradation due to proximity is greater than the improvement (if any) due to the breaking up of the strip and net effect is a degradation.

3.3 The Effect of Shunting with Normal Metal

In our tests of superconducting strip, we have noted unstable transition to normal at all currents over about 30 A, whereas currents less than 30 A result in stable quenches. By unstable, we mean that the current drops abruptly during a quench to a significantly lower value. In a stable quench, the current does not drop but simply fails to go higher.

In the early stages of the contract we attempted to stabilize our samples by placing them in contact with normal metal, but these attempts were unsuccessful because of the difficulty of making a truly low resistance connection between the superconductor and normal metal.

With the advent of spot welded connections, however, we were able to achieve the necessary low resistance connections and we were in fact, able to stabilize our samples. This was done by spot welding copper strip to our sample strip as shown in Fig. 10. Welds were made at intervals of 2 to 3 mm, over the entire sample area.

We had hoped initially that stabilization would dispel the truncation effects, but our tests have not substantiated this. To illustrate this, we present two anisotropy curves in Fig. 16, one unstabilized and the other stabilized. These samples are both approximately the same width and were both tested by the same apparatus. As seen in Fig. 16, the stabilization has not improved matters. The effect of the copper is to slow down the transients occurring during testing. For example, if the current is increased slightly above the critical value, it simply drifts back and we have in fact taken the critical value to be that value to which the current drifts back.

Even with this highly damped sample, we can force unstable behavior by suddenly increasing the current considerably over the critical value. If this is done, the current will drift back to a value lower than critical.

3.4 Potting and the Effect of Heat Transfer

Although previous experience with superconducting wire has shown that potting tends to improve performance, our experience with strip has not born this out.

Potting the dual isolated sample of Fig. 13b resulted in very poor performance and we suspected poor heat transfer to the helium to be the cause. In order to pursue this possibility, we prepared a 1 cm wide sample with all but the barest essential support structure removed. With this arrangement, we could not rotate the sample, but we obtained an H-I curve which we could compare with that of another similar sample which has been clamped between phenolic supports.

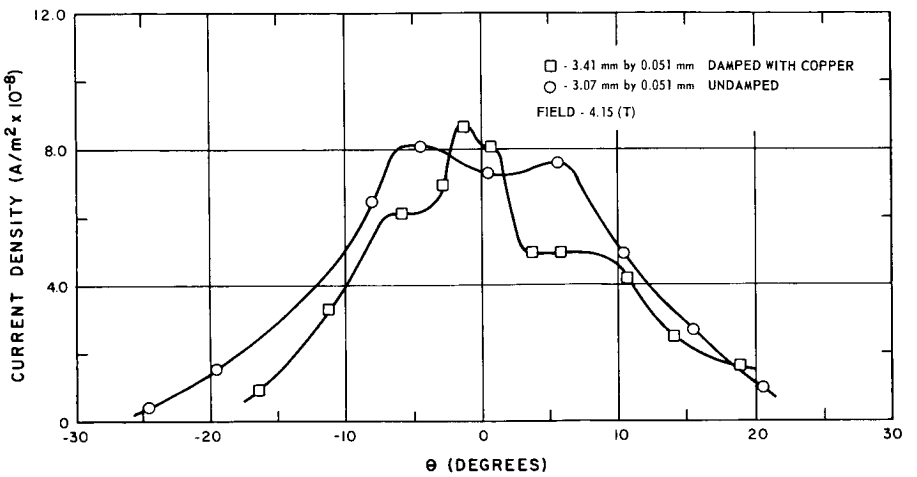

Fig. 16 Comparison of Damped and Undamped Samples

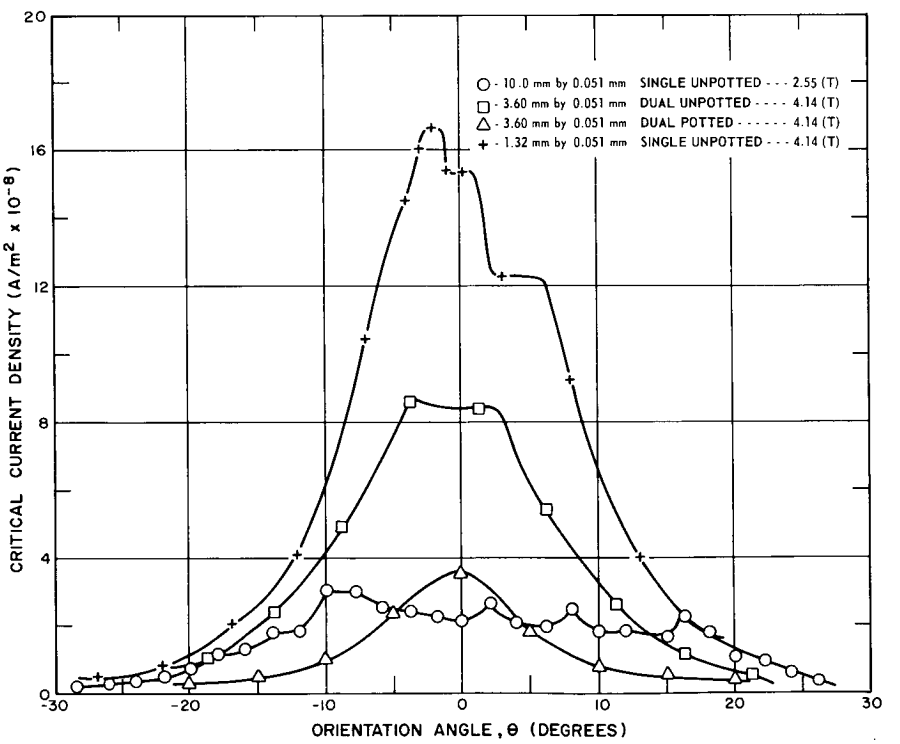

Fig. 17 The effect of the heat transfer environment on anisotropy

A2400

A2401

We thus had a total of four samples as shown in Table II.

Table II

The Effect of Cooling on Peformance

Sample Width	Type	Support	Cooling
3 mm	dual	potted	poor
3 mm	dual	clamped	fair
10 mm	single	clamped	fair
10 mm	single	minimum	good

The results are shown in Figs. 17 and 18. In Fig. 17, anisotropy curves for the two 3 mm samples are shown compared with those of the damped 10 mm sample and a 1 mm sample. In Fig. 18, the H-I curves for all four samples are compared.

These reveal three notable features: the poorly cooled samples show poor performance; the difference in performance becomes less pronounced at low fields; the potted 3 mm sample shows no truncation.

The absence of truncation on the potted sample suggests that two separate effects are at work here, a temperature effect causing a general depression of the entire, H, Θ surface, plus a truncation effect mainly width dependent.

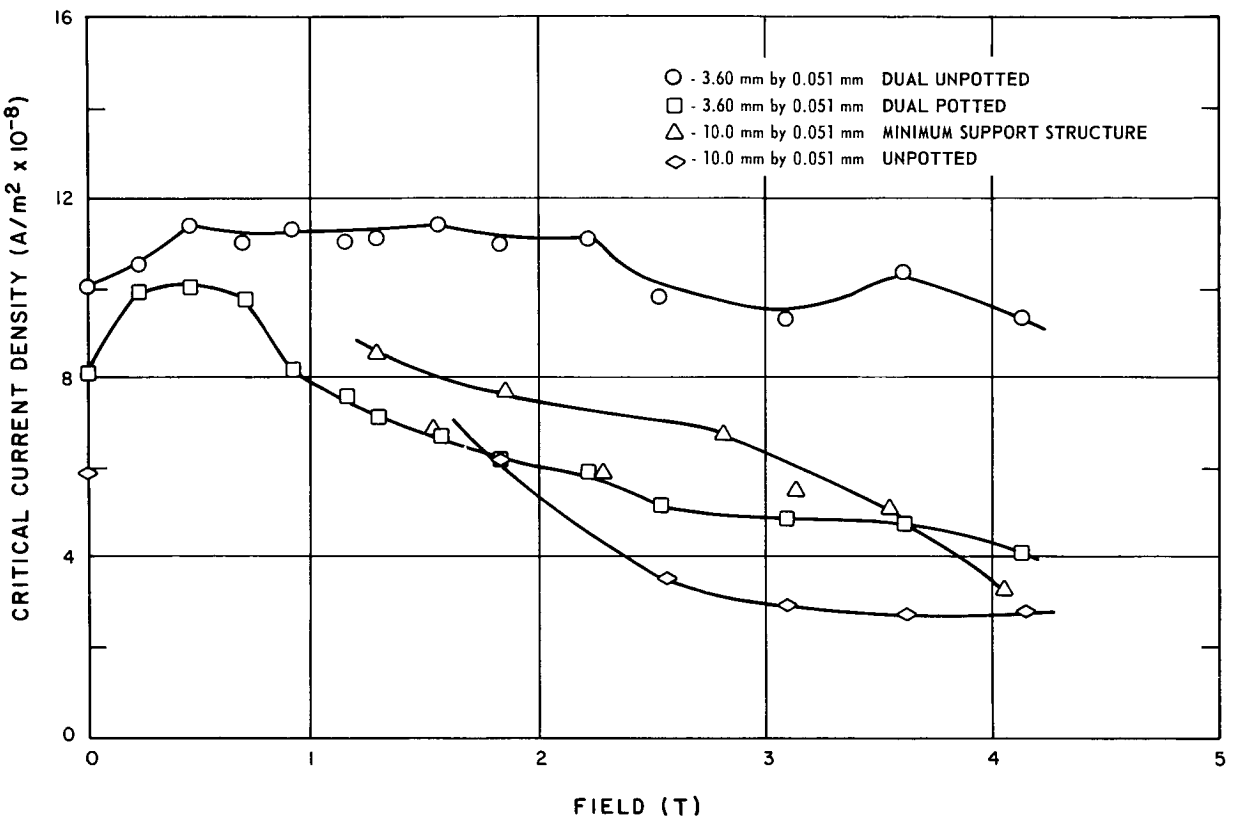

Fig. 18 The effect of the heat transfer environment on the H-I characteristic.

IV. HEAT TREATMENT AND ITS EFFECT ON PERFORMANCE

1. Introduction

Heat treatments were performed on three different superconducting materials, Nb-25% Zr, H-I 120, and pure Niobium. In general, the performance seems to be improved by annealing, but the results differ widely depending on the particular material and heat treatment. Results for the above materials are summarized below in Figs. 19 thru 24.

2. Nb-Zr

Eleven different samples of Nb-25% Zr strip were submitted to us by Kawecki Chemical Company for testing. These included two "as rolled" control samples plus 9 test samples with different proprietary heat treatments. Some of these resulted in very striking improvement in performance especially as regards anisotropy. These are shown in Figs. 19 and 20. Both display two peaks, but in sample C the peak at 90^{o} is more pronounced than that at 0^{o}.

All of the heat treated samples showed a reduction in anisotropy but in some this was at the expense of current density. The samples shown here are the best and should in fact remove the necessity of trimmer coils in strip wound magnets.

3. HI-120

Two samples of HI-120 strip were submitted to us by Westinghouse, one as rolled and the other heat treated by a proprietary process.

As shown in Figs. 21 and 22, the heat treatment greatly improves performance, but it does not remove the anisotropy as in the case of Nb-Zr.

4. Niobium

A pure niobium sample was prepared and tested before and after annealing. Heat treatment on this consisted of a 1 hour anneal at $900^{o}C$.

The results are shown in Figs. 23 and 24. Some improvement is noted in the H-I characteristic but very little change is displayed in the anisotropy.

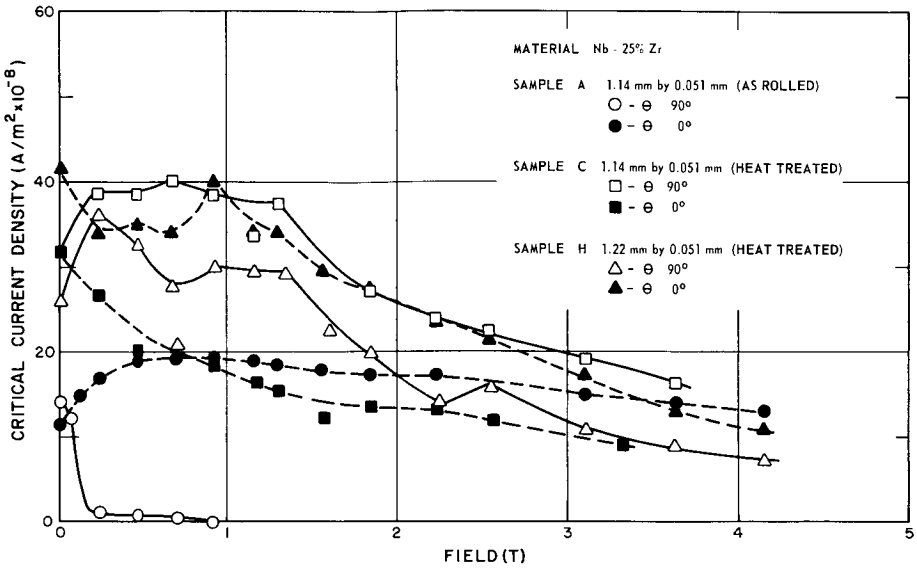

Fig. 19 The effect of heat treatment on the H-I characteristic of Nb-Zr.

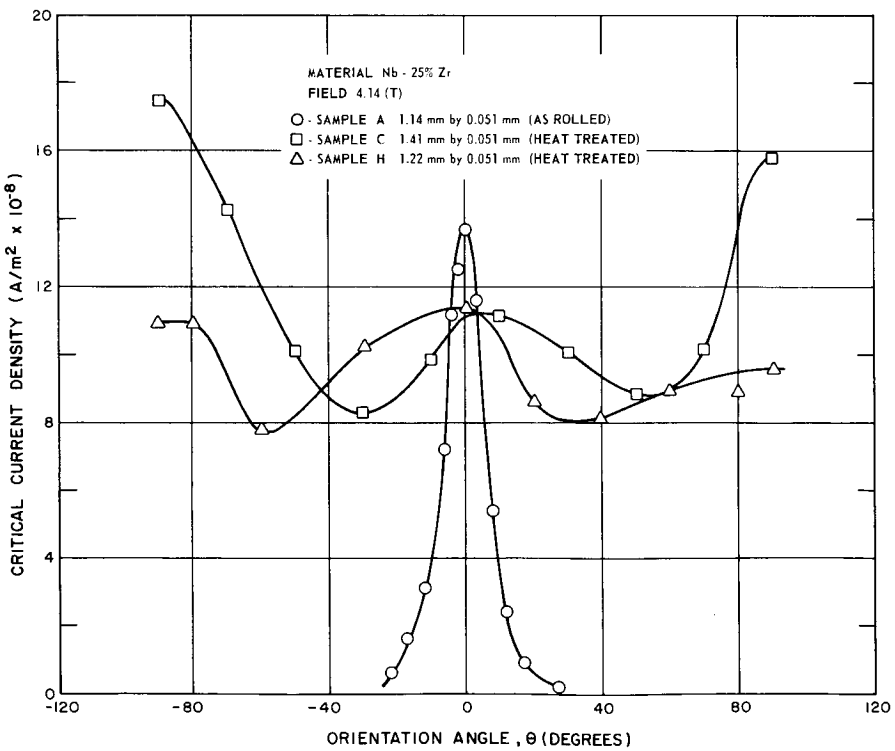

Fig. 20 The effect of heat treatment on the Anisotropy of Nb-Zr.

A2403

A2404

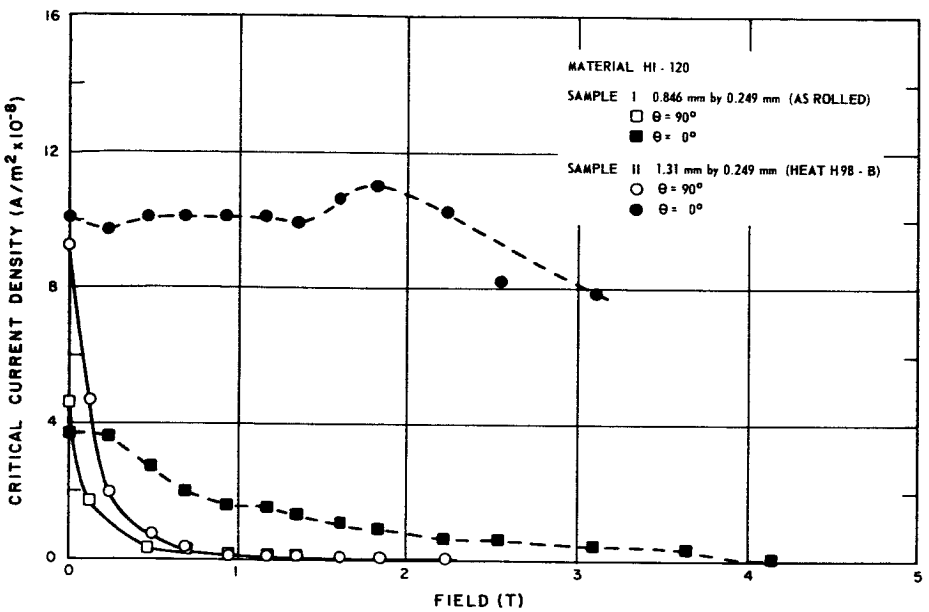

Fig. 21 The effect of heat treatment on the H-I characteristic of H-I-120.

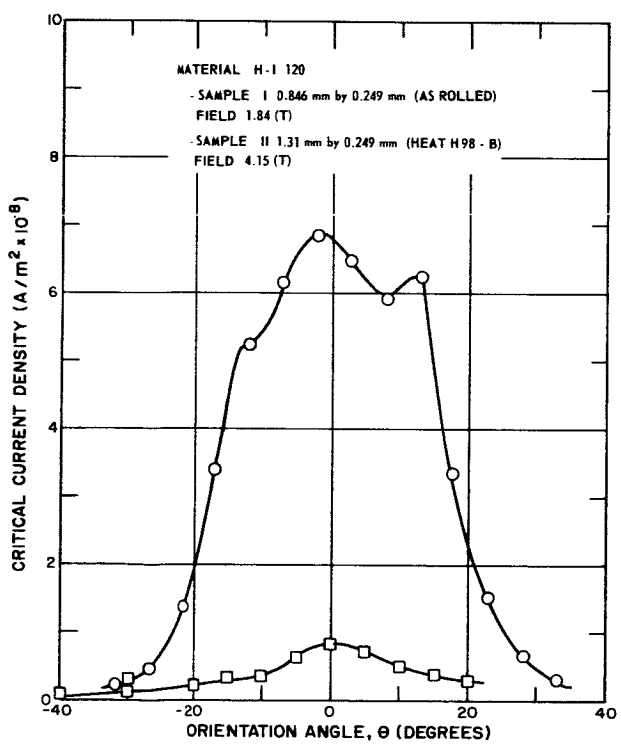

Fig. 22 The effect of heat treatment on the anisotropy of H-I-120.

A2405

A2406

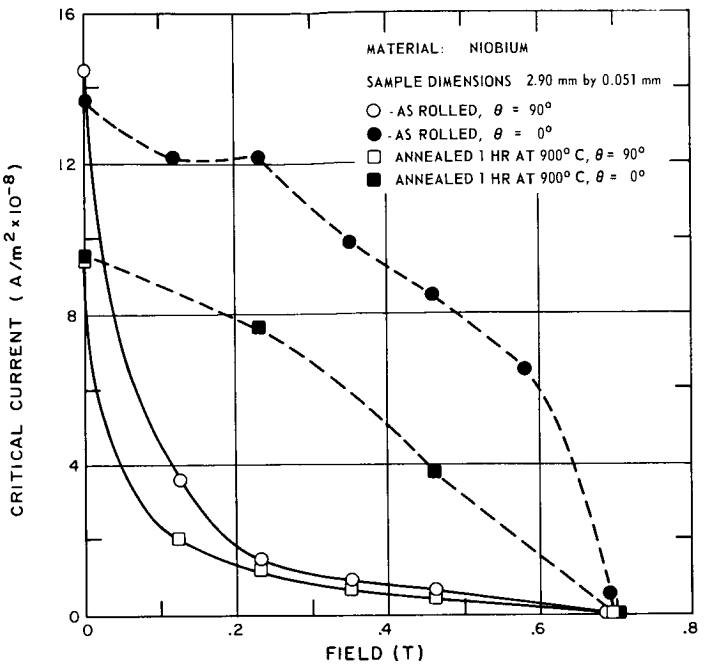

Fig. 23 The effect of heat treatment on the H-I characteristic of Nb.

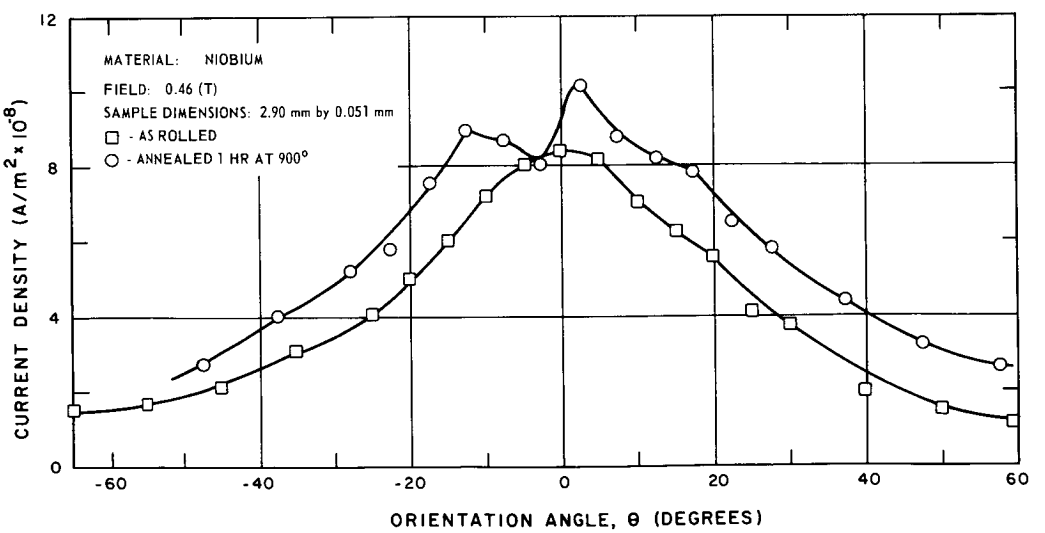

Fig. 24 The effect of heat treatment on the anisotropy of Nb.

A2407

A2408

V. MAGNETIZATION AND CURRENT DENSITY PROFILE OF SUPERCONDUCTING STRIP

1. Introduction

An optical apparatus was used to observe and photograph details of the magnetic field distribution near the surface of Nb and Nb-Zr strip. Using a superposition technique, an approximate current density profile has been calculated from these photographs.

Data has been obtained for Nb and Nb-Zr strip operating in an external field both with and without net transport current.

2. Experimental Apparatus

The device operates by virtue of the Faraday effect[3] in cerium metaphosphate glass, $Ce(PO_3)_3$ and is similar in construction to that developed by DeSorbo.[4]

A complete description of the apparatus is given in Appendix E but briefly its operation is as follows:

A second-surface mirror of magneto-optic glass is placed directly in contact with a thin strip sample of superconducting material. A light source and optical system employing crossed polarizers, as shown in Fig. E1, is used to form a photographic image which varies in intensity in a way that can be interpreted in terms of field intensity.

The sample holder, shown in Fig. E2 is provided with a small superconducting magnet capable of producing 1.2 T in a direction normal to the strip plane. A d.c. transformer is also provided for inducing transport current into the strip.

The results of these experiments are shown in the following series of photographs (Figs. 25-29). On the diagrams under each picture, the distribution of B_y, (the normal component of field) across the strip is shown. The dashed line indicates the magnitude of the externally applied field.

3. Experimental Results

3.1 Magnetization in Nb Strip

Pictures 1 through 8 show a sample of Nb strip 5.1×10^{-2} mm by 6.00 mm at 4.2°K in various stages of magnetization with no net transport current.

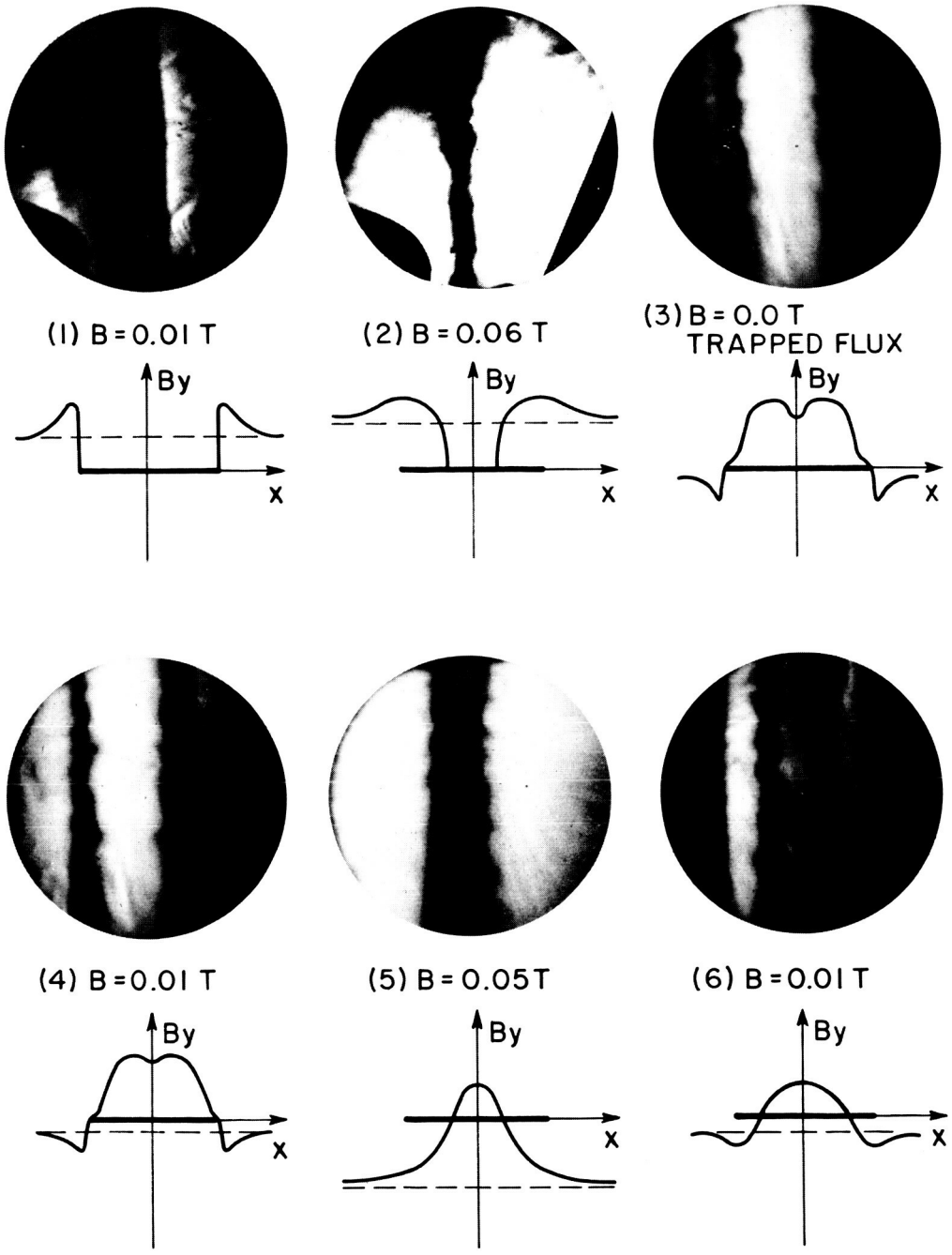

Fig. 25 Pictures 1-6, Field distributions in superconducting strip

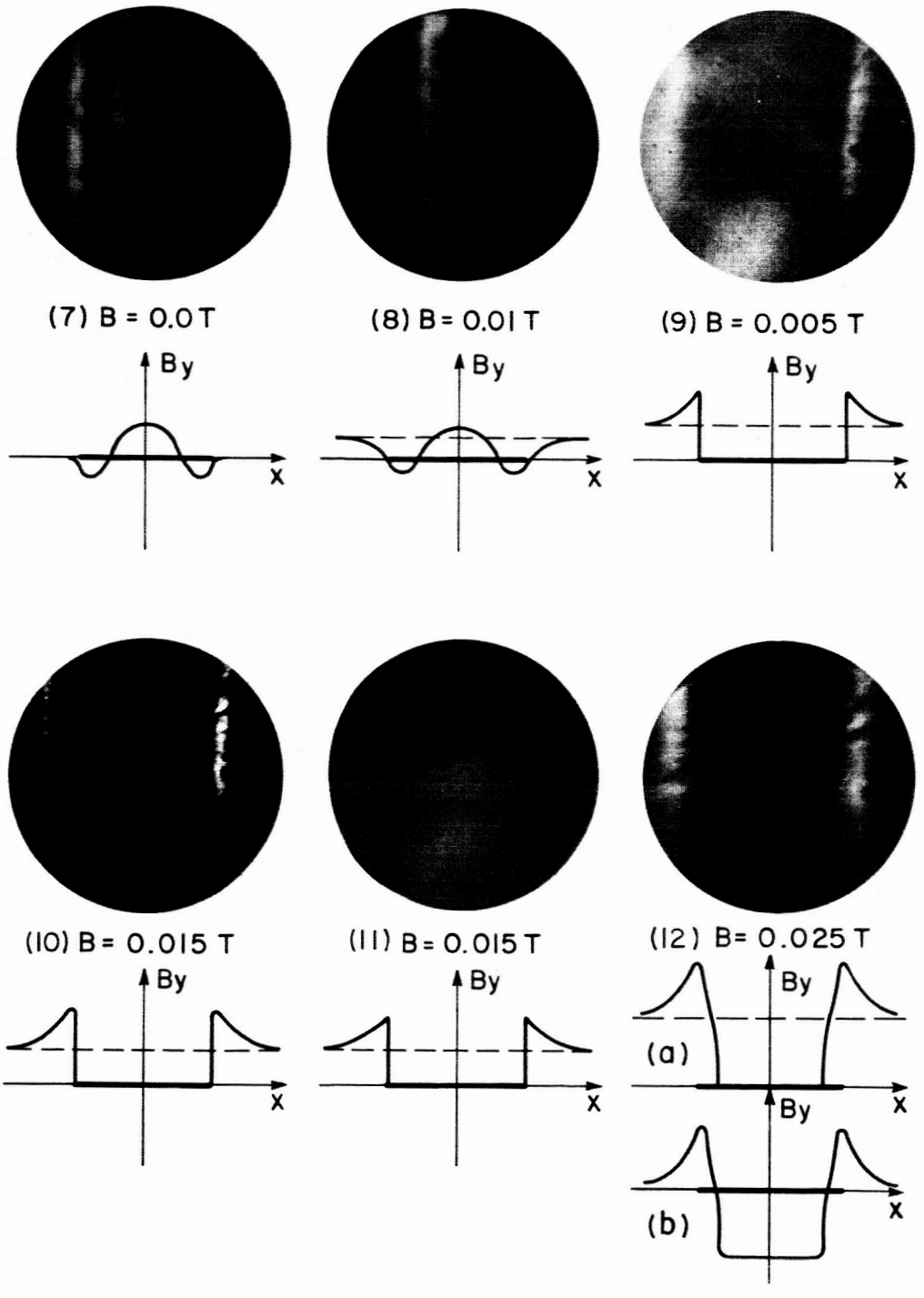

Fig. 26 Pictures 7-12, Field distributions in superconducting strip

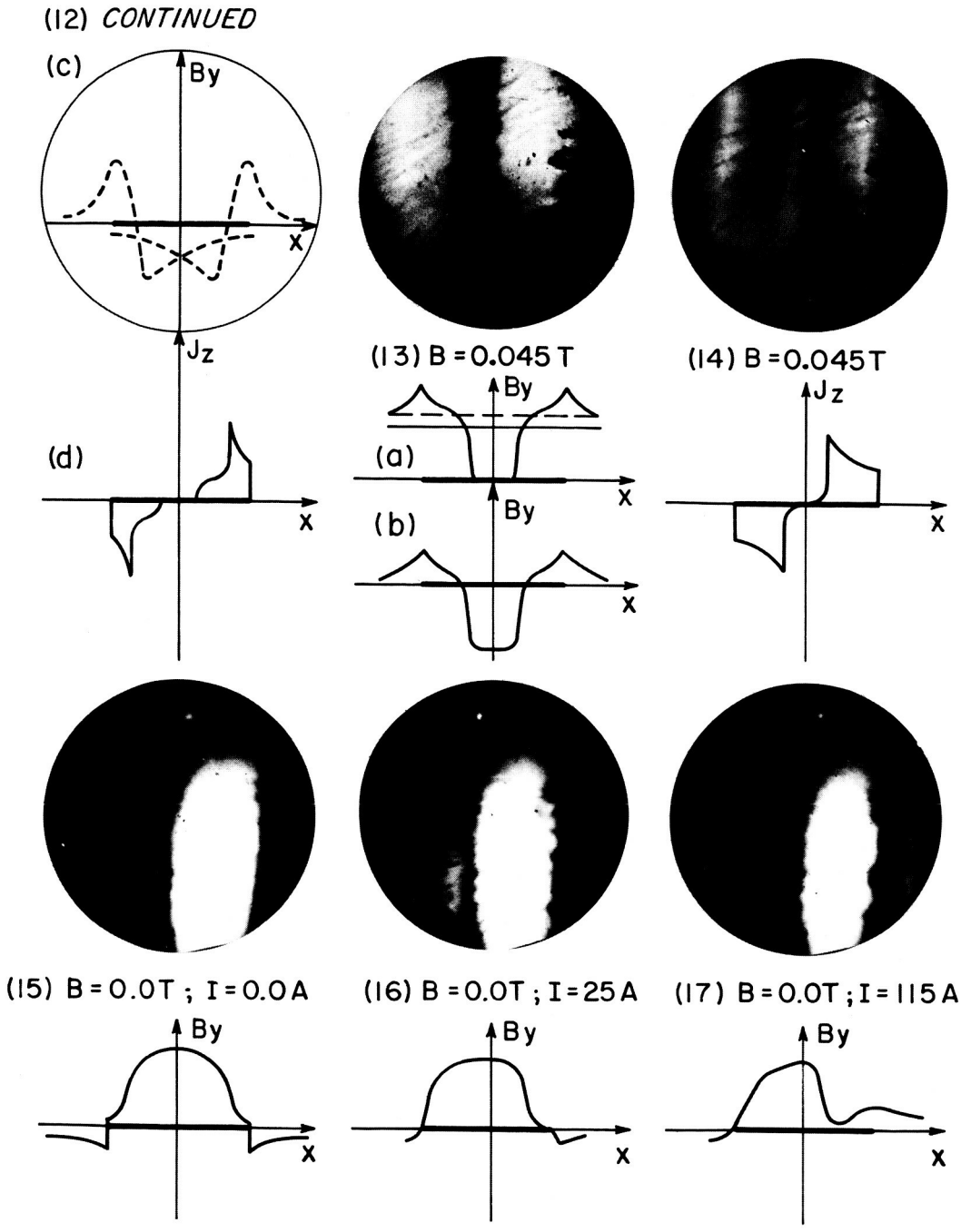

Fig. 27 Pictures 13-17, Field distributions in superconducting strip

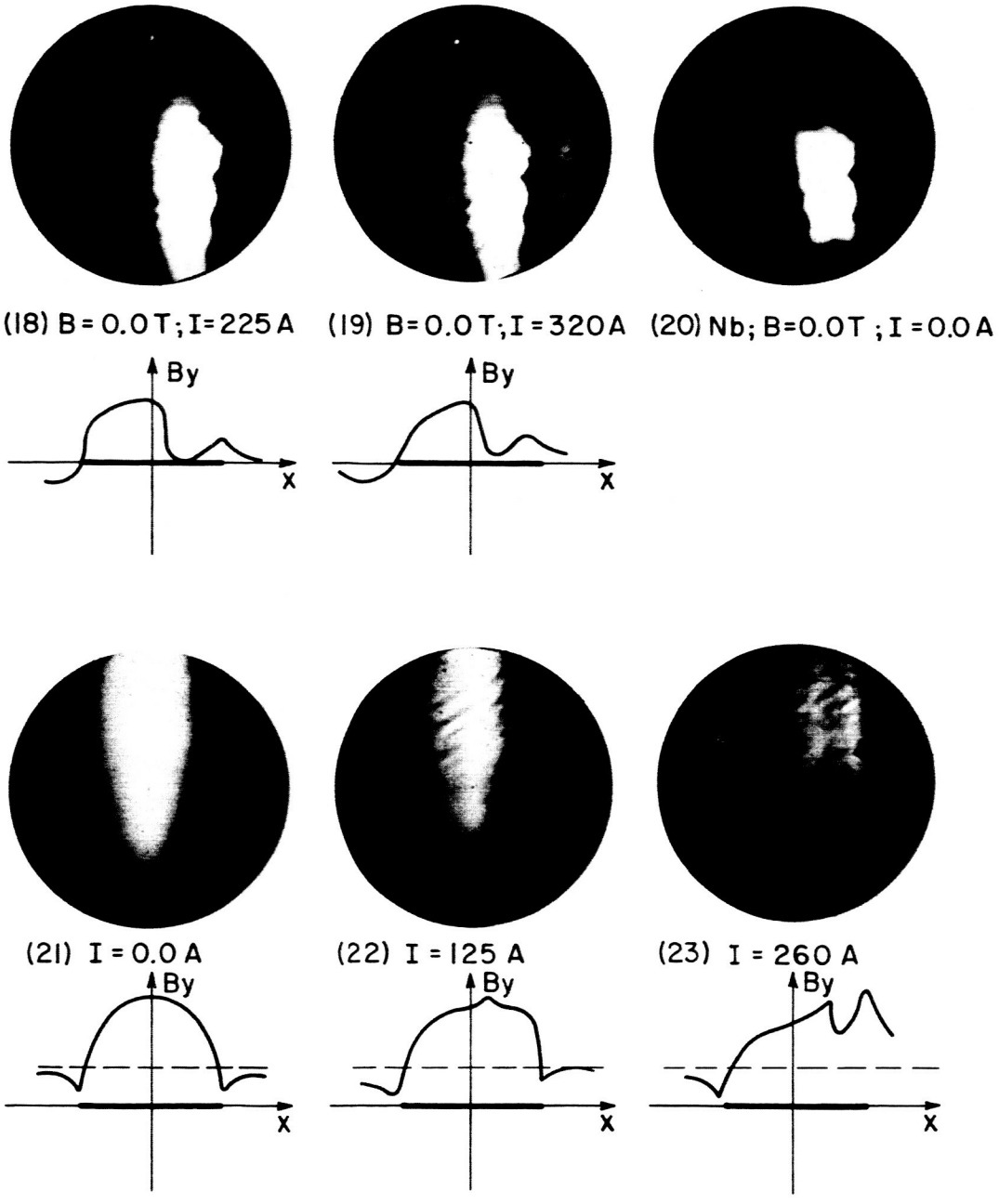

Fig. 28 Pictures 18-23, Field distributions in superconducting strip

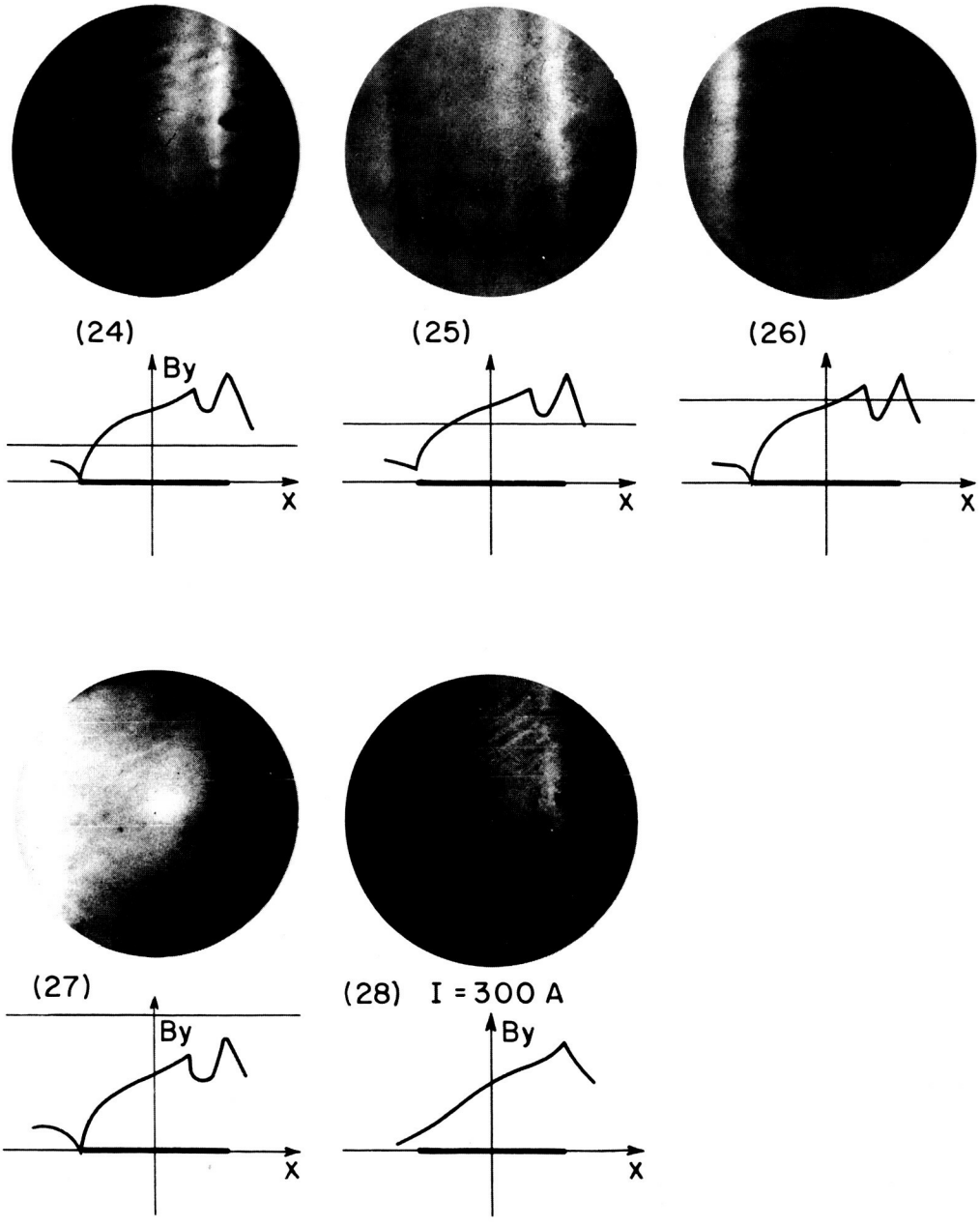

Fig. 29 Pictures 24-28, Field distributions in superconducting strip

A2413

1. With an applied field of 0.01 T, this virgin sample shows almost complete field exclusion, implying a magnetization equal and opposite to the applied field. Only at the edges, where the field is concentrated to approximately 0.02 T by the bending of the field lines, does any penetration occur. We estimate that initial penetration in Nb occurs at about 0.017 T.

2. At 0.06 T the field has penetrated approximately 2/3 of the strip, the center portion still excluding flux.

3. At zero field again, the flux which penetrated at 0.06 T can now be seen trapped, implying that the magnetization has hysteresis. The faint line down the center implies that as in (2), flux failed to penetrate the center portion.

4. With an applied field of -0.01 T, the region of trapped flux begins to recede as the new applied field begins to penetrate in the center.

5. At -0.05 T the new applied field has penetrated approximately 2/3 of the strip, while the trapped flux still remains in the center.

6. Upon reducing the applied field to -0.01 T, negative field can be seen trapped along the edges while the original positive field remains in the center.

7. At zero applied field, both positive and negative fields are seen still trapped.

8. At 0.01 T applied field can be seen just beginning to penetrate the edges as the old pattern of trapped flux begins to recede toward the center.

3.2 Magnetization in Nb-25% Zr Strip

Pictures 9 through 14 show a sample of Nb-25% Zr strip 5.1×10^{-2} mm by 7.00 mm at 2.3°K in various stages of magnetization with no net transport current.

In general with Nb-Zr at 4.2°K, we found very little detail as opposed to Nb samples under the same conditions. Evidently the magnetization in Nb-Zr, which is responsible for the patterns observed, is much less than that in Nb. Only at low temperatures (2.3°K) where the Verdet constant* and magnetization are higher, could we obtain enough contrast to photograph. In some cases, as seen in the following pictures, we rotated our analyzer so that the null occurred at some finite field instead of at zero field. This procedure often revealed detail otherwise obscured.

* See Appendix E

In this series we have made an estimate of the current density distribution responsible for the magnetization and along with one of the pictures, we have included a qualitative set of plots showing the method of superposition used to arrive at this distribution.

9. At 0.005 T the field is shown completely excluded from this virgin sample.

10. At 0.015 T the field is still almost completely excluded. Only at the edges where the field is concentrated is there any evidence of penetration.

11. Here the sample is shown again at 0.015 T but using an analyzer angle of 6^{o}, (the applied field has not been changed) so that the null now occurs at 0.028 T. This picture shows a little more detail over the strip and reveals more clearly the slight penetration near the edges.

12. At 0.025 T the field has penetrated roughly 1/4 of the strip. In the diagrams accompanying the picture (a) shows the actual field, (b) shows that part due to the magnetization; in (c) this is separated into two components and in (d) the current density profile causing these components is shown. The peaks of this profile are of the order of 10^{9} A/m^{2}.

13. At 0.045 T the field has penetrated 3/4 of the strip.

14. Here the strip is viewed again at 0.045 T with a different analyzer angle. The field at which the null now occurs is shown in diagram (a) of picture 13. Again the details of the flux pattern show up much more clearly. The current density profile for this case is shown beneath the picture. Its peaks are of the order of 10^{9} A/m^{2}.

3.3 The Effect of Transport Current in Nb

Pictures 15 through 20 show a Nb sample 5.1×10^{-2} mm by 6.00 mm at 4.2^{o}K in zero applied field but with magnetizations and various transport currents.

15. The sample is shown here at zero field and zero transport current but with maximum attainable trapped flux.

16. At 25 A the region of trapped flux can be seen moving to the left.

17. At 115 A the trapped flux continues to move to the left and diminishes in size as though some of the magnetization were being forced out.

18. At 225 A the trapped flux continues to diminish and its boundary is becoming more irregular, possibly due to flux jumps.

19. At 320 A, just 30 A below its critical current, the pattern is still much the same although accentuated somewhat.

20. The current was returned to zero by quenching with a heater elsewhere in the sample, but the magnetization remained in part of the sample in view.

3.4 The Current Density Profile in Nb-Zr Strip

Pictures 21 through 28 show a Nb-Zr sample 0.051 mm by 8.00 mm at 2.4°K with magnetization and transport current. A 0.03 T field was applied throughout the experiment.

In this series an approximate field profile was obtained by taking several photographs at the same current, but with different analyzer angles.

21. With no transport current, flux is seen trapped in the sample.

22. At 0.0125 T the maximum is off center (seen in the picture as a bright line off the center of the strip) and is 0.076 ± 0.003 T. The values of the minimums have changed; one is 0.025 ± 0.002 T, and the other is 0.01 ± 0.002 T. The total trapped flux is now less as seen by the relative magnitude of the fields with and without current, thus the magnetization of the material is decreasing.

23-27. These pictures were all taken at 260 A, but at different analyzer angles in order to obtain an approximation of the field distribution. The field at which the null occurs is indicated by the solid line in each plot. (In 23 the null is at zero field.) There are two maximums at this current, one at the edge (810 ± 30 T) and one in from the edge, (0.071 ± 0.003 T). The minimum at the other edge is 0.005 ± 0.002 T.

An estimate of the transport current profile has been made by superimposing two current distributions for which we had calculated field profiles (see Appendix F). These consisted of a parabolic profile over the entire strip plus a uniform profile over a 1.6 mm wide section along the right hand edge of the strip (see Fig. 30). The weighting factors for these profiles were then obtained by the following two requirements.

1. The current resulting from them totals 260 A.

2. The peak field due to the parabolic profile be twice that of the uniform one.

This is shown in Fig. 30 where current density, field due to this, total field, and initial magnetization are all plotted. The measured points mentioned above for the 260 A case are also included for comparison.

28. At 350 A the inner peak has disappeared leaving only the peak at the edge, implying that the current still concentrates at the edge, but that the discontinuity of the 260 A case has smoothed out.

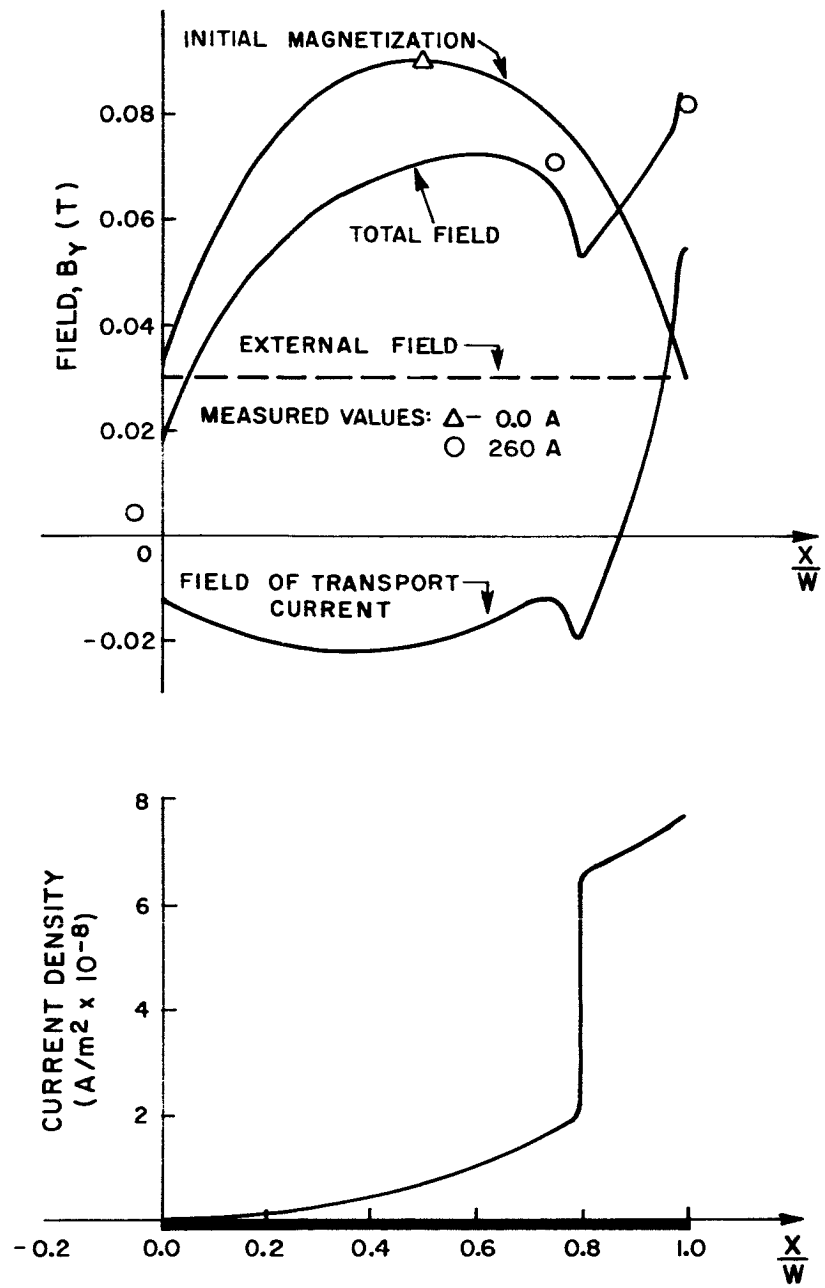

Fig. 30 Current Density Distribution in Nb-25% Zr Strip

A2414

VI. SUPERCONDUCTING STRIP COIL

1. Introduction

In order to test out some of the principles learned in the above investigations, an actual strip magnet was constructed and tested.

This coil utilized approximately 6.8 kg. of Nb-25% Zr strip 0.051 mm thick by 25.4 mm wide and was instrumented to yield information as to its stability to electrical, thermal, and mechanical disturbances.

2. Design and Structure

The design of this coil was governed by the following considerations:

1. The amount of superconducting strip available.
2. Protection against voltage breakdown or burnout during quenches.
3. The necessity imposed by anisotropy, of producing a winding in which the field is everywhere parallel to the plane of the strip.
4. The size of the dewar and the existing wire trimmer coils necessary to straighten the field lines.

These considerations led to a two-module design as shown in Figs. 31 and 32.

Each module consisted of a "pancake" winding of 440 turns in which the inner ends of the strips are brought out through slits in the inner mandrels. The winding direction of each module was such that when the two were assembled the inner ends of each strip could be spot welded together to form a continuous strip whose plane was parallel to the field lines.

During operation, the two modules were energized in series by means of the two outer ends of the strip.

The composite conductor making up each turn was composed of four elements, Nb-25% Zr strip 0.051 mm (0.002 in) thick by 25.4 mm (1 in.) wide, manufactured by Kawecki Chemical Company, copper strip (0.00254 in) (0.001 in) thick by 25.4 mm wide, aluminum strip 0.00635 mm (0.0025 in) thick by 25.4 mm wide and mylar strip 0.0254 mm thick by 30.2 mm (1.188 in) wide. The two normal metal components were for protection and stabilization of the superconductor and the mylar was for insulation between turns. The Nb-Zr strip was sandwiched between, and in direct contact with, the copper and aluminum.

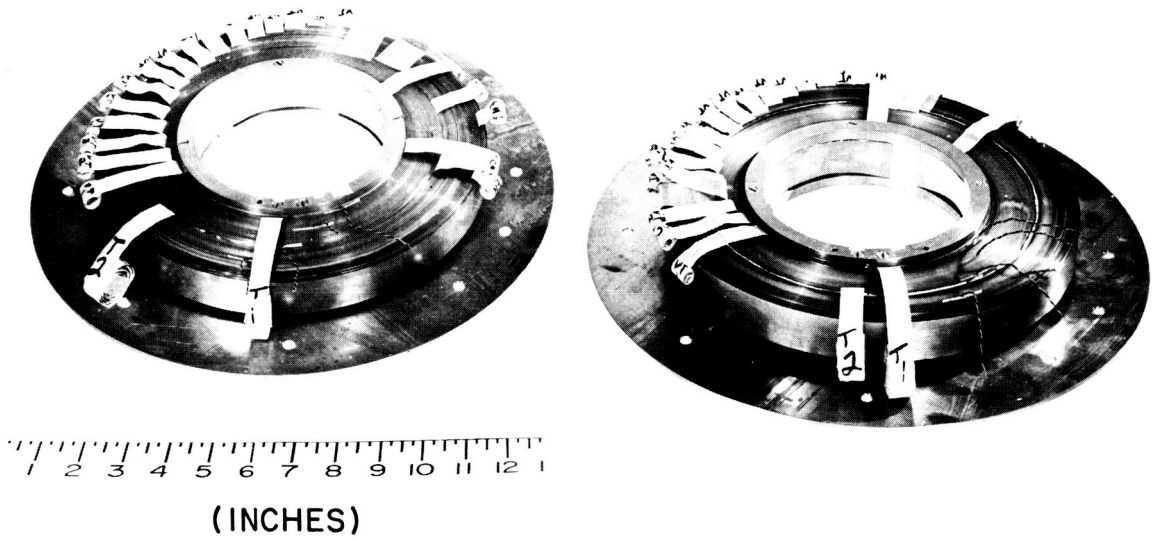

Fig. 31 Superconducting Strip Coil Modules Disassembled

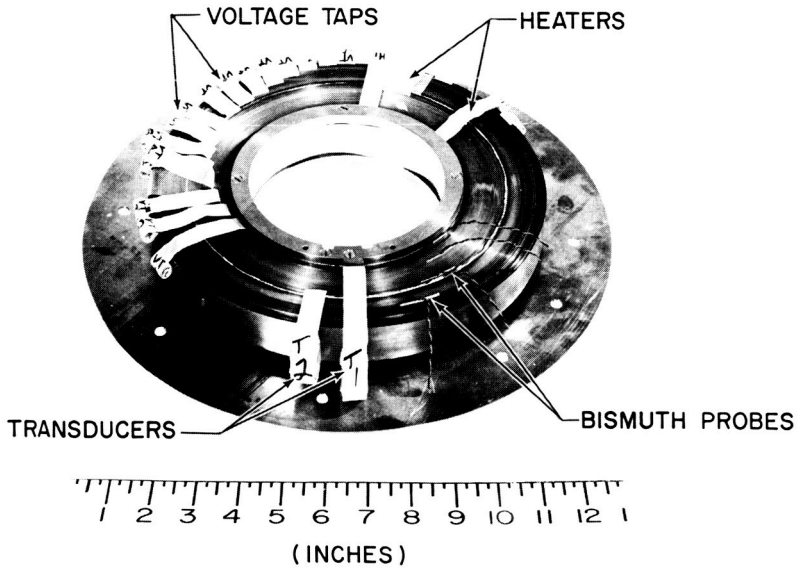

Fig. 32 Typical Superconducting Strip Coil Module showing Instrumentation

A1853

A1934

The aluminum was placed in the coil mainly to stabilize the Nb-Zr strip. It was very thin and could conform readily to the microscopic contours of the Nb-Zr strip, thereby making the best possible electrical contact. No connection was made to the ends of this strip at the inner and outer radii of the coil. It simply served as a by-pass for current to pass around local normal regions should they occur.

The copper strip, also in direct contact, served two purposes. In addition to providing local shunting, it served also as inductive protection, i.e. when the two modules are assembled its ends are connected together independently of the superconductor so as to form a complete parallel closed circuit of copper which reduces transient voltage peaks by slowing the escape of flux in the event of a quench. To prevent this "copper circuit" from shorting out the terminals of the superconducting coil, its outer terminals were connected through a copper wire coil consisting of 100 turns of No. 19 A.W.G. magnet wire (whose cross section is equal to that of the strip) wound around the outside of the main coil in a direction such as to aid or hold in the field during a quench. During charge-up, some current flows backward through this normal coil, developing a voltage across it which is applied to the superconducting coil in a direction to charge it. In this way, the extra copper in the wire coil is just as effective for inductive protection as the same mass in a single turn, but does not short out the terminals of the superconducting coil as a single turn would.

3. Instrumentation in the Coil

Each module was instrumented with 16 voltage taps for monitoring quenches, three heaters for producing local normal regions, two electromechanical transducers for introducing small local mechanical impulses, and five magneto-resistance probes to monitor the magnetic field (see Fig. 33).

The voltage taps consisted of copper strip 12.7 mm (1/2 in) wide by 0.0254 mm (0.001 in) thick insulated with mylar tape and placed in direct contact with the Nb-Zr strip at equal intervals throughout each module.

The heaters consisted of nichrome strip 6.35 mm wide by 0.0254 mm thick (0.25 by 0.001 in) with a 3.97 mm (0.156 in) section in the middle slitted to form a grid like structure as shown in Fig. 34. With most of the heat being generated in the region of the grid structure, the effective area of each heater was 50.5 mm^2, and the heat conducted into the winding exceeds that lost in the leads by a factor of 800. Electrical contact to these heaters was made by means of copper strips soldered to either end and were insulated by sheet mica (to withstand the high temperature of the nichrome) and mylar. These were placed between the copper and Nb-Zr strips in three places in each module, one near the inner radius, one midway out, and one near the outer radius.

The transducers consisted of 0.0254 mm (0.001 in) thick copper strip formed into a "strip line" type transmission line shorted at the end with a short conductor running at right angles to the magnetic field of the coil, (see Fig. 35).

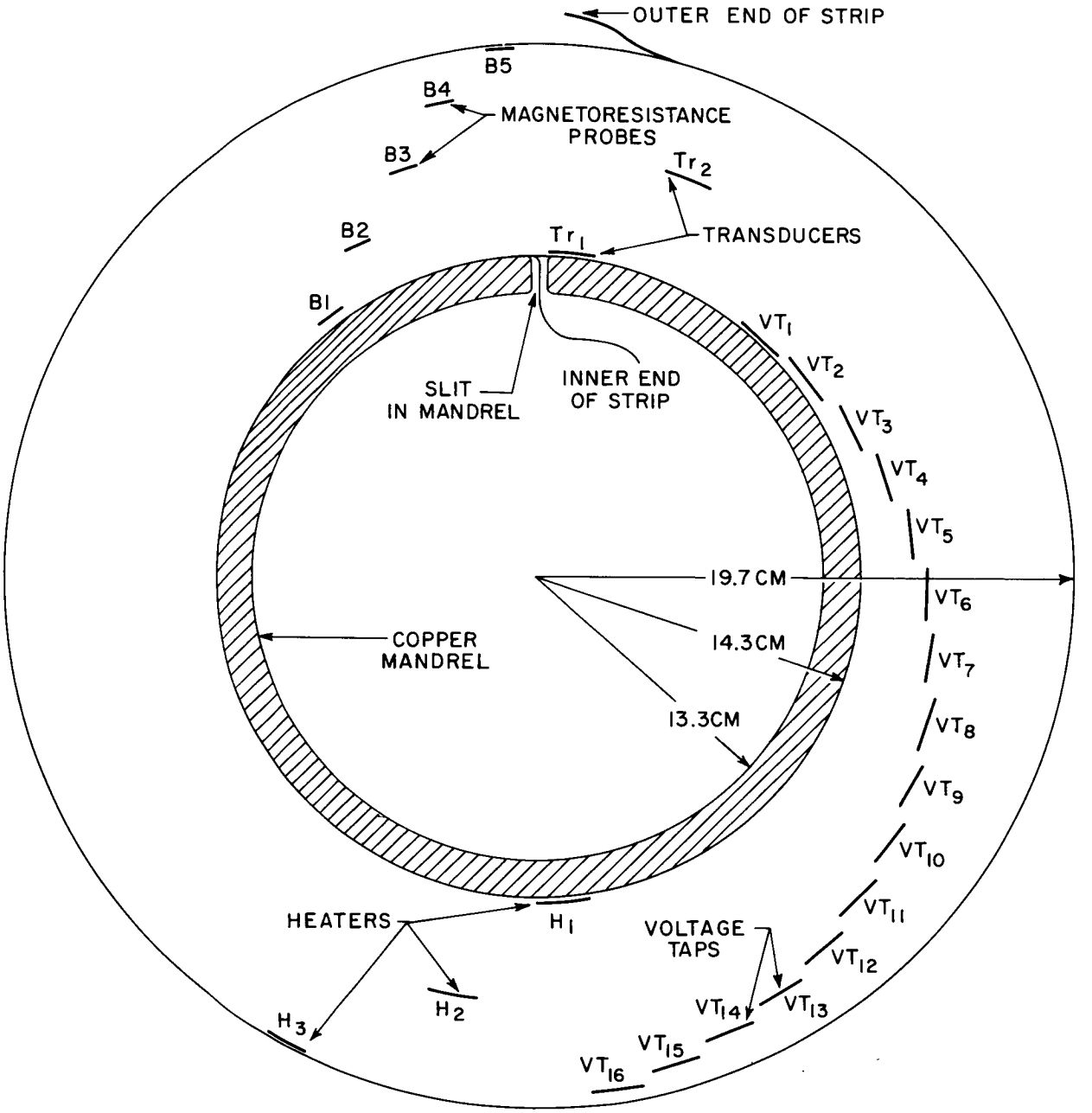

Fig. 33 Schematic of Superconducting Coil Module showing Instrumentation locations and module dimensions

A2415

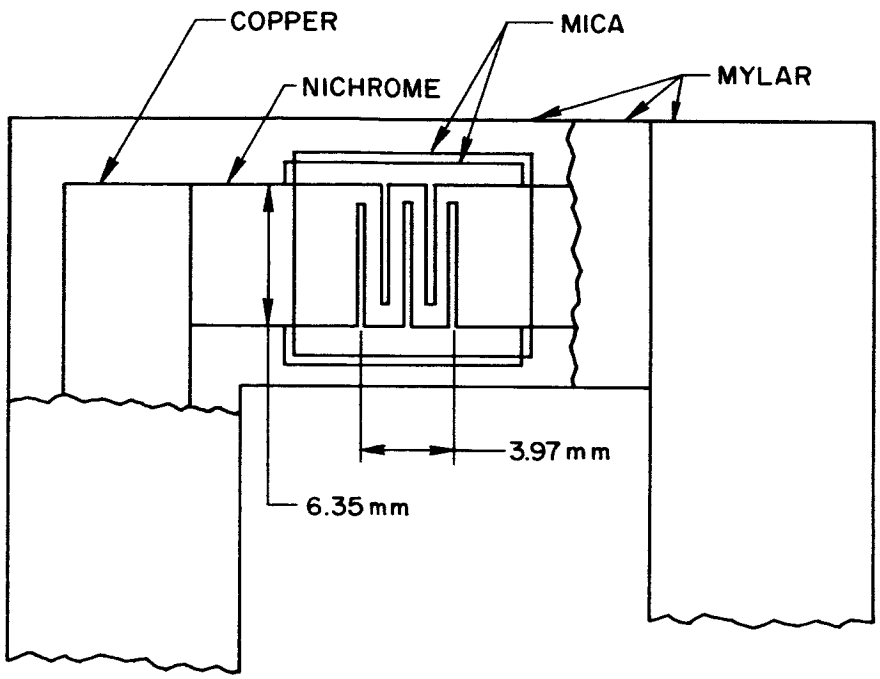

Fig. 34 Nichrome strip heater

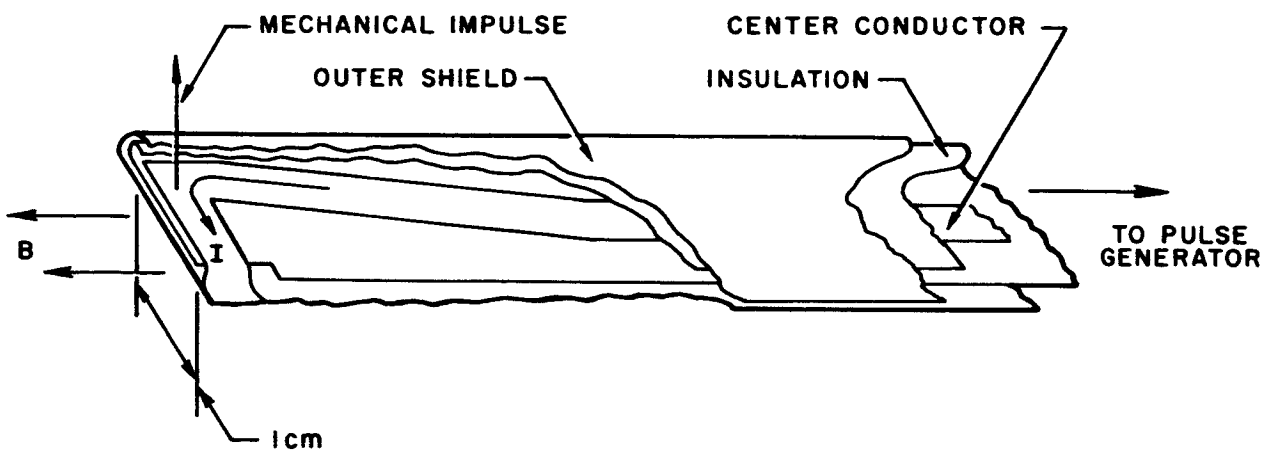

Fig. 35 Schematic of Electromechanical Transducer

A2416

A2417

Two of these were placed in each module, one near the inner radius and one midway out. They were energized by means of a small capacitor bank capable of producing a 2000 A pulse 1 ms long so that at a field of 1 T they could produce peak force of 20 N.

The magnetic field probes were commercially available units manufactured by American Aerospace Controls under the trade name Mistor, type MR-A and consist of bismuth sandwiched between Mylar insulation with two copper terminals extending from one end. They are thin and flat and can be readily inserted between the turns of a strip winding. Five of these were placed at equal intervals throughout each module, and one was placed in a styrafoam filler plug at the center of the coil assembly.

4. Winding Procedures

The winding of thin strip, particularly when such large build-ups as these are required, is something of an art. Therefore the actual winding of the coils was subcontracted. The winding was done at the Cornell Dubilier Electronics (CDE) capacitor plant in New Bedford, Massachusetts. This was done on a capacitor winding machine. Before winding the superconducting modules, a test module of stainless steel was wound in order to obtain experience in winding problems and to test the insulation proposed for the final modules. This first module was wound with a composite of four strips, a 0.051 mm thick by 25.4 mm wide (0.002 in by 1 in) stainless steel strip to simulate Nb-Zr, a 0.025 mm thick by 25.4 mm (0.001 in by 1 in) aluminum strip and two 0.025 mm by 30.2 (0.001 by 1.88 in) mylar strips to insulate the aluminum from the stainless. Since this was wound before making the final decision as to the type joint to be used, the module was wound in five electrically isolated sections, each of which contained a different type of joint.

Later each section was tested for voltage breakdown between the stainless and aluminum conductors at liquid nitrogen temperature and was found to withstand in excess of 1500 V per turn.

Packing factors between 93% and 96% of theoretical were obtained in this trial run.

The Nb-Zr strip supplied in fourteen separate lengths was spot welded end to end to form two long strips which were then wound into the two coil modules. The spot welding techniques used are described under the heading "Superconducting to Superconducting Connections" elsewhere in this report and consisted of 100 spot welds uniformly distributed over a 5 cm overlap.

The instrumentation units were placed into the coils during the winding operation; their relative locations are as shown in Fig. 33.

Upon completion of the winding operation, permanent flanges were installed and each module was potted in paraphene to prevent upset of the

winding due to $\vec{J} \times \vec{B}$ forces. Finally, the two completed modules were fastened together by means of through-bolts in the inner mandrel and the two inner ends of the Nb-Zr and copper strips were connected together, the Nb-Zr by spot welding, the copper by soldering.

5. Physical Arrangement of Components during Tests

Due to the strong anisotropy of the Nb-Zr strip from which the coil is constructed, it is necessary to straighten the field lines inside the strip winding so that they maintain as closely as possible an orientation parallel to the plane of the strip.

This was done here by means of "trimmer" coils Model SC 500 superconducting wire coils placed on either side of the strip coils, as shown in Fig. 36. They are energized by a separate power supply so that the field they produce can be adjusted to just cancel the radial components of the strip coil field over most of the strip winding.

The energizer, described in detail below, consists of an annular iron core enclosing the primary and secondary and is placed as shown in Fig. 36, surrounding the strip coil.

The entire assembly is suspended in liquid helium in the dewar by means of four stainless steel suspension rods, as shown in Fig. 37.

6. Instrumentation and Test Equipment

The nucleus of our test equipment is a 35 channel recording system using a frequency multiplexed magnetic tape recorder and a hot stylus, rectilinear chart recorder. The maximum sensitivity is 10 mV full scale with a maximum response frequency of 1 k Hz.

This system is used to continuously monitor a maximum of 34 signals (one channel needed for time resolution) from the instrumentation units in the coil. Certain signal processing units are also available in the system, e.g. a 6-channel magneto-resistance probe detector which translates probe resistance into voltage which can then be recorded, two Kiethly microvoltmeters with voltage outputs that can be fed into instrumentation channels and current shunts to translate current into voltage for recording purposes.

Available also are five 1 V, 200 A D.C. power supplies for use in direct energization of the magnet and five 10 V, 50 A power supplies for energizing trimmer coils, the energizer primary, or heaters.

The 35.6 cm (14 in) diameter dewar used in these experiments is provided with a top flange in which five hermetically sealed connectors are mounted, providing for a total of 273 instrumentation and power leads. These have been brought out to a patch panel system provided with programming plugs for rapidly changing the instrumentation during a run.

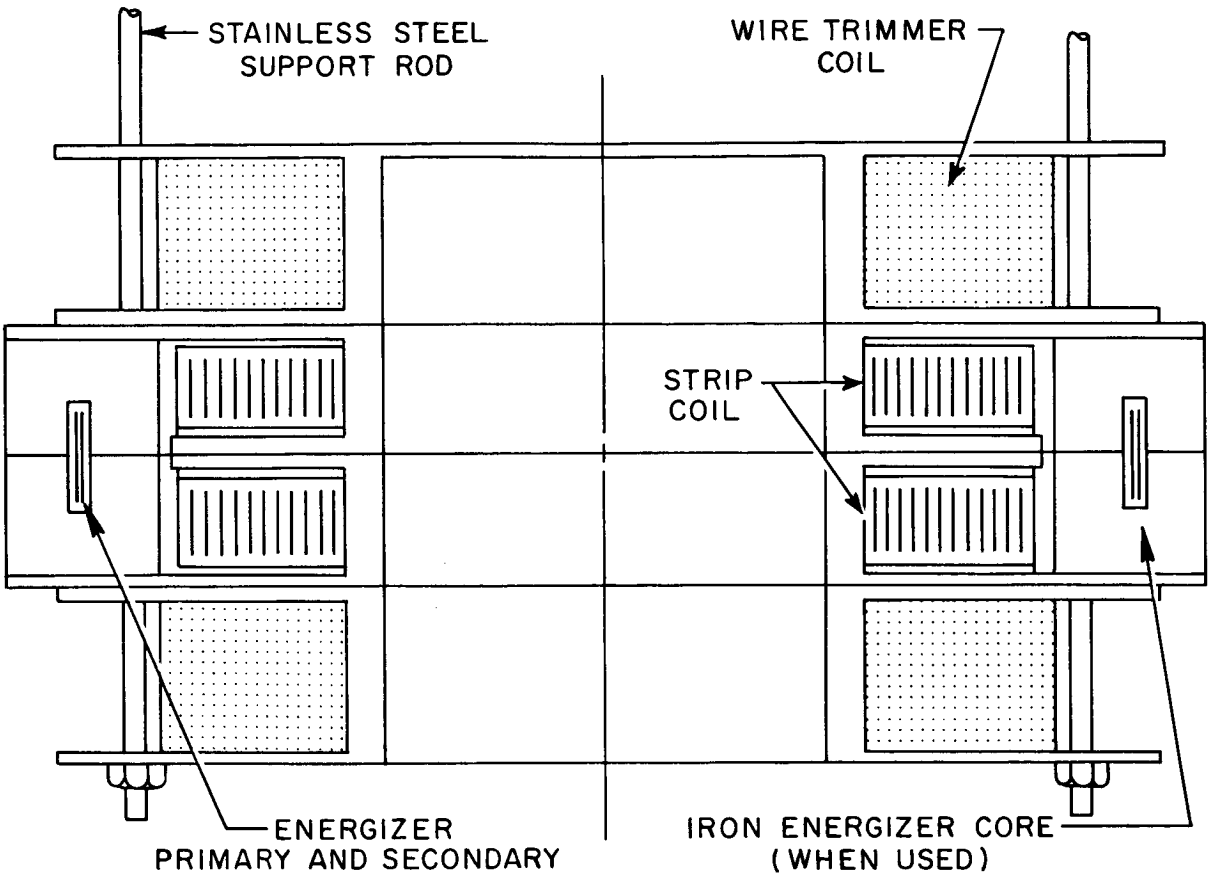

Fig. 36 Schematic of Superconducting Strip Coil Test Assembly showing Relative Positions of Strip Coils and Trimmer Coils

A2418

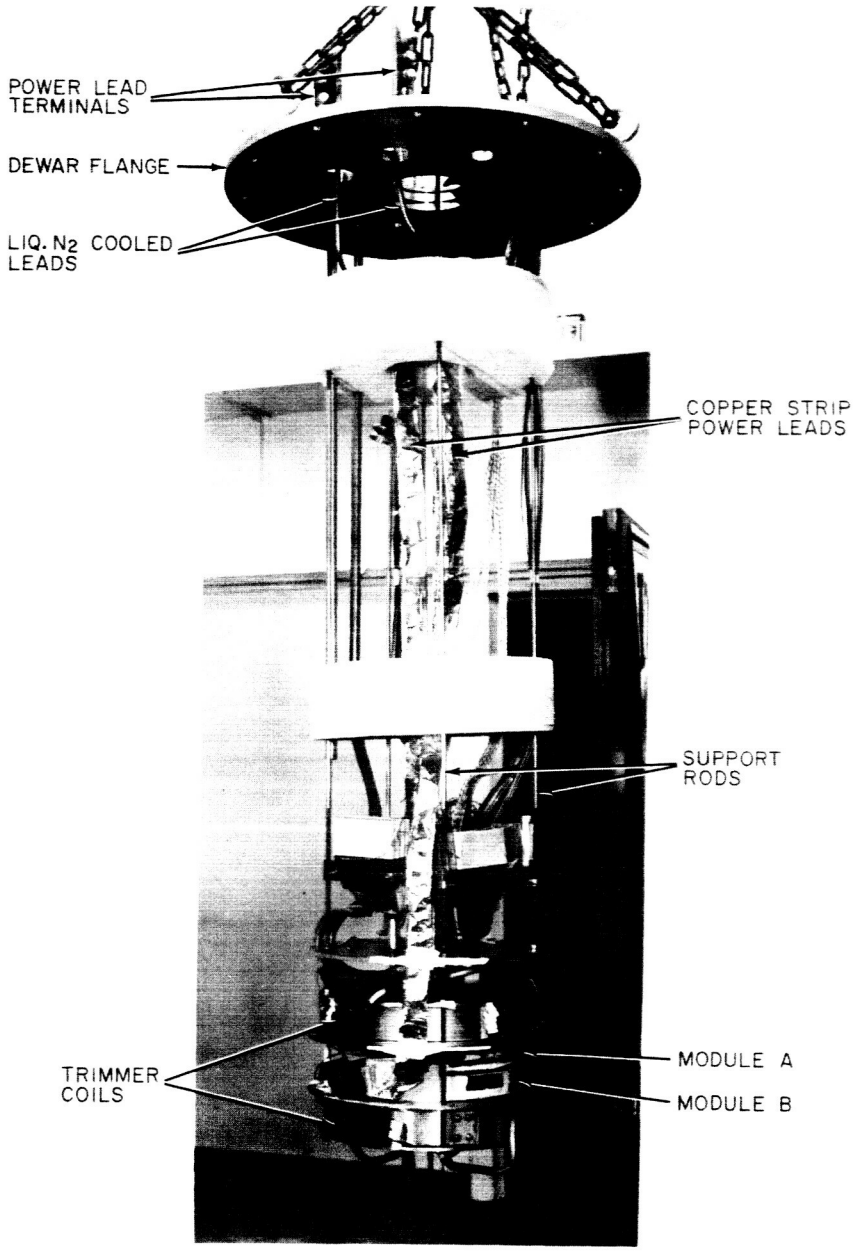

Fig. 37 Superconducting Strip Coil mounted on Support Structure ready for Test

A2419

7. Experimental Results

7.1 Test Procedure

Three energizing techniques were used on the superconducting strip magnet, one using an external power supply, one using the trimmer coils to induce current in the strip coil, and one using a flux pumping technique. Each of these techniques has advantages and disadvantages; the first is simple and straightforward, but requires that large currents be brought in and out of the helium bath; the latter two avoid this problem, but necessitate the development of an energizer and create a current measurement problem.

In each case, tests were performed to determine the stability of the coil with respect to thermal, mechanical and electrical disturbances. In addition, the magnetic field was monitored at various test locations in the coils, the diamagnetic effects were observed, and the quench transients were observed so that the origin of quenches could be located.

7.2 Conventional Energizing

7.2.1 Test Arrangement

In the test using conventional energizing techniques, the coil was provided with heavy copper leads consisting of four copper strips 50.8 mm wide by 0.051 mm thick (2" by 0.002") spot welded at the lower end to the Nb-Zr strip and soldered at the upper end to liquid nitrogen cooled terminals.

The leads were designed for minimum boil-off due to conduction and I^2R losses and the connections to the superconducting strip results in a temperature rise of less than 10^{-3} ^{o}K as calculated according to the theory of superconducting connections discussed above. The strip coil was mounted as shown in Figs. 36 and 37 between two trimmer coils used to straighten the field lines as discussed above.

When energizing, the trimmer coil current was manually adjusted to maintain a fixed proportion between the strip and trimmer currents in order to assure that the field lines remained as parallel as possible to the strip plane.

Ideally this means that the radial components of the trimmer coil field should exactly cancel the radial components of the strip coil everywhere in the strip coil. In practice, of course, cancellation can be forced at only one point in anything but an infinitely long solenoid; nevertheless with this particular geometry fairly complete cancellation was obtainable over most of the strip coil cross section.

The proper proportions between strip and trimmer currents was obtained in the following manner. Two field plots were obtained by means of a computer program, one for the strip coil by itself and one for the trimmer coils by themselves. Each of these indicated the relative magnitude and direction of the field at 32 points uniformly distributed over the strip coil cross

section. A ratio between the magnitude of the two plots was then determined such that the radial components cancelled at a point

$$r = 10.825,\ z = 1.603$$

where r and z are respectively the radial and axial dimensions in cm taken from the center of the coil. This particular point was chosen by trial and error to most nearly cause cancellations at all the other points.

7.2.2 Critical Current and Quench Characteristics

The coil quenched fairly consistently at around 160 A. Four such spontaneous quenches were recorded by means of the 32 voltage monitoring taps placed throughout the coil. From this data plots of the radial extent of the normal front as a function of time from initiation have been prepared and are shown in Fig. 38. As seen there, all the spontaneous quenches but one started at the center.

Quench number one is of interest in that a quench started independently at another location after the main quench had already progressed considerably. This is indicated in Fig. 38 where it is seen that no line connects the point at 90 turns with that at 210 turns in quench number one. Our data clearly indicates that the quench was discontinuous in this region and that a new one actually started between 210 and 240 turns.

Quench number two originating at the outside evidently did not originate in the spot welded connections. Voltages monitored across these connections showed no unusual characteristics.

In order to test the effect of the trimmer coils we purposely deviated from our constant proportionality in three quenches. In one of these, quench number three of Fig. 38, it quenched at a lower current (112 A) and can be seen to have lingered near the center for approximately one second before progressing and did not in fact quench all the way to zero current. Two other similar tests not shown here produced comparable quenches, one occurring at 90 A and the other at 80 A, neither resulting in complete current decay.

All of the quenches recorded advanced through the coil at about the same rate of 100 turns/s or 1.16 cm/s.

The maximum voltage encountered during quenches was 1.5 V taken across the whole coil, 25 mV across 60 turn taps.

7.2.3 Thermal Perturbations

Thermal perturbations of the coil were studied by energizing the small heaters placed in the winding and recording the heater current required to precipitate a quench at various coil currents.

Data were taken by recording the heater current and the voltage across the section in which heater was located while manually increasing the heater

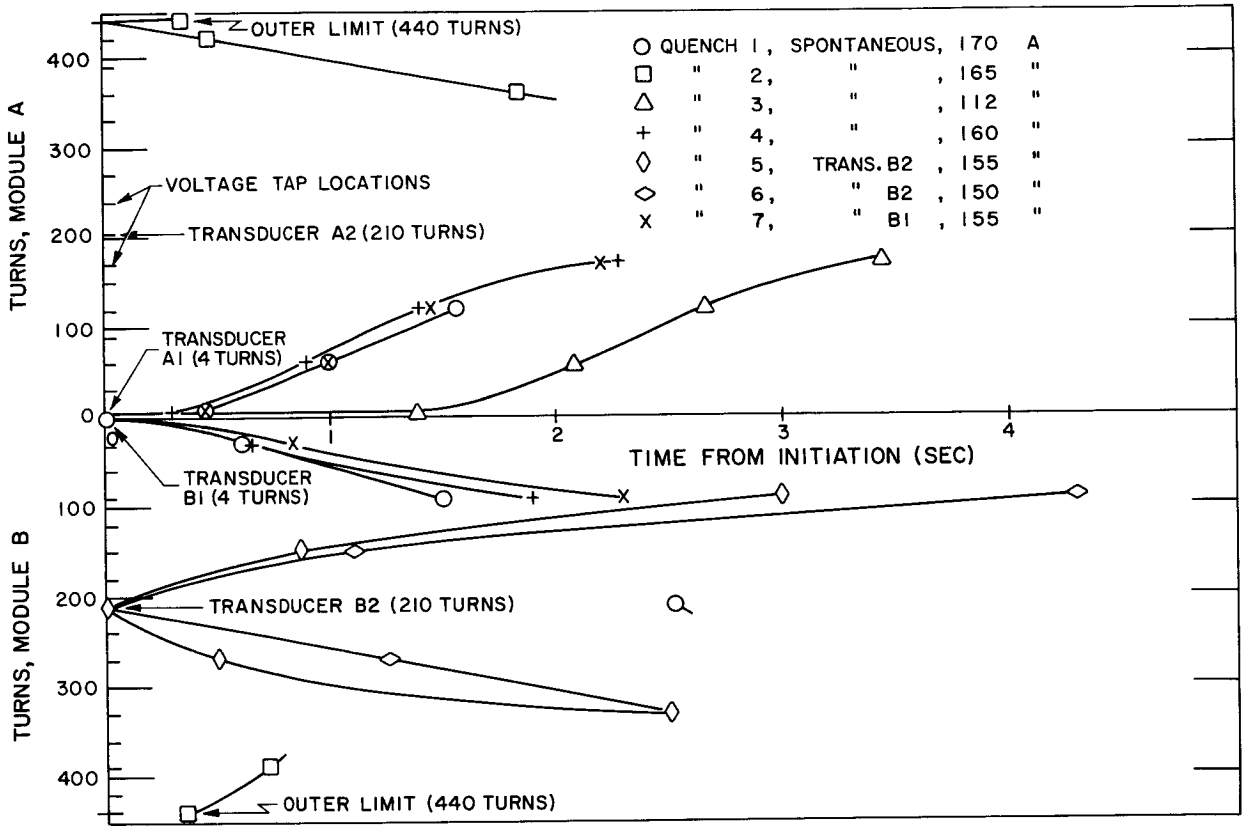

Fig. 38 Radial Extent of Normal Region as a Function of Time for several quenches

A2420

current. As soon as a voltage appeared the heater current was reduced to zero. This was done with constant coil current at approximately 20 amp intervals up to the critical current of the coil.

Of the six heaters in the coil, heater HB2 developed an open circuit and could not be used, heaters HA3 and HB3 would not produce a voltage in the coil at their maximum current. The remainder performed satisfactorily and the data obtained is shown in Fig. 39.

7.2.4 Mechanical Perturbation

The transducers described above and illustrated in Fig. 35 were used to induce small mechanical impulses into the coil.

Of the four transducers Tr B1 and Tr B2 consistently precipitated quenches at coil currents near critical, Tr A1 became open and could not be used and Tr A2 would not precipitate a quench under any circumstances.

The quenches thus produced are shown in Fig. 38 and can be seen to originate at the respective units initiating them. It is not clear, however, whether they were actually caused by heat input or mechanical impulse. Careful calculations of the temperature rise at the high pulse currents necessary to initiate a quench indicates that the superconductor could have been driven normal by heat alone.

7.2.5 Electrical Perturbations

Electrical disturbances can be produced in either of two ways: by simply applying a voltage pulse to the terminals or by inducing a voltage pulse by suddenly changing the current in the trimmer coils. Both of these techniques are really equivalent to a sudden change in the charge rate.

For most of our experiments a charge voltage of approximately 1 mV was used. A sudden one hundred fold increase in this voltage for a short period did not precipitate a quench except when it caused the current to exceed the critical value.

In general, due to the heavy damping effect of the protective circuitry in both the trimmer coils and the strip coil the trimmer coil current could not be changed rapidly enough to induce an appreciable voltage across the strip coil and in no case was a quench precipitated in this way.

7.2.6 Diamagnetic Effects

The diamagnetic properties of the coil were measured by means of the magnetoresistance probes placed in the windings. This was done with zero strip current by cycling the trimmer coil current from zero to 8 A, from 8 A to -8 A, then back to zero and recording the field inside the strip coil. Hysteresis curves, obtained at six probe locations showed hysteresis of 0.1 to 0.2 T but certain anomalies in the curves led us to suspect anisotropy of the probes (although no such anisotropy was indicated in the manufacturers specifications). A second calibration done in our transverse field magnet after dismantling the strip coil revealed extreme anisotropy in a direction which would strongly affect our data. The probes were mounted in

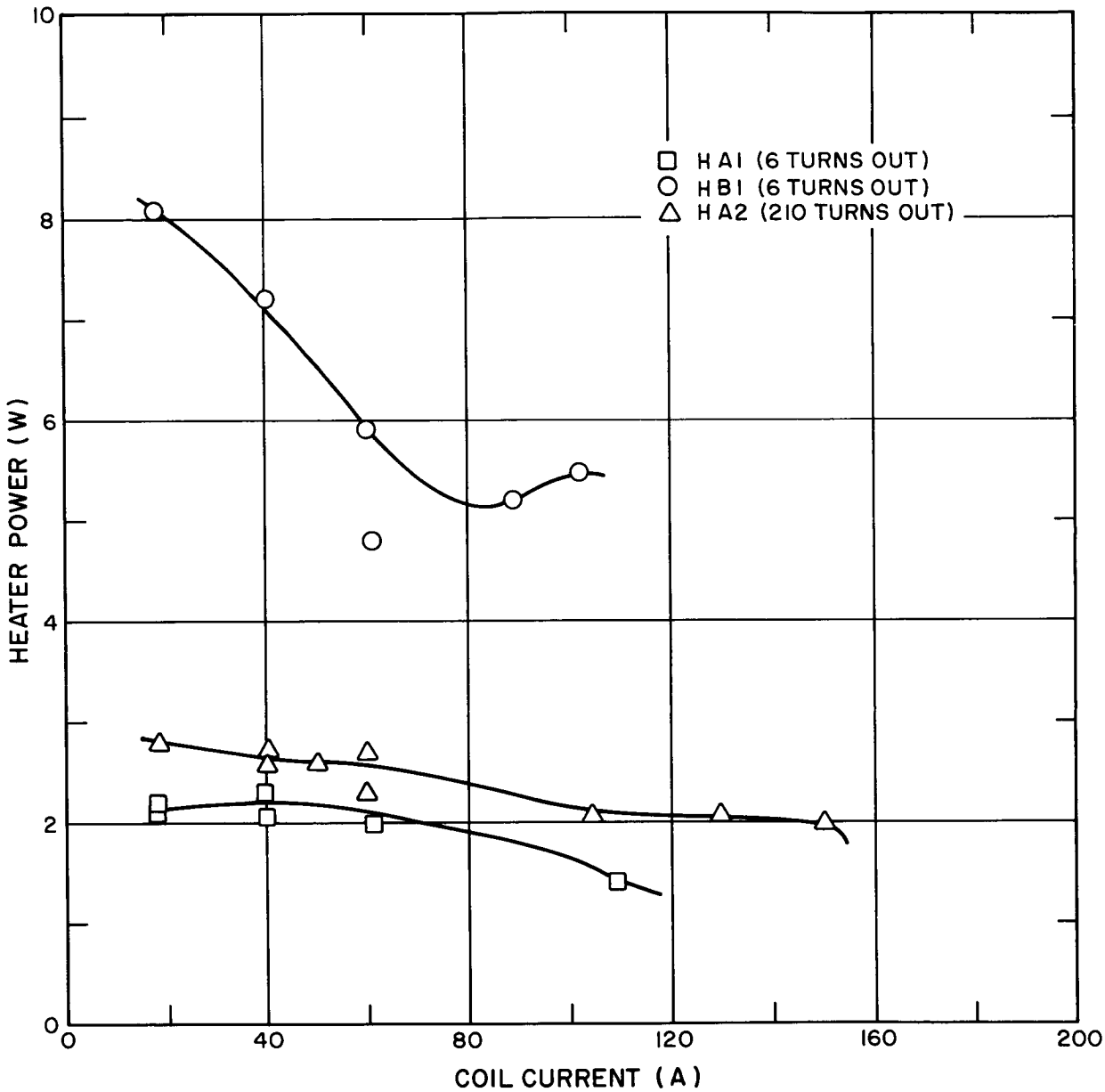

Fig. 39 Heater Power necessary to initiate a quench as a function of Coil Current

A2421

the coil in such a way that this anisotropy resulted in ten fold increase in radial field sensitivity over axial field sensitivity. Since we have no way of knowing the direction of the field vector the results of this experiment are qualitative only. The values cited above are given assuming axial orientation of the field.

7.3 Operation with an Energizer

An energizer employing two thermal persistent switches and a transformer was built and incorporated into the test assembly as shown in Figs. 36 and 41. A schematic diagram of the device is shown in Fig. 40.

The transformer core consisted of an annular ring of mild steel designed in such a way as to place the iron in the lowest fringe field region while at the same time providing a maximum core cross section. (Since it is this cross section which determines the amount of flux introduced into the coil during each cycle of operation). This cross section was such that at a saturation field of 1.5 T it would provide a saturation flux of 2.25×10^{-2} Wb.

The persistent switches consisted of lengths of Nb-Zr strip electric heaters to drive them normal and heat sinks to prevent the normal regions from spreading to other parts of the system.

Several switching sequences can be used with this circuit but the following one results in maximum efficiency because switches are opened only under zero current conditions.

1. Initially there is no current anywhere in the system
2. S_1 is opened
3. A negative voltage is applied to the primary and is allowed to remain until the transformer core is saturated in the negative direction at which time the voltage is removed.
4. S_1 is closed and S_2 is opened. (note that no currents exist in either switch before or after operation).
5. A positive voltage is applied to the primary and allowed to remain until the core is saturated in the positive direction at which time it is removed. This drives a total of twice the saturation flux into the coil.
6. S_2 is closed. (There is now a persistent current flowing through the transformer secondary, S_1 and L, the coil being charged).
7. A reverse current is passed through the primary of such magnitude as to reduce the persistent current in S_1 to zero. This in effect transfers all the current in L from S_1 to S_2.

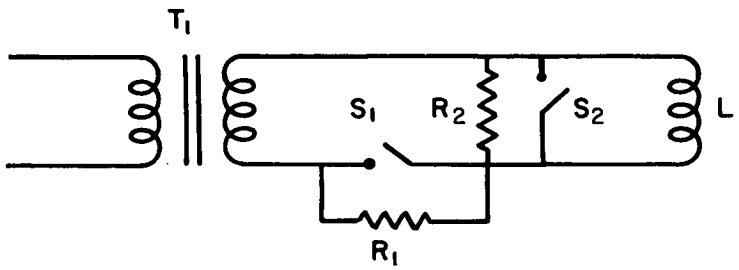

Fig. 40 Schematic diagram of Energizer

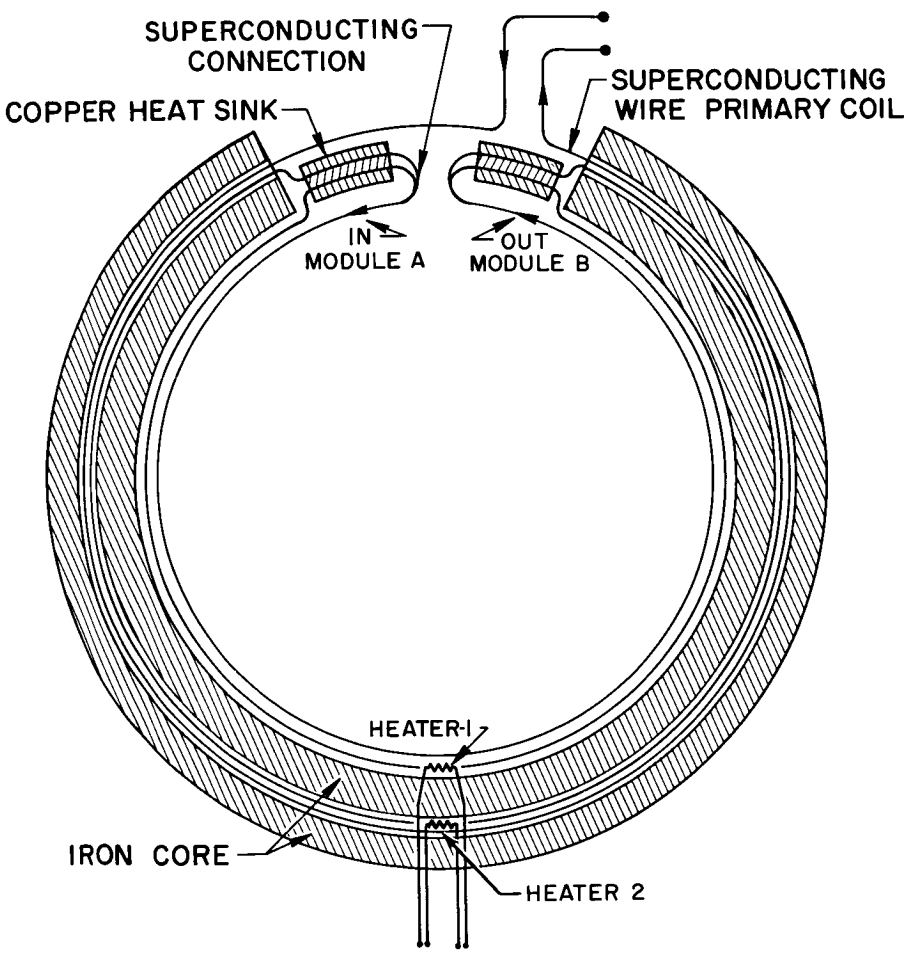

Fig. 41 Physical arrangement of Energizer Components

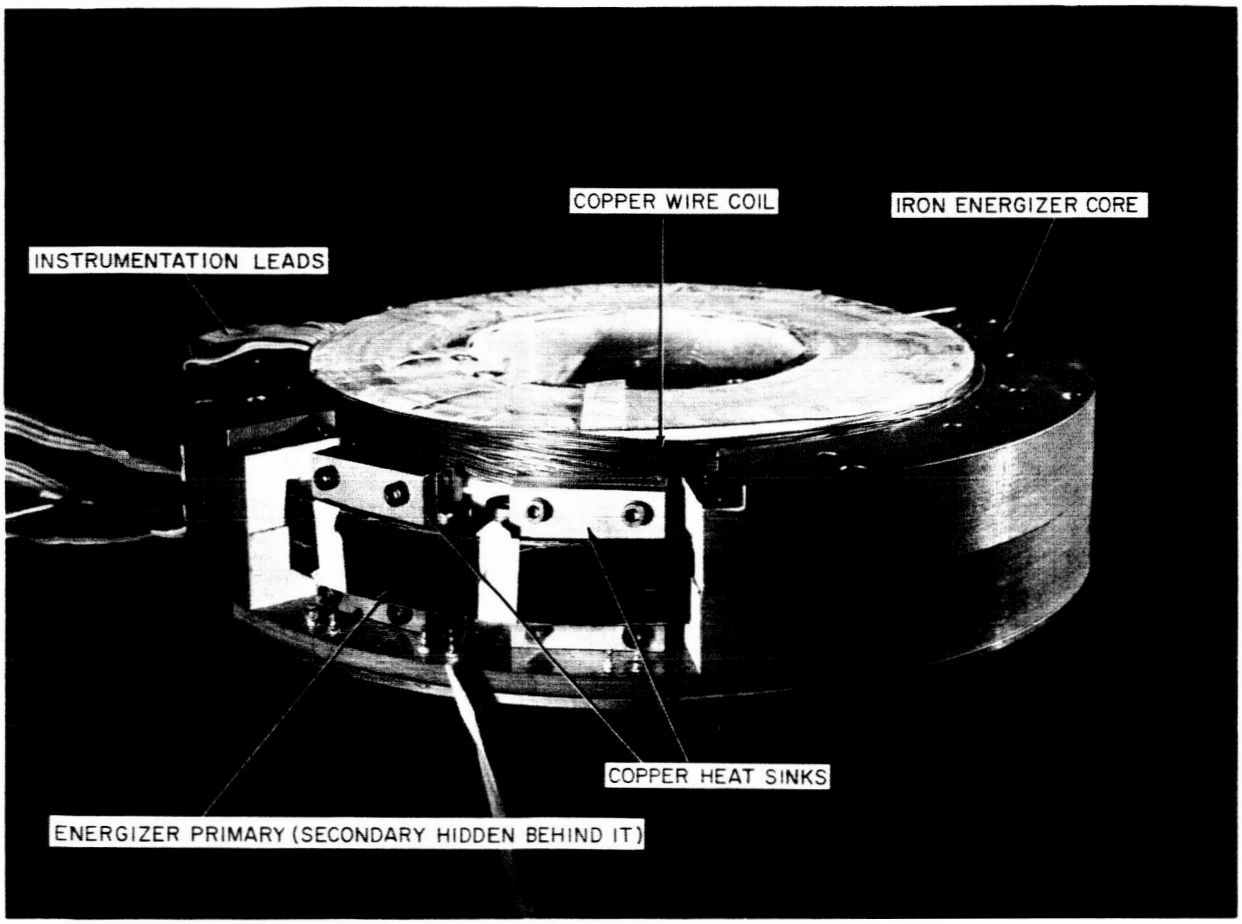

Fig. 42 Energizer shown assembled with Strip Coil Modules

A2422

8. S_1 is opened.

9. A negative voltage is applied to the primary and allowed to remain until the core is negatively saturated.

During actual tests, the device clearly demonstrated pumping action but did not come up to expectations in terms of pumping speed. According to the switching sequence described above, it should inject twice the core saturation flux, or 4.50×10^{-2} Wb into the coil with each cycle of operation.

The measured value, however was only 1.37×10^{-4} Wb. We conclude that the normal region induced by the heaters during the pumping operation was not confined by the heat sinks, but propagated into the other switch thus providing a flux leak.

7.4 Inductive Energizing

With the coil arranged for use with the energizer its outer leads are shorted together provided the energizer heaters are not activated. This makes inductive energizing possible by virtue of the mutual coupling with the trimmer coils.

When the trimmer coils are energized, a reverse current is induced in the strip coil which tends to exclude the field from the center. If the trimmer coil current is increased to the point where the strip coil quenches, or if the energizer heaters are activated, flux enters the coil and becomes trapped when the trimmer excitation is removed and the strip coil then remains energized in the persistent mode.

The method has two disadvantages; the field cannot be maintained parallel to the strip plane and current measurement is difficult. The coil was nevertheless run in this manner and persistent currents of up to 75 A were generated.

As might be expected at these low currents, no quenches could be initiated by either the transducers or the heaters in the coil. The spontaneous quenches that did occur all started at the outer diameter.

8. Conclusions

The major characteristics of the coil are shown below in Table III.

Table III

I.D.	0.127 m	(5 in)
O.D.	0.254 m	(10 in)
Length (without trimmer)	0.65 m	(2.56 in)
Turns	880	

Radial Packing Factor	Actual	0.44
	Theoretical	0.47
Inductance	.34 H (approximate)	
Field - Current Ratio (at center)		
without trimmers	$6.8 \times 10^{-3} \frac{T}{A}$	
with trimmers	$1.1 \times 10^{-2} \frac{T}{A}$	
Time Constant	4 sec	
Critical Current	160 amperes	
Max. Field at Center (with trimmer)	1.8 T	

The critical current is somewhat lower than that of the SC 500 wire coil (which is quite similar geometrically). On a simple turns ratio basis 160 A in the strip coil is equivalent to 9.4 A in an SC 500 coil.

The SC 500 coils, however quench at 12 A in a similar configuration.

The fact that all the quenches but one started at the center implies that there may have been a faulty contact there causing a premature quench.

APPENDIX A

ULTRASONICALLY SOLDERED CONNECTIONS

A superconducting to normal connection was prepared as shown in Fig. A1. It was constructed by ultrasonically tinning niobium zirconium strip with indium tin solder and then soldering this to copper electrodes.

A matrix of 1 mm diameter holes spaced at 5 mm intervals were drilled in the strip over the contact area to allow the solder to flow through and form "rivets", thus increasing the mechanical peel strength, which is ordinarily very poor in soldered or plated joints with niobium or niobium zirconium.

Three voltage taps were provided, one on the niobium zirconium and one on each copper electrode, in such a way as to monitor each interface voltage.

This joint was energized with currents up to 30 A and the resistance was measured at 4.15 T, at various orientation angles.

The results are shown in Figs. A2 and A3. Evidently, at about 9 A, stable normal region is developing at orientations around 90^{o} which gives rise to the abrupt increase in resistance noted there in both figures.

The surface resistance can be calculated from the data of Figs. 4 and 5 and turns out to be 6×10^{-11} Ω-m^2, almost two orders of magnitude greater than that of the spot welded joints. We believe the reason for this is the formation of a layer of high resistance material at the interface of the copper and indium-tin.

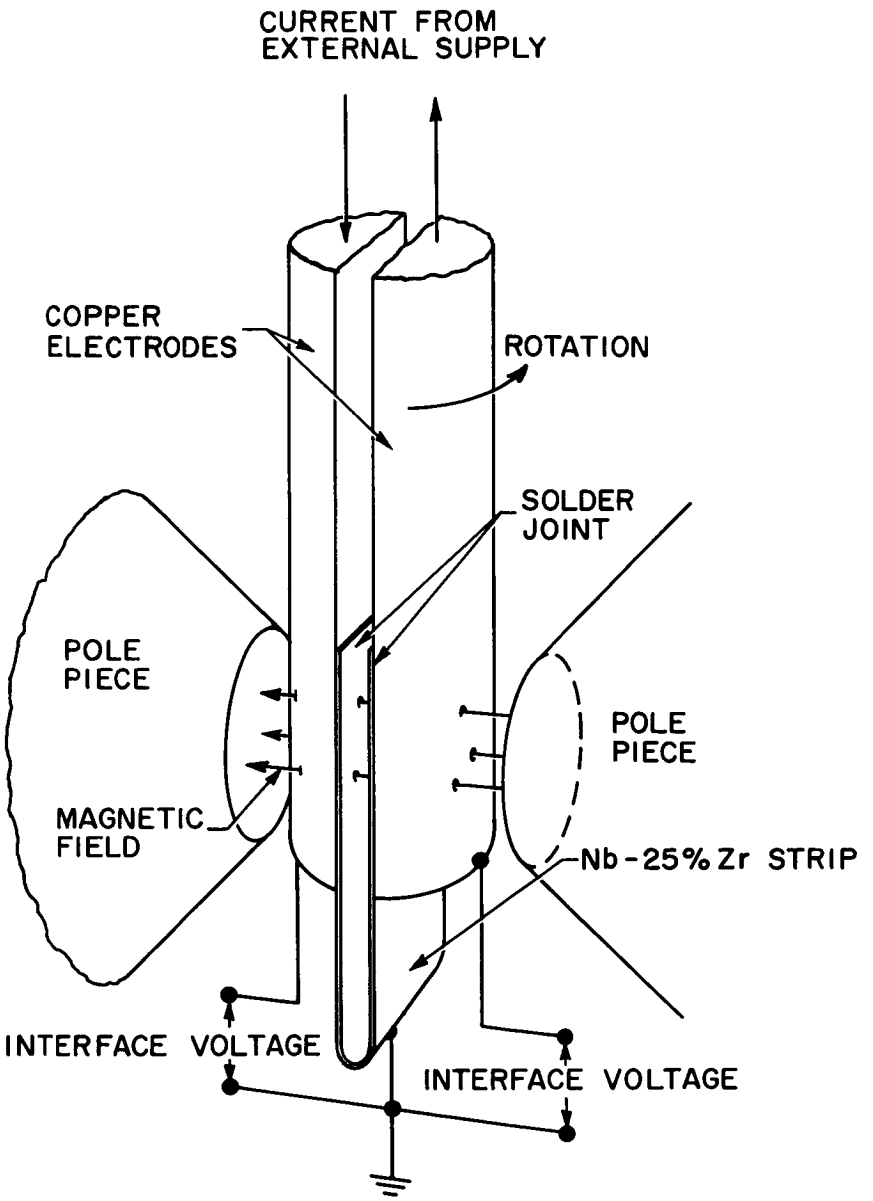

Fig. A1 Schematic of test arrangement for observing anisotropy in superconducting to normal connections.

A2423

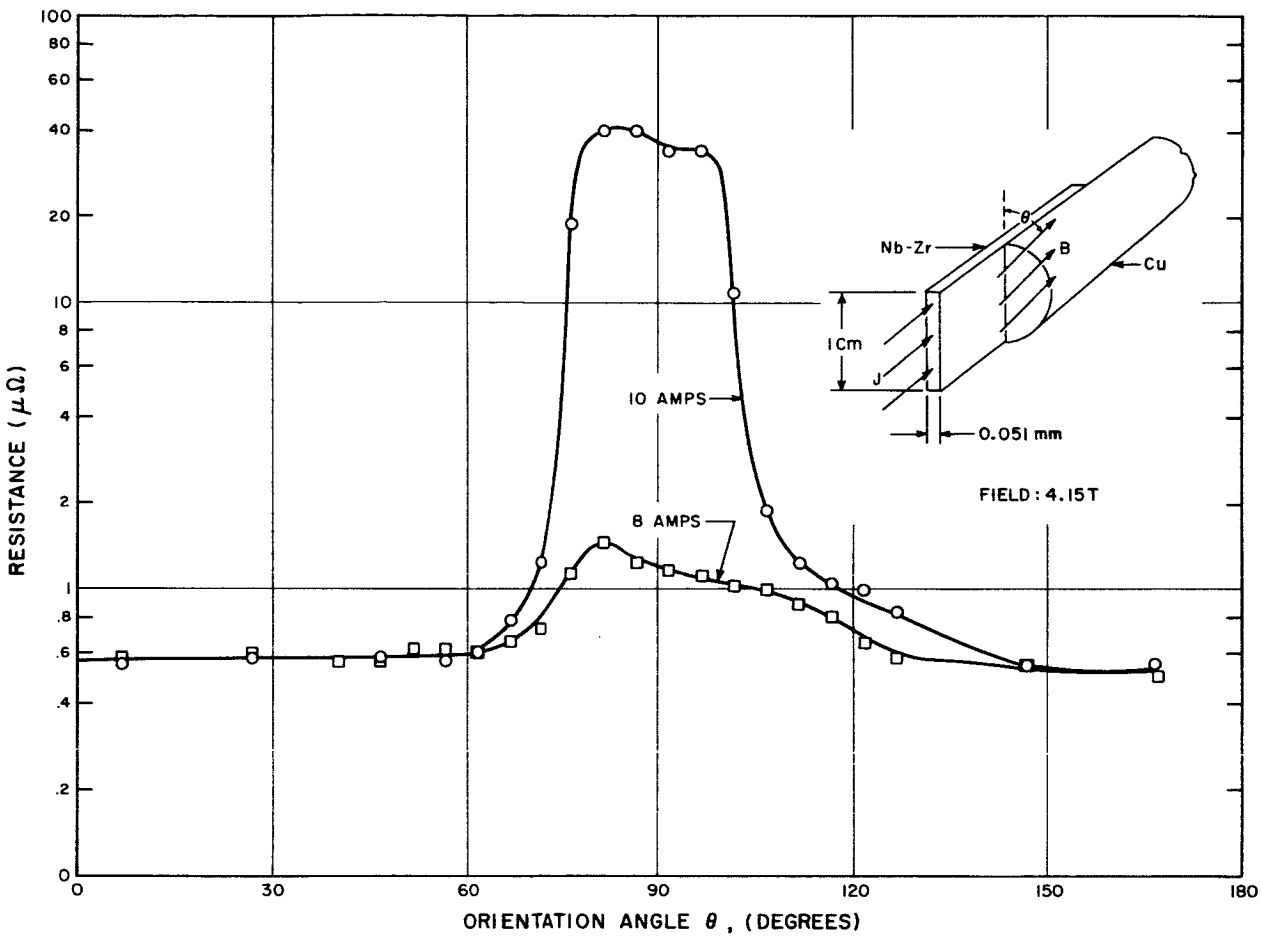

Fig. A2 Anisotropy of ultrasonically soldered superconducting to normal connection

A1742

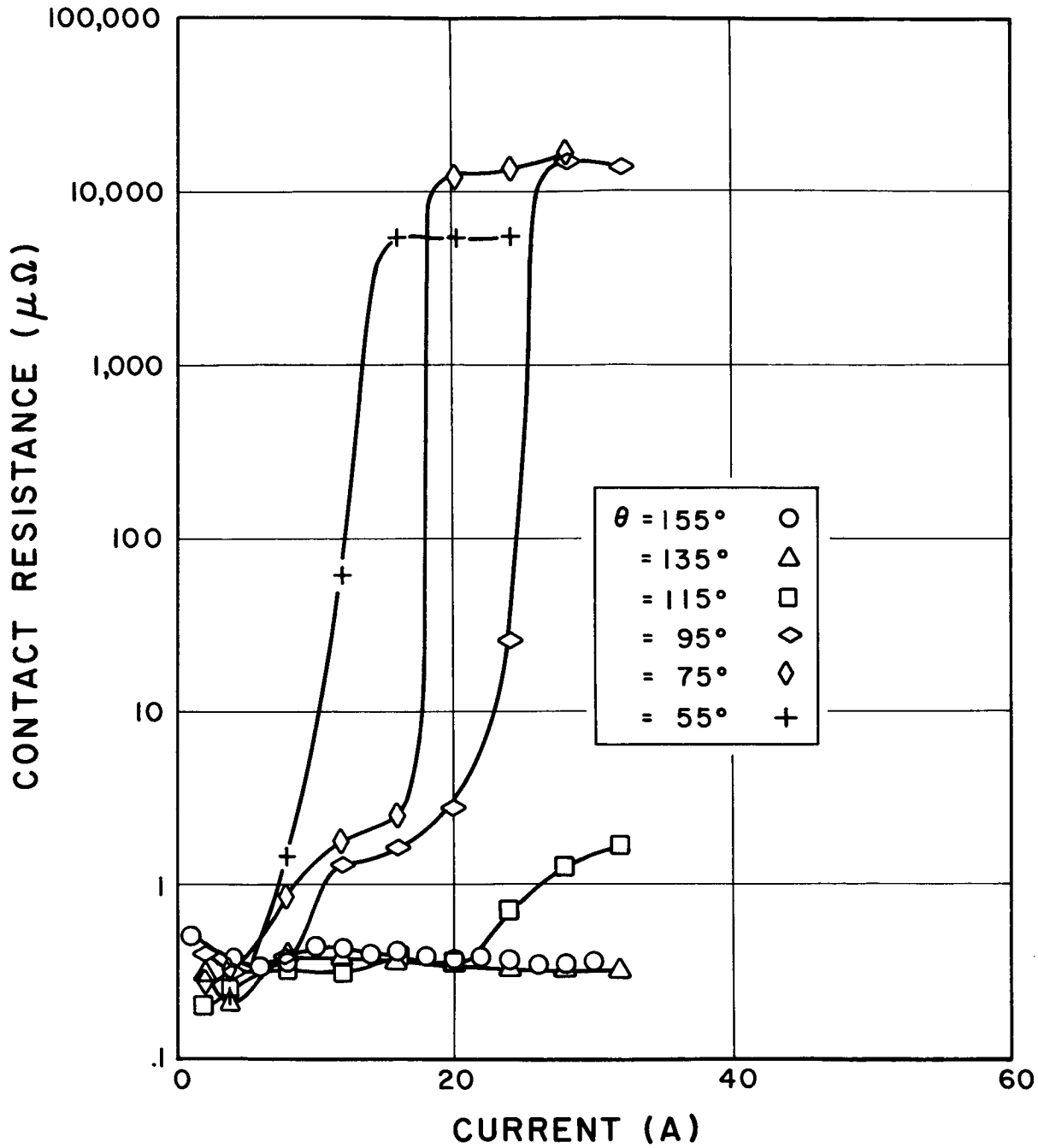

Fig. A3 Resistance vs current for various field orientations

A2424

APPENDIX B

COLD WELDED AND RIVETED CONNECTIONS

Prior to completion of the anisotropy testing apparatus, several types of joints were tested in the apparatus shown in Fig. B1. This contains a D.C. transformer for energizing the sample, a saturable reactor-type current sensor and a small iron core transformer capable of producing fields up to 1 T perpendicular to the plane of the sample.

Several samples were tested with this apparatus and their results are compared on a unit basis (i.e., current per rivet or per weld) in Fig. B2, along with the critical current density for perpendicular fields normalized arbitrarily to 100 A, in order to show the similarity in shape.

Ultrasonic Cold Welds

The data shown in Fig. B2 was taken on a 2.54 cm wide strip 0.051 mm thick welded in 6 places with a 100 W ultrasonic spot welder manufactured by the Sonoband Corporation, West Chester, Pennsylvania. These welds were made with all adjustments at maximum, i.e., maximum power, maximum weld time and maximum weld pressure, but even so, were of very marginal mechanical strength and not very repeatable.

This work, done locally on a demonstration machine proved promising enough to warrant further investigation on a larger machine (4000 W) at the Sonoband plant, and a sample was in fact prepared using this machine. Considerable time elapsed, however, before this was available for testing and in the meantime, success was realized with the resistance spot welds, so it was never tested.

Riveted and Bolted Connections

Tests were performed on joints employing the following types of fasteners:

1. 1/16" dia. stainless steel rivets
2. 1/16" dia. brass eyelets
3. 0-80 stainless machine screws

The results are shown comparatively in Fig. B2, where it is seen that the stainless rivets are the best. We feel the success of such joints is attributable to the amount of pressure with which the superconducting components are clamped together. In previous work using knife edges to apply pressure, it was found that good contacts were not realized unless enough pressure could be exerted to actually deform the superconductors.

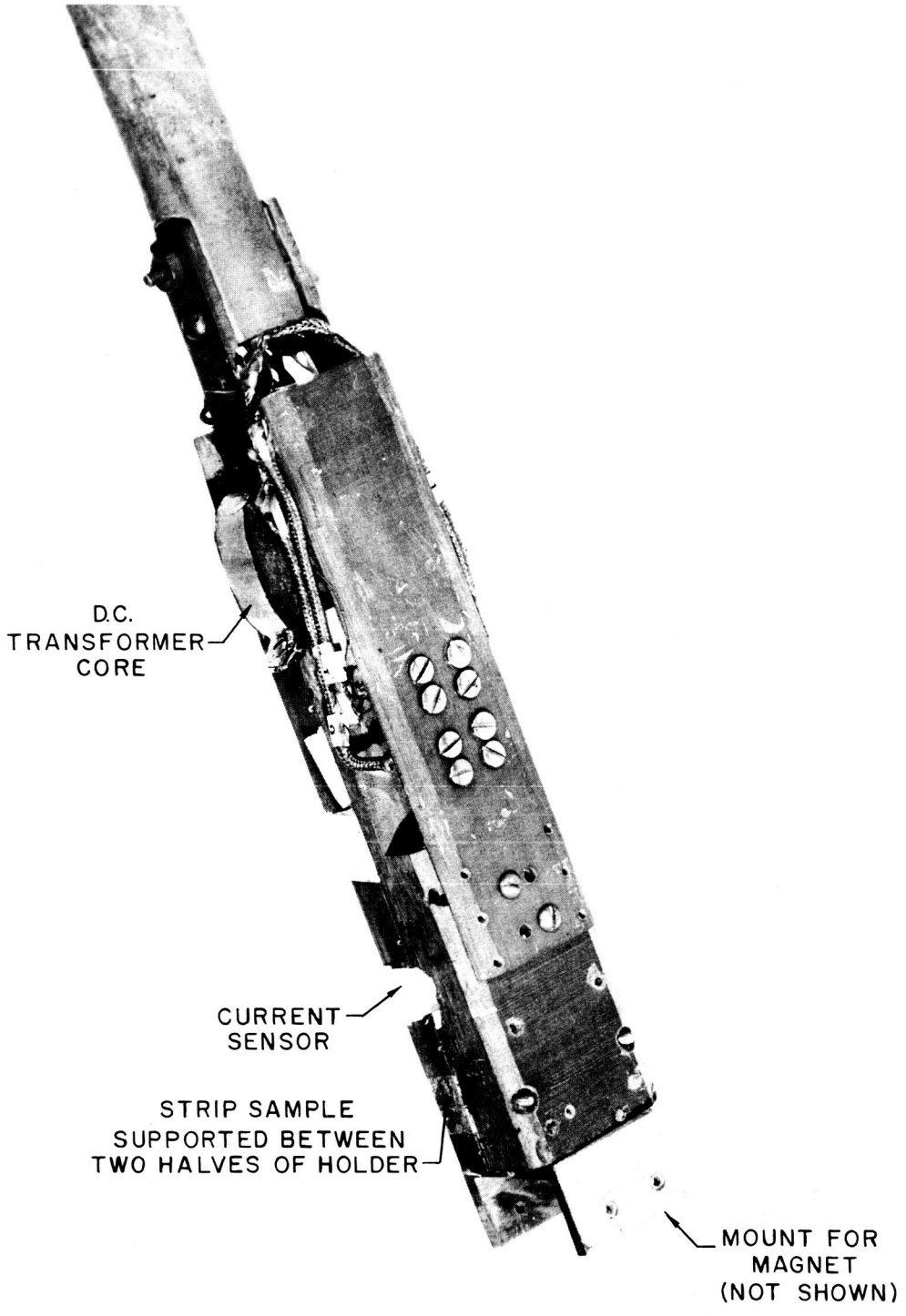

Fig. B1 Superconducting to Superconducting Contact Test Fixture

A2721

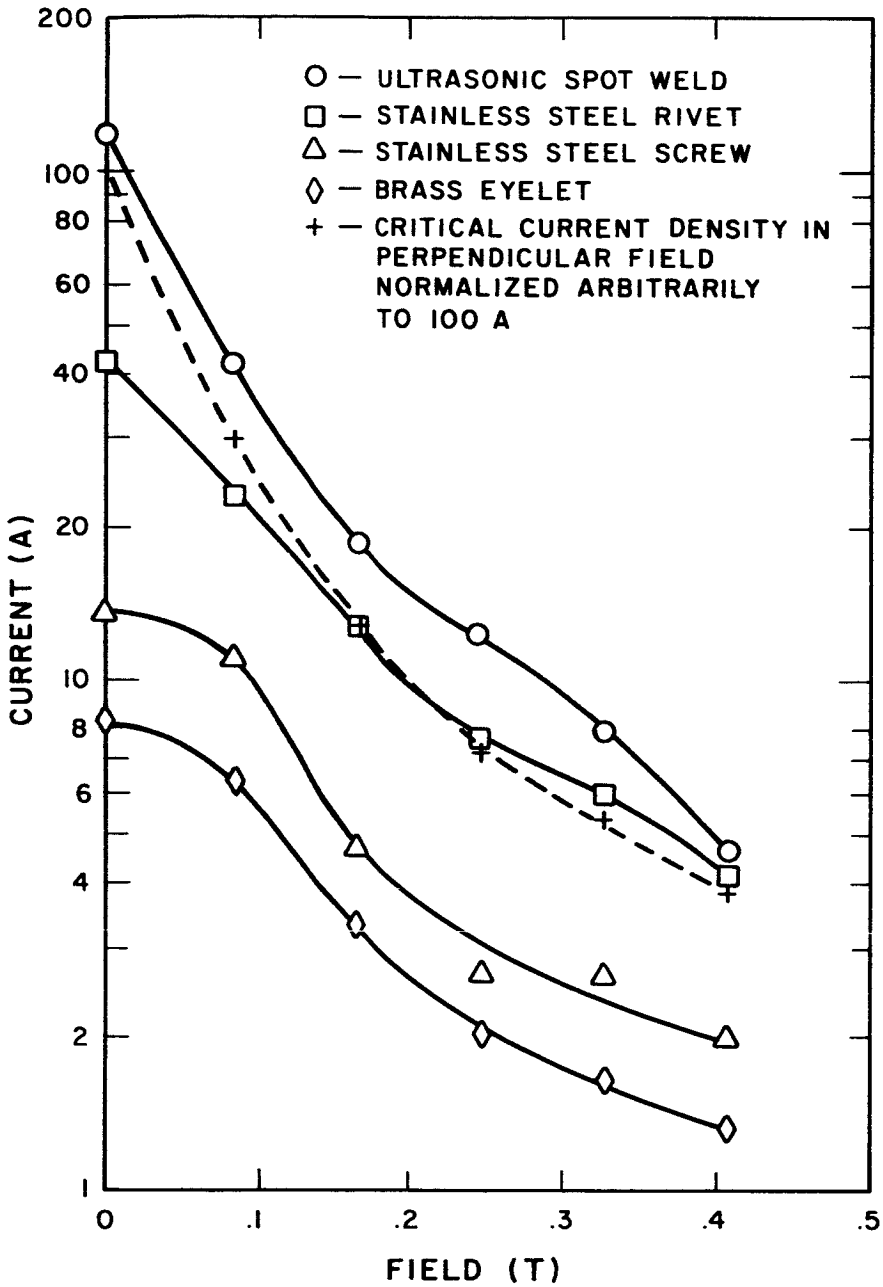

Fig. B2 Critical current vs Field as perpendicular orientation for various types of connections

A2426

APPENDIX C

THE D C TRANSFORMER

A D. C. transformer is simply a conventional A. C. transformer with a superconducting, and hence zero resistance, secondary. It allows one to generate extremely large DC currents in the secondary, by means of relatively small DC currents in the primary. Hence, by using a superconducting sample as a secondary, critical current experiments may be performed without the need for a high current room temperatue power supply, and the attendant heavy power leads.

Field Theory Discussion

We have, from Faraday's Law, that

$$\oint \vec{E} \cdot d\vec{s} = -\frac{\partial}{\partial t} \iint_A \vec{B} \cdot d\vec{A}$$

for a closed conducting loop with which ds is collinear and which circumscribes A.

Since $\vec{E} = \rho \vec{J}$, where $\vec{J}$ is current density and ρ is the resistivity of the conductor, if we allow ρ to approach zero, as it does in a superconductor, we get:

$$-\frac{\partial}{\partial t} \iint_A \vec{B} \cdot d\vec{A} = 0$$

or

$$\iint_A \vec{B} \cdot d\vec{A} = \text{constant} \qquad (1)$$

Since the total magnetic flux through the loop is constant in time, if an external field is applied, as from a transformer primary, a DC current will be induced in the loop of just the right value to cancel the introduced flux.

Although this approach gives a good qualitative feel for the operation of the transformer, circuit theory must be used to arrive at quantitative results.

Circuit Theory Discussion

Consider the circuit of Fig. C1.

Here, L_1 is the primary coil of the transformer, L_2 is that part of the secondary which is coupled to L_1 by M and L_3 is the remainder of the secondary, which has a negligible coupling with L_1. The equations are:

$$L_1 \frac{di_1}{dt} + M \frac{di_2}{dt} = V_1 \tag{2}$$

$$M \frac{di_1}{dt} + (L_2 + L_3) \frac{di_2}{dt} = 0 \tag{3}$$

Integrating the second equation gives:

$$i_2 = I_2 - \frac{M}{L_2 + L_3} i_1$$

$$= I_2 - \left[\frac{C}{N_2/N_1 + \frac{L_3}{\sqrt{L_1 L_2}}} \right] i_1 \tag{4}$$

where

$$C = \frac{M}{\sqrt{L_1 L_2}} = \text{coupling coefficient}$$

$$\frac{N_2}{N_1} = \text{turn ratio}$$

I_2 = initial current

Note that if $I_2 = 0$, as L_3 approaches zero, we get:

$$i_2 = \frac{N_1}{N_2} C i_1 \tag{5}$$

We can show from the circuit theory that the total flux linking the secondary, the $\iint_A \vec{B} \cdot d\vec{A}$ of field theory, is constant.

The flux is given by:

$$\lambda = (M\, i_1 + L_2\, i_2) + L_3\, i_2$$

Substituting for i_2 from (4), we get:

$$\lambda = (L_3 + L_2)\, I_2 = \text{constant} \qquad (6)$$

Consider the flux in the core of the transformer, λ core:

$$\lambda \text{ core} = L_1\, i_1 + L_2\, i_2$$

Substituting again for i_2 from (4), we have

$$\lambda \text{ core} = L_1\, I_1 \left[1 - \frac{C}{1 + \frac{L_3}{L_2}} \right] \qquad (7)$$

Since we may, in practice, make C approach 1, it is clear that the core flux approaches zero as L_3/L_2 approaches zero, and goes up with L_3.

Design Considerations - Core

It might appear that an air core transformer would be preferable to one with an iron core, as it could not saturate and would have a lower heat capacity.

It was found, however, that for currents above 100 A in the secondary, the coupling coefficient rapidly deteriorated. Apparently this was due to the edges of the strip going normal, and causing an effective reduction in the width of the superconductor, thus reducing the coupling coefficient.

This difficulty was largely overcome through the use of an iron core, perhaps because this prevented a concentration of flux lines due to the primary at the edges of the strip. With two transformers, identical, save for iron versus air cores, the coupling coefficient was higher by more than an order of magnitude for the iron core.

It is clear from Eq. (7) that for unity coupling and zero load impedance, no flux will ever penetrate the core. In other than ideal situations, however, flux may leak in and eventually saturate the iron.

The total flux density in the core may be found by using

$$B_{\text{core}} = \frac{\mu}{\ell} (n\, i)_{\text{core}} = \frac{\mu}{\ell} (n_1\, i_1 + n_2\, i_2) \qquad (5)$$

where ℓ is the mean path length in the core, μ is the permeability of the iron, and n_1 and n_2 are the number of primary and secondary turns respectively. Substituting for i_2 from (4), we arrive at:

$$B_{core} = \frac{\mu n_1 i_1}{e} \left[1 - \frac{C}{1 + L_3/L_2} \right] + \frac{\mu n_2 I_2}{e} \qquad (6)$$

Secondary Current Measurement

The method used in determining the current in the secondary is essentially a measurement of the field created by the current in the strip. This is done by nullifying the field due to the strip in a small region with a bias coil, as shown in Fig. C2, and using a small saturable reactor to find the null in the field in this region.

Since the bias coil acts approximately like a second piece of strip, it is convenient to wind it with 1000 turns. Then, at zero field in the interior region, the bias current in milliamperes will be equal to the strip current in amperes.

The null field detector can consist of any convenient device for sensing magnetic fields. We use a saturable reactor because of its economy and reliability. It consists of a hole drilled in the center leg of the core with a sweep winding and a pickup winding, wound into it as shown in Fig. C3.

The sweep winding, energized by a 60 Hz current drives the thin walls around the hole into saturation each cycle, and the pickup winding is fed to an oscilloscope. The presence or absence of a field in the center leg can be observed by the resulting wave shape from the pickup winding.

Design Considerations-Secondary and Center

At several points, it has been assumed that the initial current in the superconducting secondary was zero. The easiest way to achieve this is to attach a small heater to the strip. This can be done by taping a piece of nichrome, perhaps 10 mm by 100 mm by 0.1 mm, to the strip and passing a short pulse of a few amperes through it. In our design, this has been found sufficient to reduce the secondary current to zero.

Design Consideration - Construction

There follows a brief description of the actual design and arrangement of the components previously discussed. These characteristics are of course dependent on the dewars and magnets available for experimentation.

The schematic layout is shown in Fig. 8 of the main text. The transformer was designed so that a probe, containing a test section of the superconducting secondary, would fit into the iron core transverse field superconducting magnet. In this manner, both H-I and anisotropy characteristics of the strip could be measured.

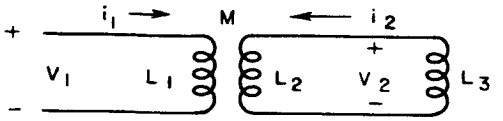

Fig. C1 Schematic Diagram of DC Transformer

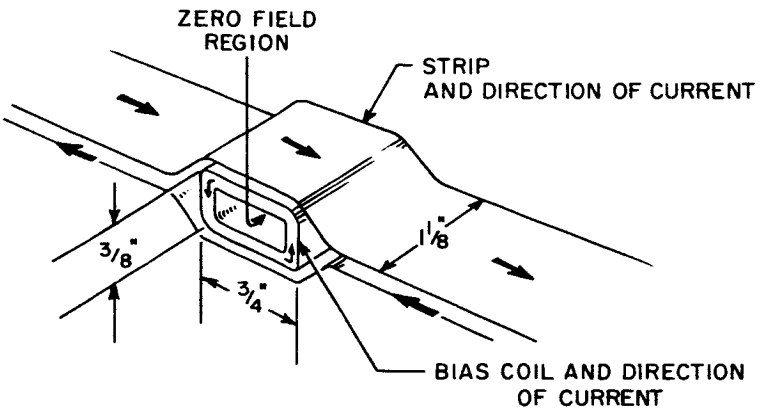

Fig. C2 Current Sensor

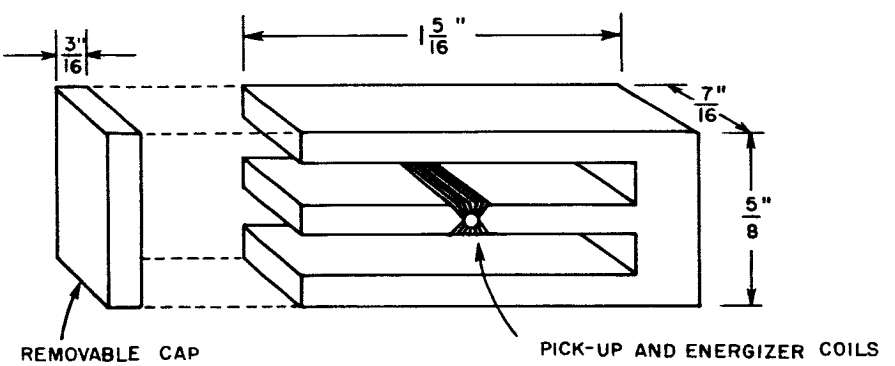

Fig. C3 Sensor Core and Saturable Reactor

A2427

A2428

A2429

On top of the flange which covers the dewar is a pointer, used for determining the angle between the strip being tested and the field applied to it. This is attached to a five foot hollow phenolic shaft, through which the electrical leads pass and to the bottom of which is attached the phenolic body of the transformer.

The primary consists of 1000 turns of Nb-Zr 0.01" dia. superconducting wire wound on a phenolic spool. The core is a ring of iron passing through this and then through one turn of the secondary. Both laminated and solid cores have been used, with no noticeable difference in performance. The strip passes through the current sensor, which has a bias winding of 1000 turns of four mil Nb-Zr superconducting wire, wound on a plastic spool. The iron sections of the current sensor are made from solid soft iron.

The windings on the current sensor consist of a primary of twenty turns of number 38 copper magnet wire, wound ten on each side of the hole in the center prong, and a secondary of two turns, one on each side of the hole. This has been found to operate well at considerably less than one volt, applied to the primary lead wires outside of the dewar.

The strip then passes through the field region inside a six-inch probe made by cutting a piece of three-eighths inch phenolic tube in half. At the extreme end, below the field, it is spot welded to form a single complete loop. It should be noted that since the L_3 of previous calculations depends on the area of the loop in the regions below the primary, every effort should be made to keep this area to a minimum. If L_3 is too large, the core becomes saturated and limits the current attainable in the secondary.

APPENDIX D

TRANSVERSE FIELD IRON CORE MAGNET

In all the anisotropy and most of the H-I experiments the magnetic field was produced by a transverse field iron core magnet capable of producing a field in a direction normal to the dewar axis. This construction allows one to make anisotropy measurements by leaving the magnet fixed in the dewar and rotating the sample.

The magnet is shown in Fig. D1 and in Fig. 8 of the main text where the shape and location of the principal parts are shown schematically. The principal parts are the superconducting coils, the iron pole pieces and the supporting structure.

The pole pieces are conical with pole faces of 1.27 cm (1/2 in.) dia. and are constructed of annealed soft iron. These are held in place by means of a superstructure which is suspended in the dewar by means of long slender stainless steel rods.

The coils are wound with 0.010" dia. Nb-25% Zr wire and have a spherical outer surface and a conical hole so that they will fit snugly over the pole pieces. The spherical outer contour allows for maximum usage of the available space in the cylindrical dewar.

Aluminum spacers are used to set the spacing of the two pole piece units and any thickness up to 1.27 cm (1/2 in.) can be used, making a maximum working gap of 1.27 cm.

Although the magnet has been operated at currents up to 28 A, 25 A is the maximum for reliable operation. At this current the magnet produces 4.17 T measured at the center of the 1.27 cm gap. Uniformity is maintained within 10% over the pole face area.

In general the design of this magnet is flexible enough so that other pole pieces can be installed, the pole spacing can be varied and with slight modification in support structure it can be changed to axial orientation with respect to the dewar.

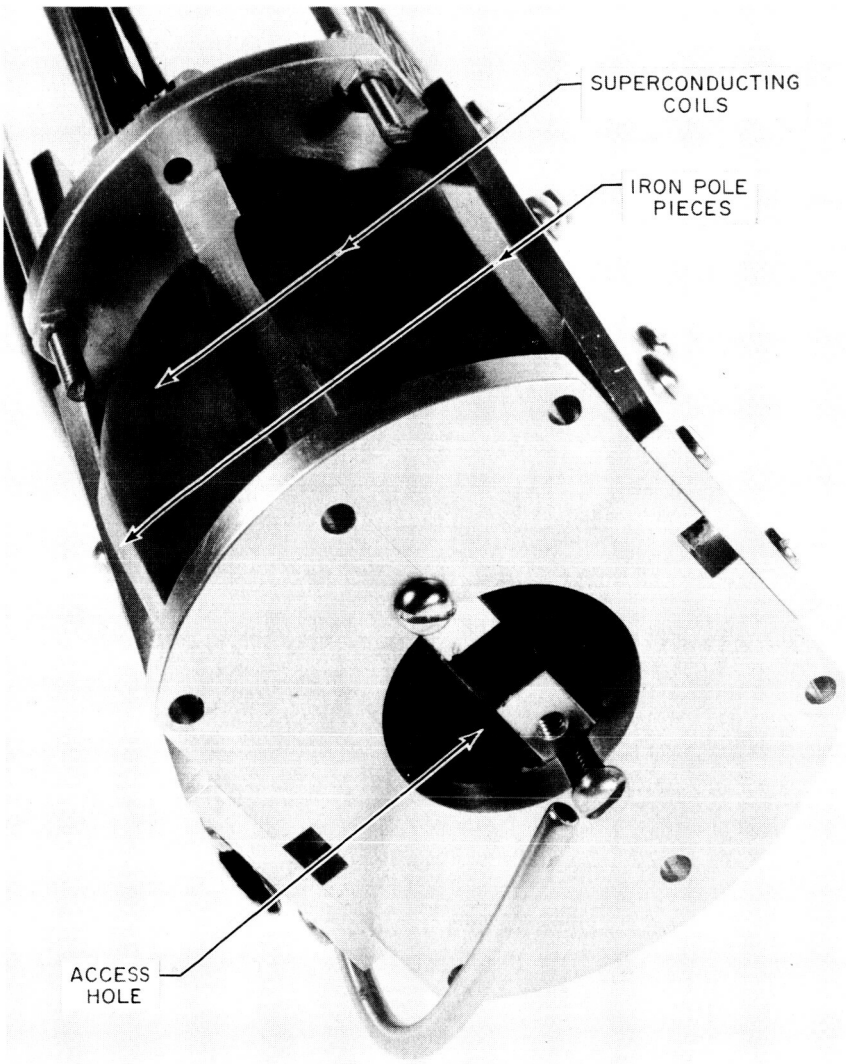

Fig. D1 Transverse Field Iron Core Superconducting Magnet

A1633

APPENDIX E

MAGNETO-OPTIC EQUIPMENT

The rotation, Θ, of the plane of polarization of plane polarized light in glass, $Ce(PO_3)_3$, exhibiting the Faraday effect is given by

$$\Theta = V(\lambda) \frac{1}{T} \int_0^{\ell} H_s \, ds$$

where $V(\lambda)$ = Verdet's constant, (a function of wavelength)

T = temperature

H_s = component of the field along the light path

ds = element of distance along the light path

ℓ = total distance travelled by the light

λ = light wavelength

For cerium metaphosphate glass, $Ce(PO_3)_3$ this relation holds in the temperature range 0-6 ^{o}K. This is one of the few substances known which exhibits the Faraday effect at these low temperatures.

This property is employed in an optical device for observing the field distribution near the surface of superconductors. A second surface mirror (i.e., a mirror which is aluminized on its back surface) of this glass is placed directly in contact with a flat sample of superconductor. A light source and optical system as shown in Fig. E1 is used to form an image which varies in intensity in a way that can be interpreted in terms of field intensity.

When a second surface mirror is used in this way $\ell = 2d$ where d = thickness of mirror. That is, the rotation is not cancelled but doubled, by reversing the direction of propagation of the polarized light.

If a mercury arc lamp is used as a light source, there are four main emission lines in the visible spectrum at 5790 Å, 5461 Å, 4358 Å, 4046 Å. The rotation is shown in Table E1.

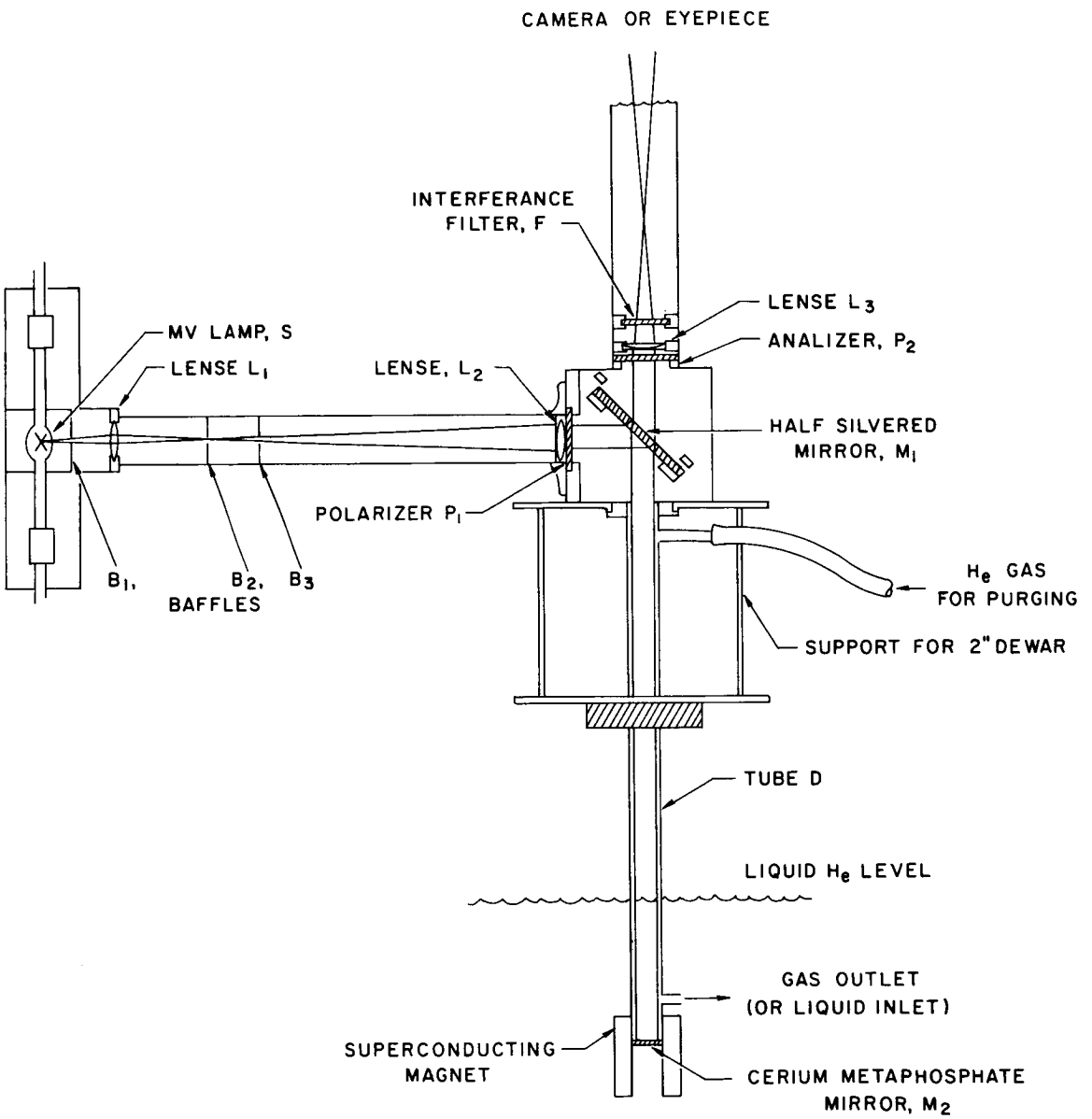

Fig. E1 Optical Apparatus

A2430

TABLE E1

Wavelength (Å)	Rotation (Degrees/T)
5790	107
5461	120
4358	190
4046	219

Thus, if a filter is used to pass only 5461 Å and the arbitrary angle measurement between the crossed polarizer and analyzer is set at zero with zero field (producing a null there), the regions of the mirror which turn bright are those where there is field present. If the angle of the analyzer is changed to some arbitrary Θ, then the regions which are nulled (appear dark) are those whose $H_{nav.}$ satisfy the given equation

$$\Theta_1 = V \frac{H_n}{T} \cdot 2d$$

where

V = Verdet constant at 5461 Å

H_n = Normal component of field

T = Temperature

d = Mirror thickness

Thus the field distribution across the surface of the mirror can be "seen" as a function of Θ_1. The relative field strengths are observed from the intensity of the regions at a constant analyzer setting.

If the filter is not used a colored image results by virtue of the dependence of the Verdet constant on wavelength. The interpretation of these images in terms of magnetic field is difficult, however, since no simple relationship exists between color and magnetic field.

Apparatus

The apparatus for observing the intermediate state is shown in Fig. E1. The main parts are:

S - Sylvania 100 W M.V. lamp - approx. 4 A, 25 V

L_1 - Double convex lens (coated) 29 mm dia., 30 mm f. l.

L_2, L_3 - Achromat (ctd) 32 mm dia., 337 mm f. l.

L_4 - Achromat (ctd) 32 mm dia., 132 mm f. l.

L_5 - Kellner eyepiece (ctd) in 31.8 mm O.D. housing 22 mm effective focal length

P_1 - Polarizer, P_2 - analyzer } { Polaroid HN 22 filter mounted between optically flat glass, 40 mm dia., 4 mm thick

M_1 - Half silvered mirror

M_2 - Second surface mirror, Ce $(PO_3)_3$ glass, 13 mm dia., 0.5 mm thick.

F - Interference filter, bandwidth 200-245 Å, max. transmission at 5450 Å

H - Rack and pinion eyepiece focusing mount, 100 mm travel, takes standard 31.8 mm O.D. eyepiece cells.

Its operation is as follows. The image of the mercury vapor light source S is formed at the pinhole in baffle B_2 which is located at the focal point of lense L_2. The light beam, thus collimated, passes through the polarizer P_1 and becomes polarized so that its electric field is normal to the plane of Fig. E1. Half silvered mirror M_1 reflects the beam down the tube to the cerium metaphosphate mirror M_2 which is mounted as shown in Fig. E2 with its silvered surface in contact with the superconducting sample. The beam is reflected from this second surface and its polarization is rotated according to the magnitude of the normal component of the magnetic field existing in the glass. The beam then continues up the tube D, through mirror M_1 to the analyzer P_2 which is crossed with respect to polarizer P_1 so that the variations in polarization are transformed into variations in color, which are then reduced to intensity variations by the filter F_1. The image can be viewed with an eyepiece or photographed.

Resolution

The resolution of the device is limited chiefly by the amount of rotation obtainable at a given field and by the sharpness of the null obtainable with the polarizers. It is not, as might be expected, critically influenced by the thickness of the mirror. Since the image is formed by virtue of differences in field rather than actual magnitudes it is of little consequence how thick the mirror is provided it is thick enough to cover the region near the surface in which the field is disturbed. The characteristic distance out from the surface within which the field is disturbed is roughly equal to the domain size or "wavelength" of appreciable change along the surface.

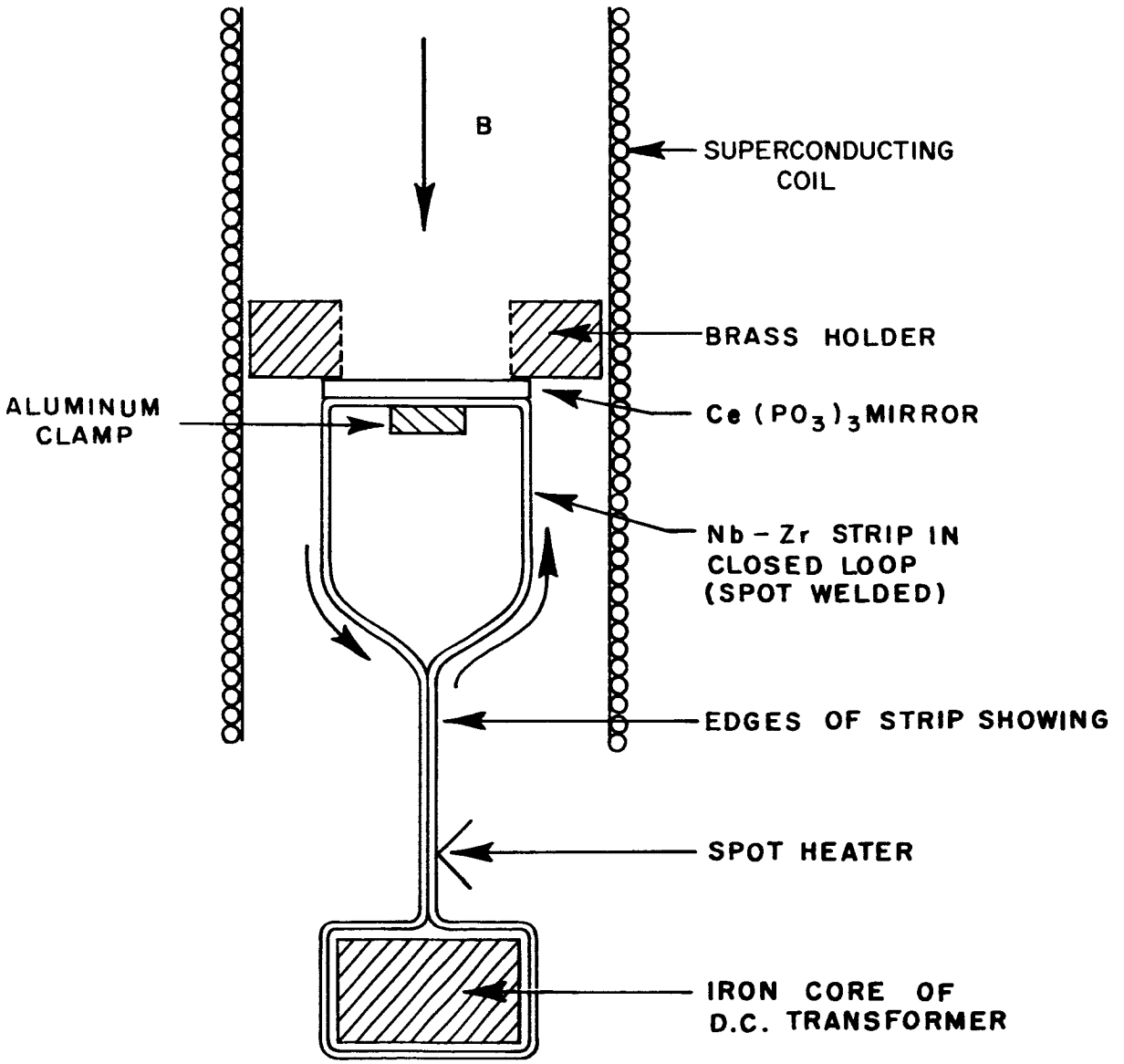

Fig. E2 Sample Holder

A2431

The mirror is therefore made at least as thick as the width of the variations one wishes to resolve. Making it thicker does not impair the resolution because out beyond the characteristic distance, the field becomes uniform again and contributes no more relative change in rotation.

A maximum thickness is however imposed by another consideration, that of stria lines in the glass. This glass is difficult to make and even at best it contains stria lines which distort the image. If the mirror is too thick, these can render the image useless.

By trial and error we have arrived at an optimum thickness of 0.5 mm for our experiments.

The maximum optical resolution is determined by the aperature stop. This is 12.7 mm in this instrument giving a resolution of

$$\ell = \frac{0.61\lambda}{D} \approx 0.03 \text{ mm}$$

for the optical system. This is sufficient to take full advantage of the resolution of the domains obtainable with the cerium metaphosphate mirror.

Sample Holder:

A sample holder as shown in Fig. E2 has been provided at the bottom end of tube D for holding the sample in close contact with the mirror. It is provided with a small superconducting magnet and a DC transformer for energizing samples.

The magnet consists of a superconducting, air core solenoid wound with 0.010" diameter Nb-25% Zr wire capable of a maximum field at the center of 1.2 T. It is permanently fixed with respect to the magneto-optic mirror so that it produces a uniform field normal to the surface of the mirror and sample.

The DC transformer is of the type described in Appendix C and is used to induce large currents into the sample while it is being viewed. A saturable reactor type current sensor (also described in Appendix C) is also included for measuring the current, and a small electric heater is provided for removing persistent currents in the sample.

APPENDIX F

FIELD DISTRIBUTION DUE TO CERTAIN CURRENT DENSITY PROFILES

In the estimation of current density profiles from photographs of surface field distribution of samples, we use a superposition technique in which certain known current profiles are superimposed on one another with appropriate weighting factors to make field distributions approximating the observed distributions.

Three current profiles were used for this purpose, uniform, linear and parabolic. For each of these profiles, the normal component of the fields was calculated at a distance 12 b out from the center plane of the strip, b being the half thickness of the strip. For the strip samples we used (5.1×10^{-2} mm in thickness) this was the distance at which the actual field equaled the average field, averaged over the characteristic length of magnetic variations.

This field was calculated by assuming the strip to be infinitely thin and having a linear current density given by

$$K = 2\,b\,J$$

where K has the dimensions amperes/meter, b the half thickness and J the actual current density in amperes/m^2.

For a strip placed in the x-z plane, the normal component of field is obtained from the expression

$$B_y = \frac{\mu_o}{2\pi} \int_{-a}^{a} \frac{K\,(x')\;(x-x')\;dx'}{(x-x')^2 + y^2}$$

The three cases for which this operation was performed are as follows in a non-dimensional form in which

$$\eta = \frac{x}{a}$$

$$\xi_1 = \frac{y_1}{a}$$

y_1 = distance above strip plane that field is being calculated

a = strip half width

b = strip half thickness

d = b/a

J_o = average current density (A/m^2)

μ_o = permeability of free space

B_y = normal component of field (T)

Case 1, Uniform

$$K = 2 J_o b$$

$$\frac{\pi B_y}{\mu_o J_o b} = \frac{1}{2} \ln \left[\frac{1 + \left(\frac{1-\eta^2}{\xi_1} \right)}{1 + \left(\frac{1+\eta^2}{\xi_1} \right)} \right]$$

Case 2, Linear

$$K = J_o b (1-\eta)$$

$$\frac{\pi B_y}{\mu_o J_o b} = \frac{1-\eta}{2} \ln \left[\frac{\xi_1^2 + (1-\eta)^2}{\xi_1^2 + (1+\eta)^2} \right]$$

$$+ \xi_1 \left[\pi - \frac{2}{\xi_1} - \tan^{-1} \left(\frac{\xi_1}{(1+\eta)} \right) - \tan^{-1} \left(\frac{\xi_1}{(1-\eta)} \right) \right]$$

Case C, Parabolic

$$K = \frac{1}{2} J_o b (1-\eta)^2$$

$$\frac{\pi B_y}{\mu_o J_o b} = \frac{1}{2} \left\{ \left[(1+\eta)^2 - \xi_1^2 \ln \left(\frac{\xi_1^2 + (1-\eta)^2}{\xi_1^2 + (1+\eta)^2} \right) \right] \right.$$

$$\left. + (1+\eta) \xi_1 \left[\frac{2}{\xi_1} + \tan^{-1} \left(\frac{\xi_1}{(1-\eta)} \right) + \tan^{-1} \frac{\xi_1}{(1+\eta)} - \pi \right] + \eta \right\}$$

REFERENCES

1. Field Dependent Anisotropy of the Critical Current in Nb-Zr Rolled Strip., M.S. Walker, M.J. Fraser, Scientific Paper 62-125-280-P1, Westinghouse Research Lab., Pittsburgh, Pennsylvania.

2. Magnetic Anisotropy in Cold Rolled Nb-Zr Superconducting Alloys, B.H. Heise, Linde Company, Tonawanda, N.Y.

3. P.B. Alers, Phys. Rev. 116, 1483 (1959).

4. W. DeSorbo and W.A. Healy, The Intermediate State of Some Superconductors, Report #61-RL-2743 M, General Electric, 1961.